USING ADVANCED FLUORESCENCE MICROSCOPY TO ANALYZE

INTRACELLULAR TRAFFICKING OF FcRn IN LIVE CELLS

APPROVED BY SUPERVISORY COMMITTEE

E. Sally Ward, Ph.D.

Raimund J. Ober, Ph.D.

Wen-Hong Li, Ph.D.

Ege T. Kavalali, Ph.D.

Philip E. Thorpe, Ph.D.

DEDICATION

First and foremost, I would like to thank my advisors Professor E. Sally Ward and Professor Raimund J. Ober for giving me an opportunity to work under their guidance. I would like to express my heartfelt respect to them for their invaluable mentorship during my doctoral studies. I would like to thank my committee members Professor Wen-hong Li, Professor Ege T. Kavalali and Professor Philip E. Thorpe for taking time to serve on my committee.

I am grateful to all current and former members of the Ward-Ober lab at the University of Texas Southwestern Medical Center at Dallas. I specially acknowledge the help, support, and discussions of Dr. Sripad Ram, Dr. Jerry Chao, Carlos Vaccaro, Alberto Puig-Canto, Dr. Prashant Prabhat, Ramraj Velmurugan, and Dr. Venkata Devanaboyina during my doctoral projects.

Finally, I would like to express my deepest gratitude to my family, especially my younger brother, sister-in-low and their lovely daughter Yijia. I would like to thank my dearest and loving wife Jingfei Zhu and son Yunwen for always being there to support me. Finally, I would like to express my sincere respect and appreciation to my grandmother Lizhong, my mom and father whose love, devotion and unconditional support of decades have prepared me to embark upon this journey.

USING ADVANCED FLUORESCENCE MICROSCOPY TO ANALYZE INTRACELLULAR TRAFFICKING OF FcRn IN LIVE CELLS

By

ZHUO GAN, B.E., M.E.

DISSERTATION

Presented to the Faculty of the Graduate School of Biomedical Sciences

The University of Texas Southwestern Medical Center at Dallas

In Partial Fulfillment of the Requirements

For the Degree of

DOCTOR OF PHILOSOPHY

The University of Texas Southwestern Medical Center at Dallas

Dallas, Texas

August, 2012

USING ADVANCED FLUORESCENCE MICROSCOPY TO ANALYZE

INTRACELLULAR TRAFFICKING OF FcRn IN LIVE CELLS

ZHUO GAN, Ph.D.

The University of Texas Southwestern Medical Center at Dallas, 2012

E. SALLY WARD, Ph.D., RAIMUND J. OBER, Ph.D.

The MHC class I-related Fc receptor (FcRn) regulates the *in vivo* half-life of immunoglobulin G (IgG) and transports IgG across cell barriers. The intracellular trafficking of FcRn is central to its diverse functions. FcRn, like all receptors, is transferred to lysosomes for constitutive degradation to maintain a balance between synthesis and breakdown. Using live cell imaging, a novel lysosomal delivery pathway for FcRn has been observed. Unlike signaling receptors that enter the intraluminal vesicles in late endosomes, FcRn remains on the limiting membrane of late endosomes and is delivered to lysosomes through a selective, primarily tubule-mediated process. Following transfer, FcRn is rapidly internalized into the lysosomal lumen. By contrast, LAMP1 remains on the limiting membrane of lysosomes. Rab5 can persist on late endosomes, which can not only fuse with lysosomes, but can also give rise to tubulovesicular carriers that enter the recycling pathway. Thus, late endosomes are functionally plastic. These observations have relevance to understanding lysosomal delivery pathways.

A combination of MUltifocal plane Microscopy (MUM) and localized photoactivation ('LP-MUM') has been developed to investigate the intracellular recycling pathway of FcRn. LP-MUM has been used to activate photoactivatable GFP (PAGFP) tagged proteins in individual sorting endosomes within cells, followed by imaging in two focal planes simultaneously. This approach has enabled the tracking of small, motile and dense transport carriers (TCs) that deliver FcRn to different destinations within the cell. The Rab GTPases, SNX4 and APPL1 play important roles in various steps of receptor trafficking pathways, and their associations with TCs has also been investigated. Four distinct itineraries taken by TCs at various stages of FcRn recycling have been characterized. In addition, the effectors associated with TCs on different pathways have been identified. APPL1+ TCs can transfer FcRn from the plasma membrane to pre-existing sorting endosomes. Interendosomal TCs migrate between sorting endosomes and are Rab4+/SNX4+ but Rab11-/APPL1-. Post-endosomal TCs that deliver FcRn to the plasma membrane are Rab11+ but Rab4-/SNX4-/APPL1-. Unexpectedly, a novel class of 'looping' TCs that leave a sorting endosome and return to the same endosome after several minutes has also been observed. The 'looping' TCs are Rab11+/Rab4+/SNX4+. The analyses of these TCs should have general relevance to other receptors and cargo on the recycling pathway.

TABEL OF CONTENT

PRIOR PUBLICATIONS

Prabhat P, Gan Z, Chao J, Ram S, Vaccaro C, Gibbons S, Ober RJ, and Ward ES. Elucidation of intracellular recycling pathways leading to exocytosis of the Fc receptor, FcRn, by using multifocal plane microscopy. PNAS 2007 104:5889-5894

Mi W, Wanjie S, Lo ST, Gan Z, Pickl-Herk B, Ober RJ, Ward ES. Targeting the neonatal Fc receptor for antigen delivery using engineered Fc fragments. J Immunol. 2008 181(11):7550-61

Gan Z, Ram S, Vaccaro C, Ober RJ, Ward ES. Analyses of the recycling receptor, FcRn, in live cells reveal novel pathways for lysosomal delivery. Traffic. 2009 10(5):600-14.

LIST OF FIGURES

CHAPTER 1 INTRODUCTION

1.1 Overview

This research project was directed towards using advanced fluorescence microscopy to investigate the intracellular trafficking pathways of the MHC class I-related Fc receptor, FcRn, and effector proteins that associate with these pathways. Investigation of the lysosomal delivery and recycling pathways of FcRn were the two foci of this research. A novel lysosomal delivery pathway has been observed. Multifocal plane microscopy and localized photoactivation techniques were used to track tubulovesicular transport carriers (TCs) and their effector proteins in the recycling pathway, resulting in novel insight into the recycling process. This chapter gives a brief overview of FcRn function, intracellular trafficking pathways and fluorescence microscopy.

1.2 The MHC class I-related Fc receptor, FcRn

The MHC class I-related Fc receptor (FcRn) is a type 1 transmembrane receptor which binds to the Fc region of IgG in a pH-dependent way (Ghetie and Ward, 2000; Roopenian and Akilesh, 2007; Simister and Mostov, 1989; Ward and Ober, 2009). FcRn is a heterodimer of an α-chain similar to the α-chains of the class I MHC molecules and a class I light chain, the β2-microglobulin (Burmeister et al., 1994). The FcRn α-chain consists of three extracellular domains (α1, α2 and α3), a transmembrane region and a

small cytoplasmic domain. The extracellular domains of the α-chain are non-covalently associated with β2-microglobulin. Several residues in the α2 domain, β_2-microglobulin and the carbohydrate of rat FcRn are critical for the pH-dependent IgG binding (Martin et al., 2001).

FcRn was first found in the intestinal epithelial cells of newborn rats and mediates IgG transport from milk to the bloodstream (Abrahamson and Rodewald, 1981; Brambell, 1966). Subsequently FcRn has been shown to be expressed in many cell types, including monocytes, macrophages, dendritic cells, endothelial cells and epithelial cells, of various mammalian species (Ahouse et al., 1993; Borvak et al., 1998; Cauza et al., 2005; Story et al., 1994; Zhu et al., 2001). FcRn expression in endothelial cells of the microvasculature and hematopoietic cells is responsible for maintaining IgG homeostasis throughout adult life (Borvak et al., 1998; Ghetie et al., 1996; Israel et al., 1996; Junghans and Anderson, 1996; Ober et al., 2004b). FcRn also mediates the transport of IgG and immune complexes across epithelial cells and other cell barriers through the transcytotic pathway (Antohe et al., 2001; Claypool et al., 2002; Dickinson et al., 1999; Firan et al., 2001; McCarthy et al., 2000; Yoshida et al., 2004; Yoshida et al., 2006). The FcRn-mediated transport of IgG and immune complexes across epithelial cells are important for mucosal immunity (Yoshida et al., 2006).

FcRn binds to IgG more tightly at acidic pH relative to near neutral pH. In its steady state, FcRn is present on the limiting membranes of sorting and late endosomes of various cell types (Ober et al., 2004b). IgG is taken into cells through fluid phase

pinocytosis and delivered to sorting endosomes (**Figure 1.1**). In acidic sorting endosomes IgG encounters and binds to FcRn since the pH is permissive for high affinity binding. Consequently, the FcRn-IgG complex is either sorted into the recycling pathway or, for polarized cells, transcytosed across the cells. IgG is released from FcRn at the plasma membrane and returned back to the extracellular environment because of the neutral pH (lower affinity). Internalized IgG is hence salvaged from being degraded, whereas unbound IgG within endosomes is transferred to lysosomes for degradation. Consequently, IgGs that bind to FcRn have long *in vivo* persistence relative to those that fail to interact with FcRn within cells. In addition, FcRn might be used to deliver therapeutic antibodies to disease sites, since it transfers IgG within cells and across cell barriers.

Because of its crucial functions in maintaining the *in vivo* persistence of IgG, FcRn can be used as a target for improving serum half-lives of therapeutic antibodies or for autoimmune diseases in which autoreactive IgGs play a role in pathogenesis (Patel et al., 2011). Engineering the FcRn-binding residues in the Fc region of IgG has resulted in modified affinities of FcRn-IgG interactions (Ghetie et al., 1997; Vaccaro et al., 2005). Mutated IgGs with higher affinity FcRn binding at pH 6.0 than wild type IgG, with retention of very low affinity at near neutral pH, will have longer *in vivo* half-lives, because these mutants can be recycled by FcRn more efficiently (Ghetie et al., 1997). This strategy can be used to improve the half-lives of therapeutic antibodies (Ghetie et al., 1997; Presta, 2008; Roopenian and Akilesh, 2007; Ward and Ober, 2009). On the other hand, some mutated IgGs have higher affinity and less pH-dependent binding to

FcRn. Our lab has developed such mutated antibodies that can enhance IgG degradation (Abdegs) (Vaccaro et al., 2005). Abdegs can serve as effective FcRn inhibitors because of three reasons. Firstly, they can bind to FcRn on the cell surface and be taken into cells by receptor-mediated uptake, rather than the less efficient fluid phase pathway. Secondly, they can bind to FcRn in sorting endosomes more efficiently than wild type, lower affinity IgGs. Finally, they are not released from FcRn at the plasma membrane following exocytosis. Thus Abdegs can be used to treat IgG mediated autoimmunity (Patel et al., 2011).

Although the crucial functions of FcRn in regulating transport and levels of IgG are well understood, the precise processes and effector proteins that are involved in the intracellular trafficking of FcRn, such as the recycling and constitutive degradation pathways, remain to be fully established. The processes are particularly relevant to improving the pharmacokinetics of therapeutic antibodies and developing therapeutic antibodies that use FcRn as a target or delivery tool. It is also of interest to know how the recycling pathway and constitutive degradation pathway of recycling receptors are related to each other. Interestingly, Abdegs have shorter *in vivo* serum half-lives than wild type IgG (Dall'Acqua et al., 2002). The process that leads to lysosomal delivery of Abdegs for degradation is also one of the topics of investigation in this research project.

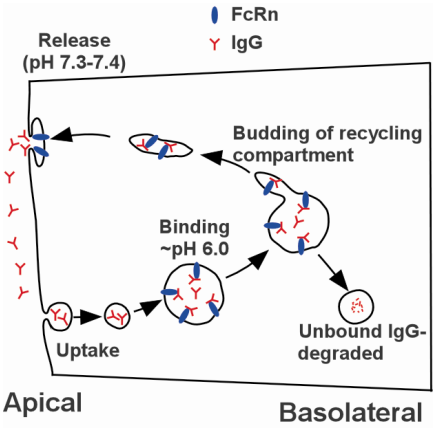

Figure 1.1

FcRn salvages IgG from degradation. In endothelial cells, IgG enters cells through fluid phase pinocytosis and is delivered to sorting endosomes. IgG can bind to FcRn in sorting endosomes because of the acidic environment. Consequently, the FcRn-IgG complex is sorted back to the apical membrane in tubulovesicular transport carriers via the recycling pathway. At the plasma membrane, IgG is released from FcRn to the extracellular environment because of the near neutral pH. IgG is hence salvaged from being degraded in the lysosomes.

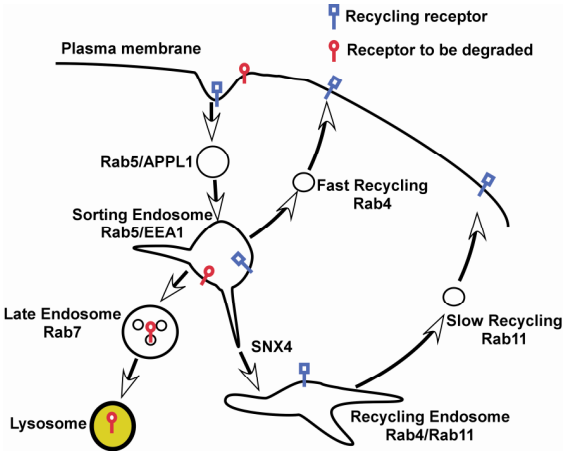

Figure 1.2

A model for the endocytic membrane/receptor trafficking pathways.

1.3 The endocytic membrane trafficking pathways

1.3.1 Receptor endocytosis

The endocytic membrane trafficking pathways, composed of transport carriers (TCs), early/sorting endosomes, recycling endosomes, late endosomes and lysosomes, regulate the internalization, sorting, recycling and degradation of membrane receptors and other macromolecules (**Figure 1.2**) (Grant and Donaldson, 2009; Maxfield and McGraw, 2004). The organelles in these pathways are connected by a complex network of tubulovesicular TCs. The transmembrane receptors to be constitutively internalized, such as FcRn and transferrin receptor, are recruited to the clathrin-coated pits in the plasma membrane. This process is mediated by sorting signals of receptors and adaptor proteins. The invagination of the clathrin-coated pits and their fission from the plasma membrane, mediated by dynamin and actin, results in the delivery of membrane receptors, their ligands and lipids into endocytic vesicles (Grant and Donaldson, 2009). Signaling receptors, such as EGFR, are selectively internalized into endocytic vesicles through clathrin-coated pits upon ligand stimulation. The surface levels of the signaling receptors are finely regulated by this ligand-stimulated internalization process. This internalization process is triggered by ubiquitination, a post-translational modification that attaches ubiquitin to the lysine residues of the receptors catalyzed by enzymes E1, E2 and E3 (Grant and Donaldson, 2009). In addition to the classical clathrin-dependent pathway, several clathrin-independent pathways exist for receptor endocytosis (Grant and Donaldson, 2009). After internalization, there are two models existing for the earlier step

of receptor endocytic pathways, *i. e.* how receptors are delivered to early/sorting endosomes after internalization. A classical model states that newly formed endocytic vesicles pinch off from the plasma membrane and fuse with preexisting, stable early/sorting endosomes to deliver cargo (Gruenberg, 2001; Mellman et al., 1986; Zerial and McBride, 2001). This concept is challenged recently by another 'maturation' model in which endocytic vesicles mature directly into early/sorting endosomes by homotypic fusion (Zoncu et al., 2009). These two models may not be mutually exclusive, since vesicles on the vesicular transport model can also mature by the addition or removal of effectors.

1.3.2 Receptor recycling

From the early/sorting endosomes, receptors can be either recycled back to the cell surface for reuse or sorted into the lysosomal degradation pathway (**Figure 1.2**] (Grant and Donaldson, 2009; Maxfield and McGraw, 2004). Recycling receptors, such as the transferrin and LDL receptors, can be transported from early/sorting endosomes to the plasma membrane directly (the fast recycling pathway) or through intermediate, perinuclear recycling endosomes/endosomal recycling compartments (the slow recycling pathway). The kinetics of transferrin receptor recycling have been shown to have two phases, consistent with slow and fast recycling, and it accumulates in the perinuclear areas of cells after 15 min incubation (Daro et al., 1996; Grant and Donaldson, 2009; Hopkins and Trowbridge, 1983; Maxfield and McGraw, 2004). The sorting of recycling receptors into the early/sorting endosomes is believed to be geometry-based (Maxfield

and McGraw, 2004). Recycling receptors remain on the limiting membrane of early/sorting endosomes. Narrow-diameter tubules can extend from the early/sorting endosomes. Recycling receptors in the limiting membrane of early/sorting endosomes can move into the tubular extension regions. The higher surface area-to-volume ratios of the tubules result in sorting of the recycling receptors on the limiting membrane from the soluble molecules in the lumen of early/sorting endosomes. The tubules then pinch off from the early/sorting endosomes to form tubulovesicular TCs which deliver cargo to different destinations. These TCs are relatively small, crowded and highly motile, making them very difficult to track in live cells. Despite extensive studies of the endocytic pathways, how the TCs and endosomal compartments in this pathway are related to each other in both temporal and spatial terms remains to be established. Specifically, the subpopulations of TCs which deliver cargos to different destinations and their effector associations are not well defined. Furthermore, although the fast and slow recycling pathways have been reported, the intracellular trafficking steps that constitute these two pathways are still unclear.

1.3.3 Lysosomal delivery

In early/sorting endosomes, ligands may be released to the lumen from their receptors due to the low pH and subsequently transferred to lysosomes. On the other hand, internalized signaling receptors are modified by cytosol ubiquitin ligases and this triggers the delivery of the receptors into the intraluminal vesicles of endosomes, a process mediated by endosomal sorting complexes required for transport (ESCRTs) (Piper and

Katzmann, 2007). Late endosomes with intraluminal vesicles are also called multivesicular bodies (MVBs). In addition, several ubiquitin-independent pathways for the entry of endocytosed membrane receptors into intraluminal vesicles have been also reported (McNatt et al., 2007; Piper and Katzmann, 2007; Reggiori and Pelham, 2001). From these intraluminal vesicles, the receptors and ligands are finally delivered into the lysosomal lumen and degraded. Lysosomes are the primary site for the stimulated and constitutive degradations of membrane receptors (Luzio et al., 2007; Saftig and Klumperman, 2009). However, the mechanisms of lysosomal biogenesis and the lysosomal delivery of receptors are not fully understood. Different models, including vesicular transport, endosomal maturation and endo-lysosomal fusion, have been proposed for the content exchange between late endosomes and lysosomes. In addition, how the recycling receptors, such as the transferrin receptor and FcRn, are transported into lysosomes for constitutive degradation is unknown. These receptors, unlike signaling receptors, remain by default on the limiting membrane of endosomes and are not ubiquitinated. It is of interest to know if these receptors are also transported to the intraluminal vesicles of MVBs prior to lysosomal delivery.

1.4 Rab GTPases

1.4.1 The Rab GTPase protein family

The Rab GTPases are a large family of small GTPases which control the intracellular membrane identity and serve as coordinators of membrane trafficking (Hutagalung and

Novick, 2011; Stenmark, 2009; Zerial and McBride, 2001). The Rab GTPases can be found either in the cytosol or associated with the limiting membranes of multiple cellular organelles (**Figure 1.3**). The Rab GTPases in the cytosol are bound to GDP and Rab GDP dissociation inhibitors (GDIs). The membrane-bound GDI displacement factors (GDFs) catalyze the dissociation of GDIs from Rabs, binding of GTP to Rabs and the insertion of Rabs into specific membranes. Therefore, Rab GTPases can switch between the GDP-bound 'off' form and the GTP-bound 'on' form. The GDP-bound Rabs are activated by releasing GDP and recruiting GTP, which requires the guanine nucleotide exchange factors (GEFs). The hydrolysis of GTP, which is catalyzed by GTPase-activating proteins (GAPs), converts the GTP-bound Rabs back to the inactive GDP-bound form.

Rab GTPases can control membrane identity by regulating membrane lipid compositions (Stenmark, 2009; Zerial and McBride, 2001). Phosphoinositides (PIs) recruit Rab effectors to specific membranes and Rab effectors phosphorylate or dephosphorylate specific phosphatidylinositols in these membranes to maintain their identities. The GTP-bound Rab GTPases regulate vesicular budding, motility of vesicles and organelles, and fusion by recruiting specific effector proteins (Stenmark, 2009; Zerial and McBride, 2001). For example, Rab GTPases can recruit adaptor proteins to sort cargo to vesicles forming on the 'donor' membrane, mediate the dissociation of coat proteins after pinching off, recruit motor adaptors or bind directly to molecular motors and recruit tethering factors to facilitate fusion.

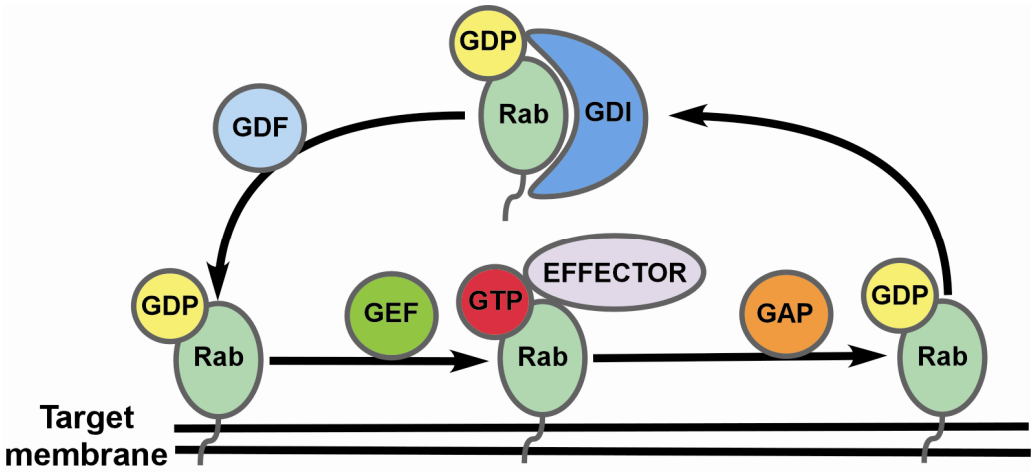

Figure 1.3

The Rab GTPase cycle. Rab GTPases in the cytosol are bound to GDP and Rab GDP dissociation inhibitors (GDIs). The membrane-bound GDI displacement factors (GDFs) catalyze the dissociation of GDIs from Rabs and the insertion of Rabs into specific membranes. The GDP-bound Rabs are activated by releasing GDP and recruiting GTP, which require the guanine nucleotide exchange factors (GEFs). The hydrolysis of GTP, which is catalyzed by GTPase-activating proteins (GAPs), converts the GTP-bound Rabs back to the inactive GDP-bound form.

1.4.2 Rab4, Rab5, Rab7 and Rab11 are involved in the endocytic trafficking pathways

Of about 70 human Rab GTPases, Rab5 is associated with early/sorting endosomes and regulates the fusion of endocytic vesicles and early/sorting endosomes (Christoforidis et al., 1999; Simonsen et al., 1998). The late endosome/lysosome associated Rab7 regulates late endosomal mobility and the formation of MVBs (Bucci et al., 2000; Progida et al., 2007). A Rab conversion model has been proposed by Rink and co-workers in which Rab5 is gradually replaced by Rab7 during endosomal maturation (Rink et al., 2005). In the recycling pathway, Rab11 is associated with both recycling endosomes and early/sorting endosomes. Internalized transferrin colocalizes with Rab11 in the perinuclear areas of cells after 30 minutes incubation (Ren et al., 1998; Ullrich et al., 1996). Rab11 regulates trafficking from early/sorting endosomes to recycling endosomes and from recycling endosomes to the plasma membrane (Lindsay and McCaffrey, 2004; Ren et al., 1998; Schonteich et al., 2008; Ullrich et al., 1996; Ward et al., 2005). An effector protein of Rab11, Rip11/Rab11-FIP5, binds to the molecular motor kinesin II to mediate receptor recycling (Schonteich et al., 2008). Other effector proteins, Rab11-FIP2 and FIP3, have been shown to interact with myosin Vb and dynein, respectively (Hales et al., 2002; Horgan et al., 2010; Wang et al., 2008). Rab4, on the other hand, is associated with sorting endosomes and is partially depleted from recycling endosomes (Sheff et al., 1999). Transferrin accumulates in the perinuclear compartments that are Rab4 negative after 15 minutes incubation (Daro et al., 1996). Rab4 regulates the formation of recycling vesicles and the fast recycling pathway through effectors such as Rabaptin-5 and Rabip4'

that interact with γ_1-adaptin (Deneka et al., 2003; Fouraux et al., 2004; McCaffrey et al., 2001; Pagano et al., 2004; Sheff et al., 1999; Yudowski et al., 2009). Interactions between Rab4 and molecular motors kinesin and dynein have also been shown (Bielli et al., 2001; Imamura et al., 2003). Rab4 and Rab11 share a common effector, D-AKAP2 (Eggers et al., 2009). However, Rab4 has been reported to not be involved in exocytic events (Ward et al., 2005).

One goal of the work in the research project was to identify the associations of Rab GTPases in FcRn trafficking pathways. For example, at which point during Rab5 to Rab7 conversion do endosomes no longer generate recycling TCs and gain competence to interact with lysosomes? How do Rab4 and Rab11 associate with different TCs in the recycling pathway of FcRn in spatiotemporal terms? These questions are particularly relevant to mechanisms regulating the constitutive degradation and recycling pathways of recycling receptors, such as FcRn and the transferrin receptor.

1.5 The adaptor protein containing PH domain, PTB domain and leucine zipper motif, APPL

Adaptor protein containing PH domain, PTB domain and Leucine zipper motif (APPL) is a Rab5 effector that was first identified as an interacting partner for inactive serine/threonine kinase AKT2 and the phosphatidylinositol 3-kinase p100α (Miaczynska et al., 2004; Mitsuuchi et al., 1999). The two homologous proteins, APPL1 and APPL2, both contain a Bin-Amphiphysin-Rvs (BAR) domain and localize to the same

compartments within cells (Miaczynska et al., 2004; Urbanska et al., 2011). The PH domain of APPL1 is insufficient for its membrane targeting (Miaczynska et al., 2004). Both the BAR and PH domains are necessary for Rab5 binding and the membrane association of APPL is dependent on Rab5. APPL1 is present in a subpopulation of early endosomes, which does not have another Rab5 effector EEA1. The APPL1+ early endosomes concentrate in the cell periphery and are smaller than the perinuclear EEA1+ sorting endosomes. The APPL1+ early endosomes are derived from clathrin-coated pits and can mature to EEA1+/PI(3)P+ early/sorting endosomes (Miaczynska et al., 2004; Zoncu et al., 2009). The maturation of APPL1+ early/sorting endosomes to EEA1+ endosomes requires PI(3)P. EGF can be internalized into APPL1+ early/sorting endosomes and bind to EGFR. Upon the delivery of EGF into APPL1+ early/sorting endosomes, APPL1 is transferred from the early/sorting endosomes to the nucleus to mediate cell proliferation by interacting with the nucleosome remodeling and histone deacetylase multiprotein complex NuRD/MeCP1, which regulates chromatin structure and gene expression (Miaczynska et al., 2004). The translocation of APPL1 upon EGF stimulation requires Rab5 hydrolysis. The APPL1+ early/sorting endosomes hence represent a subpopulation of early/sorting endosomes in the endocytic pathways where the signal transduction of EGFR can still occur.

APPL1 has also been reported to interact with multiple proteins involved in signal transduction, such as two adiponectin receptors, the netrin-1 receptor DCC, TrkA, NMDA receptor, FISH receptor, Akt, Annexin A2 and GIPC (Husi et al., 2000; Liu et al., 2002; Mao et al., 2006; Nechamen et al., 2004; Schenck et al., 2008; Urbanska et al.,

2011; Varsano et al., 2006). On the other hand, transferrin has been reported to not associate with APPL1+ early/sorting endosomes (Miaczynska et al., 2004). Since FcRn is not a signaling receptor, it is interesting to know if or how FcRn passes through APPL1+ early/sorting endosomes following internalization from the plasma membrane.

1.6 Sorting nexin 4

All members of the sorting nexin (SNX) protein family contain a phospholipid binding motif, the phox domain (Cullen, 2008; Haft et al., 1998; Worby and Dixon, 2002). The phox domains of sorting nexins consist of 100-130 amino acids and bind to specific phosphatidylinositol phosphates. Sorting nexins associate with specific membranes through their phox domains and mediate diverse membrane trafficking processes, such as endocytosis and endosomal sorting. In addition to its phox domain, sorting nexin 4 (SNX4) also contains a Bin-Amphiphysin-Rvs (BAR) domain which has a curved structure. The concave face of the BAR domain interacts with membranes and hence can sense the membrane curvature of small vesicles and tubules. The phox domain of SNX4 binds specifically to phosphatidylinositol-3-monophosphate, which is enriched in endosomes (Cullen, 2008). Hence SNX4 associates with the vesicular and tubular extensions of endosomes through its phox and BAR domains. SNX4 mediates the recycling/retrieval pathways of Ste6 and Snc1p in yeast (Hettema et al., 2003; Krsmanovic et al., 2005). In mammalian cells, SNX4 interacts with the molecular motor dynein through Kidney and Brain Protein (KIBRA) to drive the tubulation of early/sorting endosomes and mediates the transport of transferrin receptor from the

early/sorting endosomes to recycling endosomes (Traer et al., 2007). Amphiphysin 2 works together with SNX4 to mediate the intracellular trafficking of the transferrin receptor (Leprince et al., 2003). During the endosomal maturation process in which Rab4 is replaced by Rab11, SNX4+ tubulation of endosomes has been observed (van Weering et al., 2012). The tubulation of sorting endosomes is believed to be important for geometric-based sorting of membrane receptors to the recycling pathway (Maxfield and McGraw, 2004). Furthermore, SNX4 has also been reported to bind to clathrin and mediate endosome to Golgi transfer of rasin in an hVps34 dependent way (Skanland et al., 2009; Skanland et al., 2007). The TC association of SNX4 in the intracellular trafficking of FcRn is therefore of interest, since this SNX is of particular relevance to the recycling pathway.

1.7 Fluorescence microscopy

1.7.1 The principle of fluorescence microscopy

In fluorescence microscopy, the contrast of image is obtained by labeling objects, such as proteins with fluorophores. Green fluorescent protein (GFP) was first found in *Aequorea Victoria* decades ago (Shimomura et al., 1962). More recently, a large number of additional fluorescent proteins have been isolated or developed by protein engineering (Zhang et al., 2002). Genes encoding fluorescent proteins can be fused with the genes of proteins of interest by recombinant DNA techniques. The fusion proteins containing a fluorescent protein and the protein of interest can be expressed in live cells and observed

by fluorescence microscopy. This approach has revolutionized the microscopic analysis of fluorescently tagged proteins in live cells (Lippincott-Schwartz et al., 2001).

The improvement in the sensitivity of charge-coupled device detectors also allows data acquisition at higher frame rates, thus rapid events can be monitored in real time. Consequently, current microscopy approaches combined with the use of different fluorophores can be used to analyze intracellular trafficking processes at unprecedented levels of temporal and spatial resolution.

1.7.2 Multifocal plane microscopy

Conventional wide-field fluorescence microscopy monitors cellular components in a single focal plane within cells. However, cells are three dimensional structures. When observing live cells with conventional fluorescence microscopy, the organelles of interest, such as TCs and sorting endosomes may move out of the focal plane and disappear. To track the organelles that move quickly in 3 dimensions, it is desirable to image multiple focal planes simultaneously within cells. Using focusing devices, such as piezos, different focal planes can be imaged sequentially. However, the frame rates are relatively slow due to the scanning. As a result, it is difficult to track the rapid, long-distance moving organelles in multiple color channels (for different proteins). Multifocal plane microscopy (MUM), which can monitor live cells in 3 dimensions with relatively high frame rates, has been developed in our laboratory to overcome this technical barrier (Prabhat et al., 2007; Prabhat et al., 2004). In MUM, several cameras are attached to the

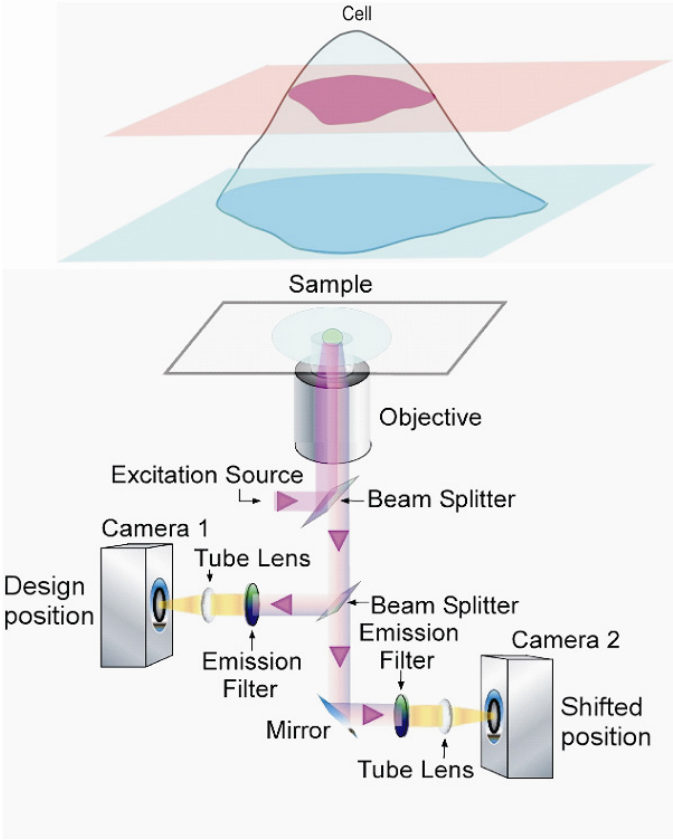

Figure 1.4

A MUM setup. Fluorescence is split into two (or more) light paths. For each of the light paths, fluorescence is projected onto a camera by a tube lens. The distances between these cameras and the tube lenses are different hence distinct planes within the cell can be imaged simultaneously by the cameras.

sideport of the microscope through dual-view adaptors **(Figure 1.4).** Fluorescence emitted by the sample is split into several light paths by beam splitters. For each of the light paths, fluorescence is projected onto a camera through a tube lens. The cameras are placed at different distances from the tube lens, and therefore focus onto different planes within samples. Therefore multiple planes within cells can be imaged simultaneously with higher frame rates. Fast moving organelles which travel in 3 dimensions can be tracked using MUM (Prabhat et al., 2007; Prabhat et al., 2004; Ram et al., 2008).

1.7.3 Localized photoactivation

Photoactivatable fluorescent proteins (PA-FPs), whose emission spectral properties can be changed significantly upon illumination with light of specific wavelengths, have been developed and used for imaging protein dynamics, fluorescence pulse labeling, fluorescence resonance energy transfer and localization-based super resolution imaging (Betzig et al., 2006; Demarco et al., 2006; Kim et al., 2006; Lippincott-Schwartz et al., 2003; Patterson and Lippincott-Schwartz, 2002; Schuster et al., 2011b). Some PA-FPs, such as PhotoActivatable GFP (PAGFP), emit little or no fluorescence under the original excitation wavelengths of GFP (488 nm). However, the emission of PA-GFP increases significantly upon transient photoactivation with UV light (Patterson and Lippincott-Schwartz, 2002). Others, such as EosFP, switch peak emissions from one wavelength to another upon photoactivation (Wiedenmann et al., 2004). When labeling proteins with conventional fluorescent proteins, there are frequently too many labeled organelles containing these proteins in the field of view. Furthermore, some of these compartments

might be moving rapidly within the cell. The individual organelles of interest are difficult to distinguish from surrounding structures in sequential frames because of the high density and mobility. Tracking of single organelles or vesicles over relatively long time periods is therefore difficult due to loss of identities. The background fluorescence from out-of-focus, labeled structures also limits the capacity of identifying and tracking single structures within live cells. In some cases the proteins to be tracked, such as Rab GTPases, are also present in the cytosol and give rise to fluorescent haze.

The use of PA-FPs facilitates the tracking of movement of proteins within cells, if PA-FPs on one individual organelle can be specifically 'switched on' rapidly and efficiently, whereas PA-FPs in other structures within cells are left inactivated. Activated organelles are easy to identify throughout all frames, since other organelles within cells emit very low fluorescence and are almost invisible. For the same reason the background fluorescence is also very low. The quantification of fusion and fission events of TCs with endosomes or other organelles is difficult when using conventional fluorophores. For example, when smaller, low fluorescent intensity TCs fuse with bigger, brighter structures such as a sorting endosome, the intensity change in the sorting endosome is minor compared with its original intensity. Using PA-FPs and activating only one individual organelle in cells facilitates confirmation of merging events by quantification of intensity analyses because the 'acceptor' organelles will have lower fluorescence. Therefore the intensity changes in the organelles are significant in relation to its original intensity.

In this research project, a Localized Photoactivation-MUltifocal plane Microscopy (LP-MUM) setup which combines both MUM and photoactivation has been developed to investigate the intracellular trafficking pathways of FcRn. in live cells. In particular, the use of LP-MUM, has enabled the tracking of small, motile TCs in the FcRn recycling pathway in three dimensions, leading to novel insight into the intracellular trafficking steps that contribute to FcRn recycling.

CHAPTER 2 MATERIALS AND METHODS

The details of the sample preparations, experimental conditions and data processing are presented in this section. This project was a collaborative effort of the current and former members of Drs. E. Sally Ward/Raimund J. Ober lab. The cell culture, molecular cloning and transfection were done by Dr. E. Sally Ward, Z. Gan, C. Vaccaro, S. Gibbons, J. Zhou and A. Puig-Canto. Live and fixed cell imaging experiments and data analyses were conducted by Z. Gan.

2.1 Media

2.1.1 Tissue culture media

MCDB 131 medium was prepared by mixing 500 mL of MCDB 131 (without L-glutamine, Invitrogen, Carlsbad, CA), 50 mL of FCS, 5 mL of penn/strep and 5 mL of L-glutamine.

Ham's F-12 K medium was prepared by mixing 7.14 grams of Ham's powder (US Biological, Swampscott, MA), 1.25 grams of sodium bicarbonate, 500 mL of Milli-Q water, 50 mL of IgG-depleted FCS, 5 mL of penn/stryp, 5 mL of L-glutamine, 77.5 mg of calcium chloride, 50 mg of heparin salt and 15 mg of endothelial cell growth supplement.

2.1.2 Bacterial media

No salt medium was prepared by mixing 20 grams of tryptone, 20 grams of yeast extract and 1 Liter of distilled water. The pH value of medium was adjusted to 7.2 with NaOH.

4 x TY medium was prepared by mixing 20 grams of tryptone, 10 grams of NaCl, 20 grams of yeast extract and 1 Liter of distilled water. The pH value of medium was adjusted to 7.2 with NaOH.

2.2 Plasmid constructs

2.2.1 Plasmid constructs obtained

Plasmid constructs that are obtained from outside are listed in Table 2.1.

2.2.2 Plasmid constructs made in our lab

In this research project, FcRn with GFP appended to N-terminus is written as GFP-FcRn, and FcRn with GFP appended to C-terminus is written as FcRn-GFP etc. Plasmid constructs encoding human and mouse FcRn (hFcRn and mFcRn) fused at the C-terminus or N-terminus with enhanced GFP or mRFP, and human or mouse β2-microglobulin (β2m) have been described (Ober et al., 2004b; Vaccaro et al., 2005). The wild type hFcRn gene in hFcRn-GFP was replaced by a mutated variant of human FcRn (’79-

Table 2.1 Plasmid constructs obtained

Constructs	Description	Generously provided by or purchased from
LAMP-1-GFP	rat LAMP-1 with GFP appended to C-terminus	Professor P. Luzio (University of Cambridge, UK)
GFP-Rab4	human Rab4a with GFP appended to N-terminus	Professor M. Zerial (Max Planck Institute of Molecular Cell Biology and Genetics, Germany)
GFP-Rab5	human Rab5a with GFP appended to N-terminus	Professor M. Zerial (Max Planck Institute of Molecular Cell Biology and Genetics, Germany)
GFP-Rab7	human Rab7a with GFP appended to N-terminus	Professor M. Zerial (Max Planck Institute of Molecular Cell Biology and Genetics, Germany)
GFP-Rab11	human Rab11a with GFP appended to N-terminus	Professor M. Zerial (Max Planck Institute of Molecular Cell Biology and Genetics, Germany)
GFP-SNX4	human SNX4 with GFP appended to N-terminus	Prof. P. Cullen (University of Bristol, UK).
mCherry-SNX4	human SNX4 with mCherry appended to N-terminus	Prof. P. Cullen (University of Bristol, UK).
GFP-APPL1	human APPL1 with GFP appended to N-terminus	Addgene (Cambridge, MA)
mRFP-APPL1	human APPL1 with mRFP appended to N-terminus	Addgene (Cambridge, MA)

89/136-147') that has higher affinity for binding to IgG (Zhou et al., 2005) to generate the hFcRn_mut-GFP construct. The plasmid construct encoding LP pHluorin-hFcRn (Miesenbock et al., 1998) has been described previously (Prabhat et al., 2007). The wild type FcRn gene in LP GFP-hFcRn and LP-mRFP-hFcRn was replaced by the mutated variant of human FcRn ('79-89/136-147') as a Bglll-Sall fragment to make the LP GFP-hFcRn_mut and LP mRFP-hFcRn_mut. The FcRn_mut-stop construct was generated by inserting a stop codon between the C-terminus of the FcRn_mut gene and the N-terminus of the GFP gene in the FcRn_mut-GFP construct. To make the hFcRn_mut-PAGFP, the hFcRn_mut gene in the hFcRn_mut-mRFP construct was recloned into the PAGFP-N1 vector (generously provided by Dr. George Patterson, NIBIB) as an EcoRl fragment. In order to make the LP PAGFP-hFcRn, the PAGFP gene was recloned into the LP mRFP wt hFcRn to replace the mRFP gene as a Kpnl fragment. The wild type FcRn gene in this construct was then replaced with the mutated variant of human FcRn ('79-89/136-147') as a Bglll-Sall fragment to make the LP PAGFP-hFcRn_mut.

The plasmid constructs encoding mRFP-Rab5 and mRFP-Rab7 have been described previously (Gan et al., 2009). Genes encoding human Rab11a and Rab4a were recloned into the mRFP-C1 vector that is made by replacing the EGFP gene in the pEGFP-C1 vector (Clontech, Palo Alto, CA) with the mRFP gene as a NheI-Bgl II fragment, as KpnI-BamHI fragments to make the mRFP-Rab4 and mRFP-Rab11 constructs, respectively. To make PAGFP-Rab11 and PAGFP-Rab4, the human Rab11a and Rab4a genes in the mRFP-Rab4 and mRFP-Rab11 constructs were recloned into the PAGFP-C1 vector as Kpnl-BamHl fragments, respectively. To make PAGFP-SNX4, the human

SNX4 gene from mCherry-SNX4 was recloned into the PAGFP-C1 vector (Dr. George Patterson) as a HindIII-Xmal fragment.

2.3 Expression of PAGFP

The PAGFP gene in a PAGFP-C1 vector was recloned into a pUC19 vector designed for periplasmic secretion (Ward, 1992; Ward et al., 1989) as an EcoRI-NcoI fragment to generate an *E. coli*. expression vector for the production of soluble PAGFP. The plasmid construct was transformed into *E. coli*. Transformed *E. coli* cells were grown for 14 hours in 4 x TY. The protein expression was induced in no salt medium for 4.5-5 hours and the cells were osmotically shocked as described previously (Ward, 1992). The soluble PAGFP protein was then purified from the osmotic shocks fractions using Ni-NTA-agarose resin (Qiagen, Valencia, CA). The purified protein was dialyzed against PBS with 0.02% NaN_3 at 4 °C overnight, harvested and concentrated by centrifuging at 4 °C at 2,300 rpm using Amicon 10,000 MWCO ultra filtration units (Millipore, Billerica, MA).

2.4 Antibodies and reagents

Alexa 488, 555, and 647-labeled dextran (10,000MW, anionic, fixable) were purchased from Invitrogen.

MST-HN, an mutated human IgG1 (or 'Abdeg') that is engineered to bind with higher affinity and less pH-dependence to FcRn in the range pH 6.0–7.4 (Vaccaro et al., 2005)

was labeled with Atto 647N-NHS ester (Atto-Tec, Siegen, Germany) or Alexa fluor 555 (Invitrogen) as recommended by the manufacturer's methods.

Mouse IgG2a anti-Rab5 and mouse IgG1 anti-EEA1 antibodies were purchased from BD Biosciences (San Jose, CA). Mouse IgG1 anti-LAMP-1 antibody (H4A3) was purchased from the Developmental Studies Hybridoma Bank (Iowa City, IA). The rabbit polyclonal anti human APPL antibody was purchased from Abcam (Cambridge, UK). Secondary antibody conjugates Alexa 647-labeled goat anti-rabbit IgG, Alexa 350-labeled donkey anti-rabbit IgG, Alexa 488-labeled goat anti-mouse IgG2a and Alexa 555-labeled goat anti-mouse IgG1 were purchased from Invitrogen.

2.5 Cell culture and transfections

The human endothelial cell line HMEC-1 is a dermal-derived microvasculature cell line (generously provided by F. Candal, CDC). HMEC-1 cells were maintained in MCDB131 medium (Invitrogen) before transfection. HMEC-1 cells were transiently co-transfected with different combinations of expression constructs using nucleofector technology (Amaxa Biosystems, Cologne, Germany) and the protocol recommended for the transfection of human endothelial cells. Immediately after transfection, cells were plated in phenol red-free Ham's F-12K medium on MatTek dishes (35-mm, glass-bottom, 10 mm microwell dishes; MatTek, Ashland, MA) for live cell imaging experiments. In some experiments, the glass bottoms of MatTek dishes were substituted by coverglasses (part number 72224-01, Electron Microscopy Sciences, Hatfield, PA) using polymount

because HMEC-1 cells were found growing better on the EMS coverglasses after transfection. For fixed cell imaging experiments, transfected cells were plated on coverslips (size 1.5, 12 mm diameter; Fisher Scientific, Houston, TX) in a 24-well plate or MatTek dishes with EMS coverglasses. These combinations are: FcRn-GFP (human) (1 μg) and human β2m (1 μg); FcRn-GFP (mouse) (1 μg) and mouse β2m (1 μg); mRFP-FcRn (human) (1 μg) and human β2m (1 μg); FcRn-mRFP (human) (1 μg) and human β2m (1 μg); LAMP-1-GFP (rat) (1 μg), mRFP-FcRn (human) (1 μg), and human β2m (1 μg); GFP-Rab5 (0.5 μg), mRFP-FcRn (human) (1 μg), and human β2m (1 μg); GFP-Rab7 (0.5 μg), mRFP-FcRn (human) (1 μg), and human β2m (1 μg); mRFP-Rab5 (0.5 μg) and GFP-Rab7 (0.5 μg); GFP-FcRn (1 μg) and human β2m (0.5 μg); FcRn-PAGFP (1 μg), human β2m (0.5 μg) and mRFP-Rab4 (0.2 μg); mRFP-FcRn (1 μg), human β2m (0.5 μg) and GFP-APPL1 (0.2 μg); FcRn-stop (1 μg), human β2m (0.5 μg) and GFP-APPL1 (0.2 μg); GFP-SNX4 (0.2 μg) and mRFP-Rab4 (0.2 μg); GFP-Rab11(0.2 μg) and mCherry-SNX4 (0.2 μg); mCherry-SNX4 (0.2 μg) and GFP-APPL1 (0.2 μg); mRFP-Rab4 (0.05 μg); FcRn-stop (1 μg), human β2m (0.5 μg), GFP-Rab11 (0.2 μg) and mCherry-SNX4 (0.2 μg); GFP-SNX4 (0.2 μg), human β2m (0.5 μg) and mRFP-FcRn (1 μg); mCherry-SNX4 (0.2 μg) and GFP-Rab11 (0.2 μg); mCherry-SNX4 (0.2 μg) and PAGFP-Rab4 (0.2 μg); mRFP-Rab4 (0.2 μg), human β2m (0.5 μg) and FcRn-PAGFP (1 μg); PAGFP-Rab4 (0.2 μg) and mCherry-SNX4 (0.2 μg); mCherry-SNX4 (0.2 μg) and PAGFP-Rab11 (0.2 μg); PAGFP-Rab11 (0.2 μg), human β2m (0.5 μg) and mRFP-FcRn (1 μg); GFP-FcRn (1 μg), human β2m (0.5 μg) and mCherry-SNX4 (0.2 μg); pHluorin-FcRn (1 μg), human β2m (0.5 μg) and mRFP-APPL1 (0.2 μg).

To ensure that the expression of Rab proteins and SNX4 does not affect the recycling pathway in transfected cells, HMEC-1 cells were co-transfected with different combinations of SNX4 and Rab proteins. Recycling rates of labeled transferrin were analyzed using flow cytometry as described previously (Ward et al., 2005). For cells co-expressing Rab proteins and SNX4 at the levels used for imaging in this research project, no significant differences in the transferrin recycling rates were observed between transfected and untransfected cells.

For live cell imaging experiments, cells were maintained at 35 – 37 °C using an objective heater. Experiments were carried out between 19–27 hours post-transfection. To mark lysosomes with labeled dextran, cells were incubated with Alexa 488, 555 or 647-labeled dextran (500 μg/ml in phenol red-free Ham's F-12 K medium at ≈ pH 7.4) for 2 hours. Cells were then washed and chased in phenol red-free Ham's F-12 K medium at ≈ pH 7.4 for 1–6 hours. To label FcRn with Atto 647N or Alexa 555-labeled IgG (MST-HN mutant), cells were incubated with 5 μg/ml IgG conjugates in phenol red-free Ham's F-12 K medium at ≈ pH 7.4 for 2 min to 24 hours.

For immunofluorescence staining, cells were fixed using 3.4% or 1.7% paraformaldehyde with 0.1% glutaraldehyde (10 min on ice) and permeabilized using 0.5 mg/ml saponin in phosphate buffered saline (PBS). Cells were then pre-blocked with 4% BSA in PBS and incubated with the primary antibody in 1% BSA in PBS for 25 min at room temperature. Cells were blocked with serum (100X dilution with 1% BSA in PBS) from the same host-animal in which the secondary antibody was raised, and incubated with the secondary

antibody conjugate for 25 min at room temperature. If cells were on coverglasses in a 24-well plate, cells were washed and the coverglasses were mounted on slides with Prolong (Invitrogen) and sealed with polymount. If the cells were on MatTek dishes, the mounting and sealing steps are not required. Instead, cells were immersed in 1.5 – 2 ml of 1% BSA in PBS containing 0.05% sodium azide.

2.6 Immobilization of recombinant PAGFP

Mowiol (Calbiochem, La Jolla, CA) coverslip mounting solution was prepared by mixing 6 g glycerol, 2.4 g Mowiol, 6 mL distilled water and 12 mL 0.2 M Tris (pH 8.5). The solution was stored at -20 °C. To immobilize recombinant PAGFP, the Mowiol solution was warmed to 37 °C and mixed with a solution of purified PAGFP. 100 µL mixed solution was transferred immediately to the microwell areas of MatTek dishes. The mixed solution was pipetted up and down to ensure good mixing on the microwells. The MatTek dishes were left in dark place overnight to allow the gel to solidify. The entire dishes were covered with 2.5 mL of 1X PBS before imaging.

2.7 LP-MUM

The details of the LP-MUM configuration and validation are described in APPENDIX A. For LP-MUM imaging, cells were maintained at 35 – 37^{o}C using an objective heater. For PAGFP activation, individual sorting endosomes were identified in the mCherry/mRFP channel. A 405 nm laser beam was focused on the sorting endosomes and transiently

turned on to photoactivate PAGFP in sorting endosomes. The photoactivation resulted in the significant increase of PAGFP fluorescence. The cells were then continuously excited by a 488 nm and a 543 nm lasers during acquisition. The exposure time was 300 ms per frame for all 4 cameras.

2.8 Wide field live cell imaging

Cells were maintained at 35 – 37 °C using an objective heater. Data were collected using a Zeiss Axiovert S100TV inverted fluorescence microscope with a Zeiss (Thornwood, NY) 1.4 NA 100× Plan-APOCHROMAT objective and a Zeiss 1.6× Optovar. Three laser lines were used for wide field excitation with a custom-built, right side-facing filter cube. A 488-nm laser (Laser Physics, West Jordan, UT) was used for GFP excitation, a 543-nm laser (Research Electro-Optics, Boulder, CO) for mRFP or Alexa 555 excitation, and a 633-nm laser (JDS Uniphase, San Jose, CA) for Atto 647N or Alexa 647 excitation. Images were acquired with an Andor (South Windsor, CT) iXon camera. A beamsplitter 488/543/633 and emission filters Z488/543/633m, HQ590/50m, HQ525/50m, and HQ690/90m from Chroma Technology (Brattleboro, VT) were used. A filter wheel was used to mount and cycle the single band emission filters. Three shutters were used to cycle the three lasers sequentially. The exposure time for each color channel was 500 ms, and a set of images for all three color channels was acquired every 1.5 s.

2.9 Wide field fixed cell imaging

Fixed cell images were acquired using a Zeiss Axiovert 200 M inverted fluorescence microscope with a Zeiss 1.4 NA100× Plan-APOCHROMAT objective or a Zeiss 1.4 NA 63× Plan-APOCHROMAT oil DIC objective. In some cases, a Zeiss 1.6× Optovar was used. Exciter HQ 470/40x, dichroic Q495LP, and emitter HQ 525/50m were used for the GFP/Alexa 488 channel, exciter HQ 545/30x, dichroic 570LP and emitter HQ 593/40m were used for the mRFP/mCherry/Alexa 555 channel, exciter HQ 640/20x, dichroic Q660LP and emitter HQ 700/75m were used for the Atto 647N/Alexa 647 channel, and exciter D365/10X, dichroic 380 DCLP and emitter D460/50m were used for the Alexa 350 channel. All filters and dichroics were purchased from Chroma Technology. Images were collected with a Hamamatsu Orca 100 CCD camera.

2.10 Imaging analyses

All data were processed and displayed using the custom-written Microscopy Image Analysis Tool (MIATool) software package (www4.utsouthwestern.edu/wardlab) in MATLAB (Mathworks, Natick, MA). For data presented in Chapter 3, the intensities of acquired data were linearly adjusted. Images from two or three color channels were overlaid and annotated. In overlay images, the intensities of the individual color channels were adjusted to similar levels. The final images were exported for presentation in Canvas 9 (ACD Systems, Miami, FL). For intensity analyses of sorting endosomes and lysosomes, regions of interest (ROIs) were segmented manually, and a threshold value

was applied to the ROIs to determine pixels belonging to analyzed compartments. A background intensity value was subtracted from each pixel. The resulting values were added together to obtain the total mRFP (FcRn), Atto 647N (IgG) or GFP (LAMP-1 or Rab7) fluorescence intensities of the analyzed compartments. For photobleaching analyses, a background intensity value was subtracted from each pixel. The average intensities per pixel of the complete image for each frame were multiplied by the maximum pixel numbers of the 'donor' compartments, and the resulting values were plotted over time.

For (LP-)MUM data presented in Chapter 4, the first step of image processing is registration (Appendix A). After registration, the intensities of images from each camera were linearly adjusted to similar levels to properly display the events of interest. In some cases (e.g. relatively long time of imaging), photobleaching was compensated by applying different linear intensity adjustments to different time-contiguous segments of images from a given camera. For intensity analysis, the GFP-APPL1+ endosomes were manually segmented for each frame. A background intensity value was subtracted from each pixel. The resulting values were added together to obtain the total GFP fluorescence intensities of the compartments in each frame. For photobleaching analysis shown in **Figure 4.10**, a 141X141 ROI within the cell was selected and a background intensity value was subtracted from each pixel. The resulting values were added together to obtain the total GFP fluorescence intensities of the ROI in each frame. The total GFP fluorescence intensities of the endosome and ROI were normalized and plotted over time.

For core/annulus intensity analyses of exocytic events shown in **Figure 4.29**, methods analogous to those described previously (Prabhat et al., 2007) were used. This approach was used to determine the change in fluorescence intensity for two concentric ROIs encompassing the exocytic site. The total fluorescence intensity of each ROI was calculated for every frame, and the intensity of the smaller ROI designated the core intensity. The difference between the intensity of the larger and smaller (core) ROI was calculated to yield the annulus intensity.

CHAPTER 3 ANALYSES OF THE LYSOSOMAL DELIVERY PATHWAY THAT MEDIATES DEGRADATION OF FcRn AND ABDEGS

3.1 Introduction

Lysosomes are a primary site of protein degradation in cells. In the current Chapter, microscopy experiments have been conducted to investigate the lysosomal delivery of FcRn on the constitutive degradation pathway. In addition, the delivery of a class of engineered antibodies called Abdegs, that are known to have relatively short *in vivo* half-lives (Vaccaro et al., 2005), to lysosomes has been analyzed. The results in this chapter have been published in *Traffic* (Gan et al., 2009). The temporal aspects and modes of lysosomal delivery of FcRn and Abdegs have been analyzed.

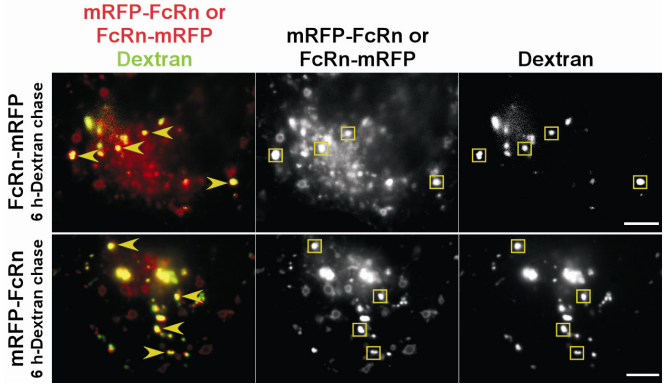

Figure 3.1

mRFP-tagged FcRn can be detected in lysosomes. HMEC-1 cells were co-transfected with mRFP-FcRn and human β_2m or FcRn-mRFP and human β_2m. Cells were pulsed with Alexa 647-labeled dextran for 2 hours and chased for 6 hours. Compartments in the single color data for FcRn and dextran are highlighted with rectangles of the same color as the arrowheads in the overlay data. Scale bars = 5 µm. Yellow arrowheads in the overlay data indicate dextran+ lysosomes with mRFP-tagged FcRn in the intraluminal space. Both N- or C-terminally tagged FcRn can be detected in lysosomes.

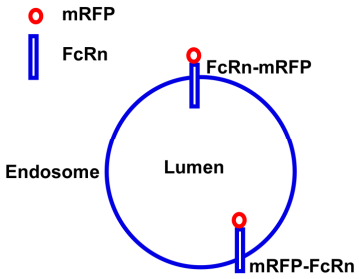

Figure 3.2

FcRn is a type I transmembrane protein. For FcRn-mRFP fusion protein, the fluorescent protein mRFP is appended to the C terminus of FcRn and in the cytosol if FcRn is on the limiting membrane of endosomes. For mRFP-FcRn, mRFP is appended to the N terminus of FcRn and in the intraluminal space of endosomes.

3.2 Distribution of FcRn

HMEC-1 cells were transfected with mRFP tagged FcRn (human) and pulse chased with Alexa 647-labeled dextran to label lysosomes (2 hours pulse, 6-24 hours chase). mRFP fluorescence could be clearly detected in the intraluminal space of the dextran+ lysosomes, in addition to being present on the limiting membrane of abundant early endosomes as described previously (Ober et al., 2004b) (**Figure 3.1**). FcRn is a type I membrane protein, so that C-terminal tagging results in the localization of the fluorescent protein in the cytosol if the receptor is on the limiting membrane of intracellular organelles (**Figure 3.2**). Importantly, the detection of mRFP in the intraluminal space is not due to cleavage of mRFP from FcRn on the limiting lysosomal membrane followed by release into the lumen, since it is observed for both N- and C-terminally tagged FcRn. In cells transfected with C-terminally tagged FcRn, 94% (n=50) of dextran+ lysosomes are mRFP+ and for N-terminally tagged FcRn, 96% (n=55) of dextran+ lysosomes are mRFP+, indicating that the fusion of mRFP to FcRn does not impact the intracellular trafficking pathway of FcRn. However, from the analyses using mRFP tagged FcRn, whether FcRn is also present on the limiting membrane of lysosomes in addition to the intraluminal space could not be determined. Therefore experiments with FcRn tagged at the C-terminus with GFP (FcRn-GFP) were also carried out to investigate this. GFP has very low fluorescence at lysosomal pH (Katayama et al., 2008; Patterson et al., 1997) and is susceptible to proteolysis (Daniels and Amara, 1999; Delamarre et al., 2005; Katayama et al., 2008). It is therefore hypothesized that GFP fluorescence from C-terminally tagged FcRn would not be detectable if FcRn were rapidly internalized into the intraluminal

space following transfer to lysosomes. Although GFP-labeled FcRn could be seen on the limiting membrane of endosomes as described previously (Ober et al., 2004b), GFP is not observed in lysosomes when the fluorophore was linked to either the N- or C-terminus of FcRn (**Figure 3.3**, and data not shown). This suggests that the internalization of FcRn from the limiting membrane into the intraluminal space of lysosomes is relatively rapid, so that the steady state distribution is primarily within the lumen. The lysosomal accumulation of FcRn is most likely due to the constitutive turnover of this receptor.

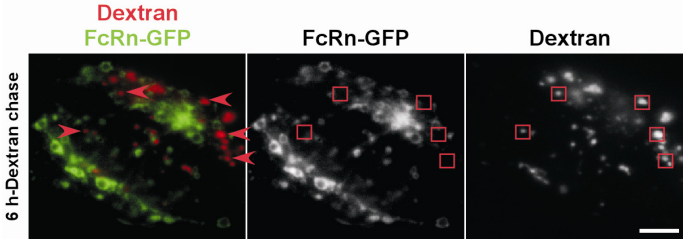

Figure 3.3

FcRn-GFP cannot be detected in lysosomes. HMEC-1 cells were co-transfected with FcRn-GFP and human β_2m. Cells were pulsed with Alexa 647-labeled dextran for 2 hours and chased for 6 hours. Compartments in the single color data for FcRn and dextran are highlighted with rectangles of the same color as the arrowheads in the overlay data. Scale bar = 5 µm. Red arrowheads in the overlay data indicate dextran+ lysosomes without FcRn-GFP in the intraluminal space.

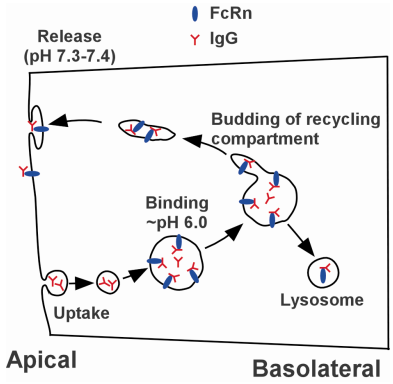

Figure 3.4

MST-HN IgG (Abdeg) serves as a FcRn tracer. MST-HN IgG can bind to FcRn on the plasma membrane of the cell. It also can be taken up through fluid phase pinocytosis and delivered to sorting endosomes. It can bind to FcRn in sorting endosomes because of the acidic environment. Consequently, the FcRn-IgG complex is sorted back to the plasma membrane via the recycling pathway. At the plasma membrane, unlike wild type IgG, MST-HN IgG is not released from FcRn into extracellular environment. MST-HN therefore serves as an intracellular marker for FcRn within the cell.

3.3 Temporal aspects of lysosomal delivery

The constitutive expression of mRFP tagged FcRn in transfected cells precludes an analysis of the temporal aspects of lysosomal delivery of this receptor. A fluorescently labeled Abdeg IgG ('MST-HN') that has been engineered to bind through its Fc region with high affinity to FcRn in the pH range 5-7.4 (Vaccaro et al., 2005) was therefore used to track receptor behavior over time periods that could be regulated by IgG delivery. In addition, to facilitate the use of labeled IgG as a tag for FcRn, a mutated variant of human FcRn (Zhou et al., 2005) that is engineered to have higher affinity for IgG was used throughout these studies. The relatively high affinity of the interaction of this mutated FcRn for binding to MST-HN in the range pH 6.0-7.2 (Kd at pH 6.0 = 1 nM; Kd at pH 7.2 = 4.5 nM, (Prabhat et al., 2007)) reduces the possibility of dissociation of MST-HN from FcRn in endosomes and at the cell surface so that it can be used as a tracer for FcRn on both the recycling and endolysosomal pathways within cells (**Figure 3.4**). By contrast, wild type IgG1 binds with substantially lower affinity to FcRn (mutant) at pH 6.0 and with immeasurably low affinity at near neutral pH (Vaccaro et al., 2005; Zhou et al., 2005) and is therefore unsuitable as a ligand for tracking FcRn.

mRFP-FcRn transfected cells were pulse-chased with Alexa 488-labeled dextran (MW 10,000 Da) to label lysosomes, followed by addition of 5 µg/ml Atto 647N-labeled IgG. Cells were imaged at different times up until 24 hours following IgG addition (**Figure 3.5**). After a pulse time of ~1-3 hours with labeled IgG, the antibody shows extensive colocalization with mRFP-FcRn (**Figure 3.5**; or FcRn-mRFP, data not shown) in

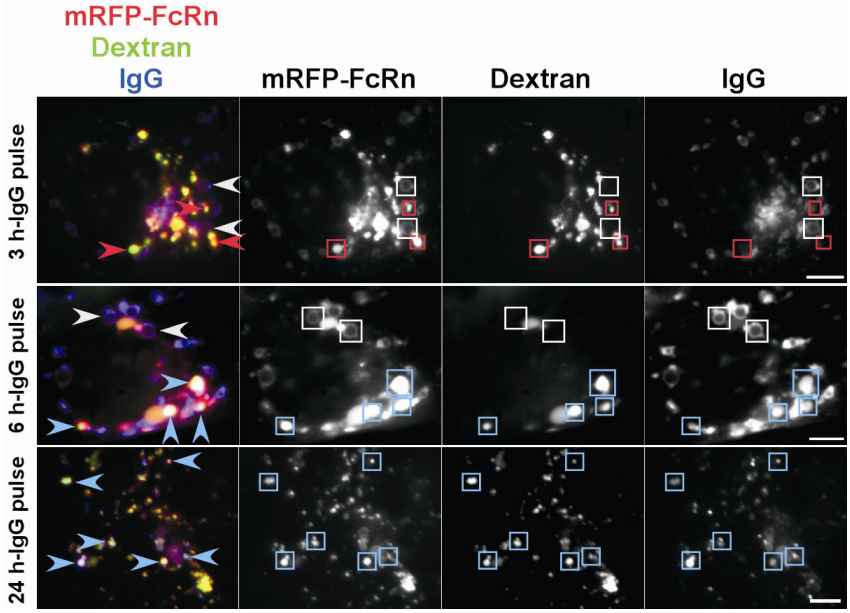

Figure 3.5

Temporal aspects of lysosomal delivery of FcRn. HMEC-1 cells were co-transfected with mRFP-FcRn and human β2m. Cells were pulsed with Alexa 488-labeled dextran for 2 hours and chased for 1 hour. Cells were then incubated with 5 μg/ml Atto 647-labeled IgG for different times as indicated. Compartments in the single color data for FcRn, IgG and dextran are highlighted with rectangles of the same colors as the arrowheads in the overlay data. Scale bars = 5 μm. White arrowheads indicate endosomes with mRFP-FcRn+/IgG+ limiting membrane. Red arrowheads indicate mRFP-FcRn+/dextran+ lysosomes without detectable IgG following 3 hours of IgG incubation. Blue arrowheads indicate mRFP-FcRn+/dextran+/IgG+ lysosomes following 6 or 24 hours of IgG incubation.

endosomal structures or smaller tubulovesicular compartments (all of 50 mRFP-FcRn+ or FcRn-mRFP+ endosomes analyzed are IgG+), consistent with our earlier studies (Vaccaro et al., 2005) with little or no colocalization with lysosomes (2% of 51 dextran+/FcRn+ lysosomes analyzed are IgG+). However, following 4-6 hours of IgG addition, significant amounts of labeled antibody are colocalized with dextran and mRFP in the intraluminal space of lysosomes (**Figure 3.5**; 85% of 46 dextran+/FcRn+ lysosomes analyzed are IgG+), although a substantial proportion of this antibody remains associated with FcRn in endosomes (**Figure 3.5**; all of 62 FcRn+ endosomes analyzed are IgG+). At later times (6-24 hours), the amount of IgG in lysosomes relative to endosomes increases, until about 16-24 hours when the majority is located in lysosomes (**Figure 3.5**; 98% of 50 dextran+/FcRn+ lysosomes analyzed are IgG+). Thus, within several hours of addition, IgG ligand and FcRn can be detected in the intraluminal space of lysosomes and the accumulation continues to increase thereafter. The behavior of the MST-HN mutant contrasts with that of wild type IgGs which, due to their marked pH dependent binding to FcRn, are in general sorted into the recycling/transcytotic pathway and exocytosed (Ober et al., 2004a; Ober et al., 2004b). Since the MST-HN mutant is an effective tag of FcRn, this data establishes the timing of FcRn transfer to lysosomes.

3.4 Modes of FcRn transport from late endosomes to lysosomes

To analyze the details of the dynamic processes that are involved in the transfer of FcRn to lysosomes, HMEC-1 cells were co-transfected with mRFP-FcRn and lysosomal associated membrane protein-1 (LAMP-1)-GFP to demarcate late endosomes (dim for LAMP-1, mannose-6-phosphate receptor (M6PR) positive and dextran negative; data not shown) and lysosomes (bright for LAMP-1, M6PR negative, dextran positive). The use of fluorescently labeled LAMP-1 allows the limiting membrane of the lysosomes to be demarcated. Consistent with the analyses using dextran pulsed cells (**Figure 3.1**), mRFP could be detected in the intraluminal space of LAMP-1+ (bright) lysosomes (**Figure 3.6**).

Figure 3.6 shows the delivery of mRFP-labeled FcRn from a late endosome to a closely apposed lysosome via a tubule that extends from the late endosome (13.5 s), fuses with a lysosome and immediately separates from the 'donor' endosome within a time period of about 3 s. Subsequent to FcRn transfer, a smaller lysosome fuses with the first lysosome in a homotypic fusion event (28.5-30 s). In **Figure 3.7**, a FcRn+ tubule that is longer than that shown in **Figure 3.6** is extended from a late endosome and delivers FcRn to the lysosome. This tubule merges with the lysosome (19.5 s) and disconnects from the lysosome 4.5 s following the merging event. The intensity changes for mRFP fluorescence in both the donor endosome (decrease in intensity) and the acceptor lysosome (increase in intensity) for these two transfer events are shown in **Figure 3.8**. For all intensity plots in this research project, to exclude the possibility that the intensity decreases in donor compartments are due to photobleaching, the average photobleaching

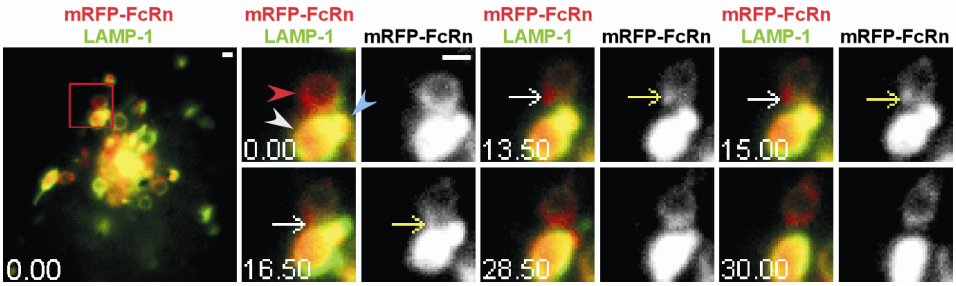

Figure 3.6

Tubule-mediated transfer of FcRn from the limiting membrane of a late endosome to a lysosome. HMEC-1 cells were co-transfected with LAMP-1-GFP, mRFP-FcRn (human) and human β2m. Individual images are presented with the time (in seconds) at which each image was acquired (first image is arbitrarily set to time 0). Images on the left hand side show a complete cell, with the boxed region expanded as cropped images for the 0 second and later images. White arrows in the overlay images show the event of interest that are also indicated in the single color (mRFP-FcRn) data by yellow arrows. Images are individual frames of Movie 3.1. Scale bar = 1 μm. A mRFP-FcRn+ tubule extends from a late endosome (red arrowhead) to a lysosome (white arrowhead) from 13.5–16.5 s. At 16.5 s, the tubule merges with the lysosome and separates from the late endosome. An additional lysosome (blue arrowhead, 0 s) merges with the first lysosome (white arrowhead at 0 s) at 28.5–30 s.

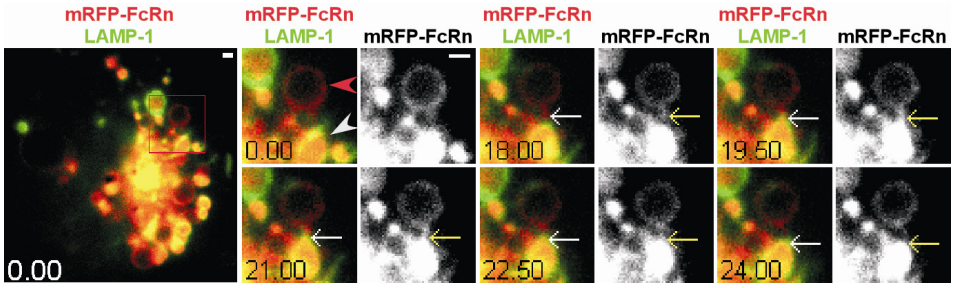

Figure 3.7

Tubule-mediated transfer of FcRn from the limiting membrane of a late endosome to a lysosome. HMEC-1 cells were co-transfected with LAMP-1-GFP, mRFP-FcRn (human) and human β2m. Individual images are presented with the time (in seconds) at which each image was acquired (first image is arbitrarily set to time 0). Images on the left hand side show a complete cell, with the boxed region expanded as cropped images for the 0 second and later images. White arrows in the overlay images show the event of interest that are also indicated in the single color (mRFP-FcRn) data by yellow arrows. Images are individual frames of Movie 3.2. Scale bar = 1 μm. A mRFP-FcRn+ tubule extends from a late endosome (red arrowhead) towards a lysosome (white arrowhead) at 0 s, merges with the lysosome at 19.5 s and breaks away from the recipient lysosome at 24 s.

rates are determined. The average intensity decays are much less than the measured intensity decreases in donor compartments, indicating that intensity decreases in donor compartments are not due to photobleaching (**Figure 3.9**). In both examples of transfer events, the lysosomes already have substantial amounts of mRFP (FcRn) in their vacuole. Taken together with the absence of FcRn-GFP on the limiting membrane of lysosomes (**Figure 3.3**), this suggests that the internalization of FcRn into the intraluminal space is efficient.

Due to the constitutive expression of mRFP in transfected cells, the 'brightness' of mRFP in the majority of recipient lysosomes limited our ability to detect relatively small changes in intensity due to transfer of FcRn (tagged with mRFP) to lysosomes. Therefore, to facilitate the analysis of such intensity changes, the pathways of late endosome to lysosome transfer were further investigated using labeled (Atto 647N) MST-HN IgG (Vaccaro et al., 2005), for which accumulation in lysosomes only started shortly following IgG addition to cultures. In a subset of analyses mouse FcRn instead of human FcRn was also used since, unlike human FcRn, it does not have a cytosolic tail lysine (Ahouse et al., 1993; Story et al., 1994) which could serve as an ubiquitination target (**Figure 3.12**, **Figure 3.14** and **Figure 3.16**). Similar distribution and transport modes were observed for both mouse and human FcRn in HMEC-1 cells in this and other studies, indicating that the trafficking pathway of human FcRn from late endosomes to lysosomes is not ubiquitin dependent.

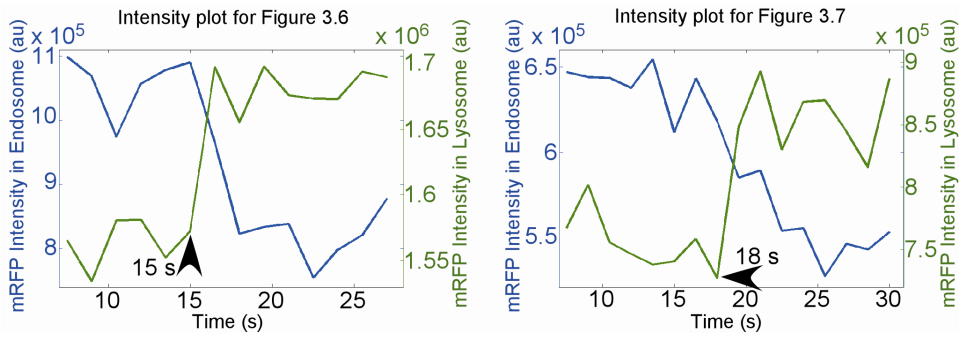

Figure 3.8

Fluorescence intensity plots for mRFP in the interacting compartments in Figure 3.6 and Figure 3.7.

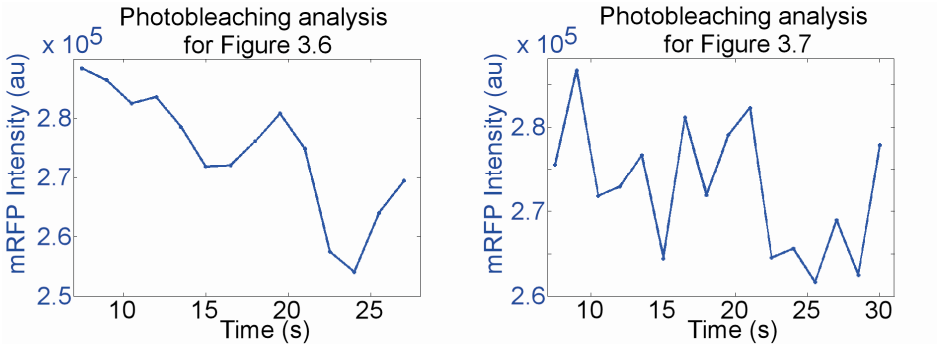

Figure 3.9

mRFP Photobleaching analyses for Figure 3.6 and Figure 3.7 The average intensities per pixel of each frame were multiplied by the maximum pixel numbers of the 'donor' compartments, and the resulting values were plotted over time. The mean mRFP intensity decays (≈ 40000 and 20000 units, respectively) during the transfer events showed in **Figure 3.6** and **Figure 3.7** are less than the measured mRFP intensity decreases (≈ 300000 and 100000 units, respectively) of the 'donor' compartments showed in **Figure 3.8**. These photobleaching analyses hence indicate that the intensity decreases shown in **Figure 3.8** are not due to photobleaching.

In **Figure 3.10**, a FcRn+/IgG+ late endosome interacts with a dextran+/IgG+ lysosome over a time period of 67.5 s (until the data collection is stopped). During a three second period (43.5-46.5 s), detectable levels of IgG transfer can be observed. The intensity changes for Atto 647N fluorescence in both the donor endosome (decrease in intensity) and the acceptor lysosome (increase in intensity) for this transfer event are presented in **Figure 3.11**. By contrast with **Figure 3.10**, **Figure 3.12** shows IgG transfer between an adjacent late endosome and lysosome via a process that does not involve a detectable tubule and resembles kiss-and-linger events (Bright et al., 2005; Gandhi and Stevens, 2003; Ryan, 2003; Storrie and Desjardins, 1996). In the example shown, detectable levels of IgG transfer occur over a time period of ~460 s (**Figure 3.12**). An analysis of the intensity changes for Atto 647N fluorescence in the two compartments involved in this transfer event is presented in **Figure 3.13**. The intensity changes over time provide support for the transfer of material from the late endosome to lysosome. In another example of IgG transfer to lysosomes, we observed two tubules extending simultaneously from an FcRn+/IgG+ endosome (**Figure 3.14**): one tubule interacts with a lysosome for 25.5 s and transfers detectable levels of IgG over a shorter period of 3 s (30-33 s). A second tubule appears to contact an endosome for about 46.5 s. FcRn(-GFP) and IgG could be detected in both tubules (**Figure 3.14**), and instead of separating from the donor endosome, both tubules retract following interaction with their partner organelles. The intensity changes for Atto 647N fluorescence in the donor and acceptor compartments in **Figure 3.14** are consistent with the transfer of IgG (**Figure 3.15**). Subsequently, FcRn and IgG leave the donor endosome in a tubulovesicular transport container (**Figure 3.16**),

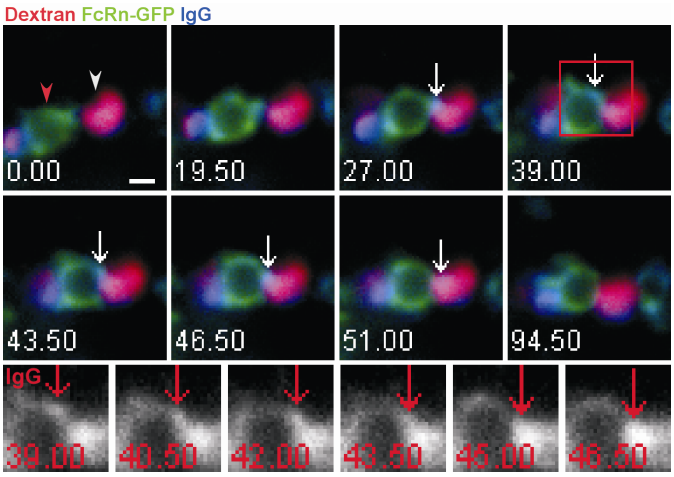

Figure 3.10

Tubule-mediated transfer of IgG from an endosome to a lysosome. HMEC-1 cells were co-transfected with FcRn-GFP (human) and human β2m (A). Cells were pulsed with Alexa 555-labeled dextran for 2 hours, chased for 1 hour and incubated with 5 μg/ml Atto 647N-labeled IgG for 7 hours. Individual images are presented with the time (in seconds) at which each image was acquired (first image is arbitrarily set to time 0). Images shown are individual frames of Movie 3.3. Scale bar = 1 μm. A dextran+/IgG+ lysosome (white arrowhead) interacts with an endosome (red arrowhead, FcRn+/IgG+ limiting membrane) for an extended time period (27-94.50 s, when data collection was stopped). Detectable levels of IgG are transferred from the endosome to the lysosome (43.5-46.5 s). The event of interest is indicated by white arrows. The boxed region marked at 39 s is subsequently presented as cropped, single color (IgG) images in the lower row, with red arrows indicating the same event.

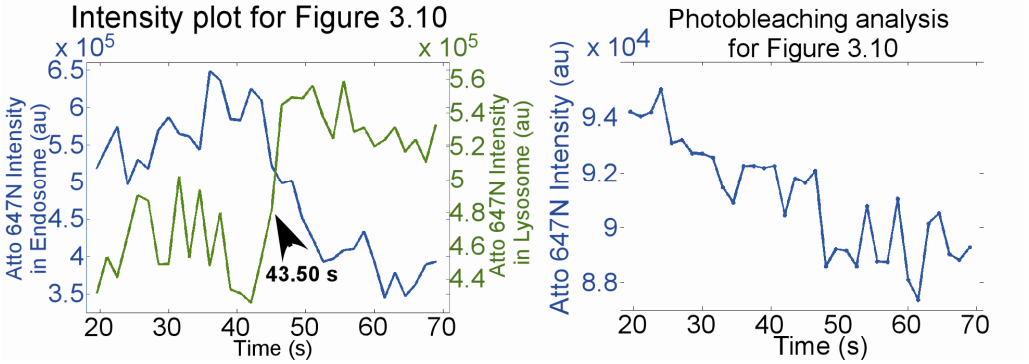

Figure 3.11

Photobleaching analysis and fluorescence intensity plots for Figure 3.10. The mean Atto 647N intensity decay (≈ 6,000 units) during the transfer event shown in **Figure 3.10** is significantly less than the measured Atto 647N intensity decrease (≈ 150,000 units) of the 'donor' compartment. The photobleaching analysis indicates that the intensity decrease is not only due to photobleaching.

suggesting that late endosomes can both transfer FcRn and/or ligand to lysosomes and generate recycling compartments.

Collectively, these analyses indicate that the majority (71%, n=24 from 24 different cells) of transfer events for FcRn involve tubular extensions from late endosomes to lysosomes, with the remainder resembling kiss-and-linger (five events) or rarely, full fusion to form hybrid compartments (two events; data not shown). However, the frequency of kiss-and-linger might be an underestimate, since we frequently observed late endosomes and lysosomes in close proximity without detectable transfer of material. Of the 17 events for which tubular transfer could be observed, 88% involved long lived contacts between late endosomes and lysosomes (> 3 s). All five transfer events that did not occur via visible tubules involved contact between participating organelles that lasted for prolonged time periods (> 200 s).

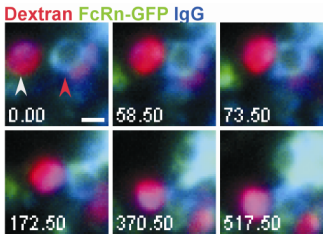

Figure 3.12

A lysosome and endosome interaction without tubules involved. HMEC-1 cells were co-transfected with FcRn-GFP (mouse) and mouse β2m. Cells were pulsed with Alexa 555-labeled dextran for 2 hours, chased for 1 hour and incubated with 5 μg/ml Atto 647N-labeled IgG for 5 hours. Individual images are presented with the time (in seconds) at which each image was acquired (first image is arbitrarily set to time 0). Images shown are individual frames of Movie 3.4. Scale bar = 1 μm. A FcRn+/IgG+ late endosome (red arrowhead) interacts with a dextran+/IgG+ lysosome (white arrowhead) for a prolonged period (58.5-517.50 s, when data collection was stopped) to transfer IgG without detectable tubular extension(s).

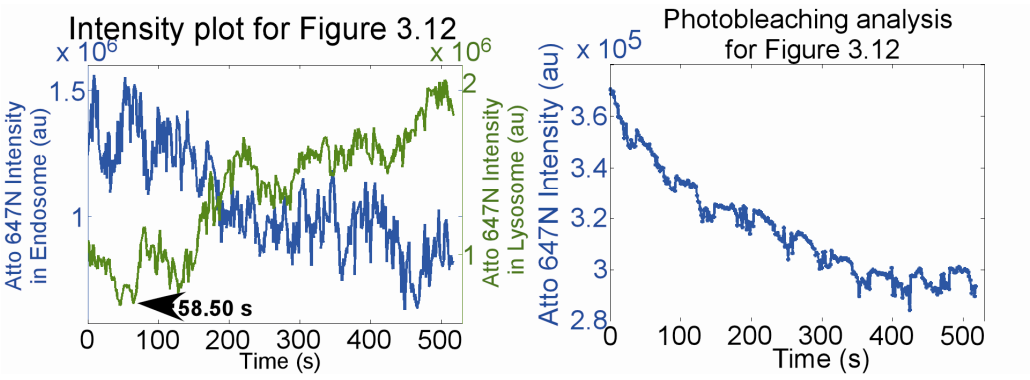

Figure 3.13

Photobleaching analysis and fluorescence intensity plots for Figure 3.12. The mean Atto 647N intensity decay (≈ 70,000 units) during the transfer event shown in **Figure 3.12** is significantly less than the measured Atto 647N intensity decrease (≈ 700,000 units) of the 'donor' compartment. The photobleaching analysis indicates that the intensity decrease is not only due to photobleaching.

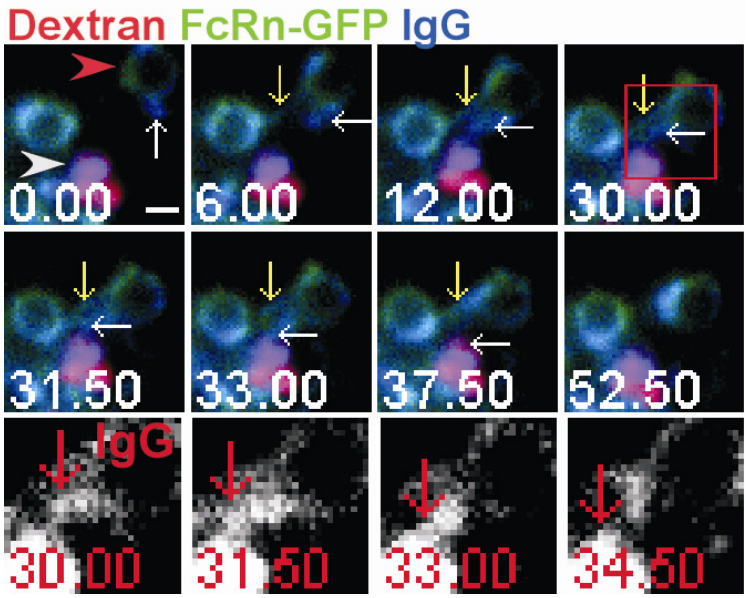

Figure 3.14

Tubule-mediated transfer of IgG from an endosome to a lysosome. HMEC-1 cells were co-transfected with FcRn-GFP (mouse) and mouse β2m. Cells were pulsed with Alexa 555-labeled dextran for 2 hours, chased for 1 hour and incubated with 5 μg/ml Atto 647N-labeled IgG for 4 hours. Individual images are presented with the time (in seconds) at which each image was acquired (first image is arbitrarily set to time 0). Images shown are individual frames of Movie 3.5. Scale bar = 1 μm. A FcRn+/IgG+ tubule, indicated by white arrows, extends from a 'donor' endosome (red arrowhead) towards a dextran+/IgG+ lysosome (white arrowhead), and contacts this lysosome for 25.5 s (12-37.5 s) before retracting. Detectable levels of IgG are transferred from this tubule to the lysosome (30-33 s). A second tubule, indicated by yellow arrows, extends from the 'donor' endosome and interacts with another endosome (6-52.5 s) prior to retracting. The boxed region at 30 s is presented as cropped, single color (IgG) images in the lower row, with red arrows indicating IgG transfer from the 'donor' endosome to the lysosome.

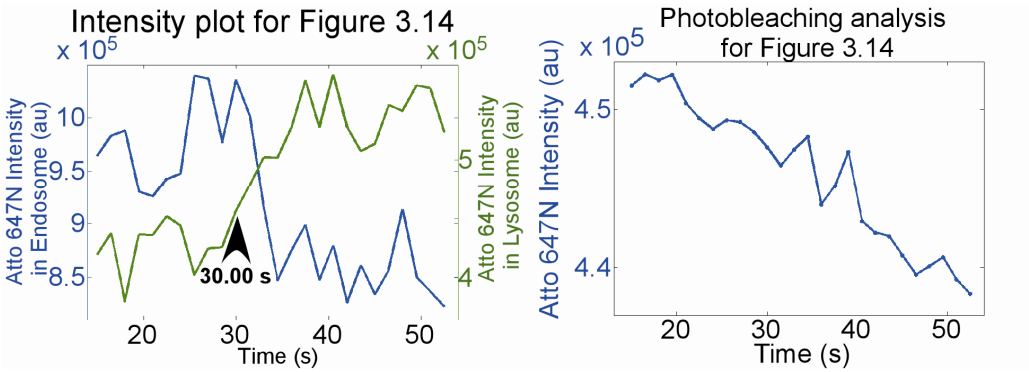

Figure 3.15

Photobleaching analysis and fluorescence intensity plots for Figure 3.14. The mean Atto 647N intensity decay (≈ 12,000 units) during the transfer event shown in **Figure 3.14** is significantly less than the measured Atto 647N intensity decrease (≈ 150,000 units) of the 'donor' compartment. The photobleaching analysis indicates that the intensity decrease is not only due to photobleaching.

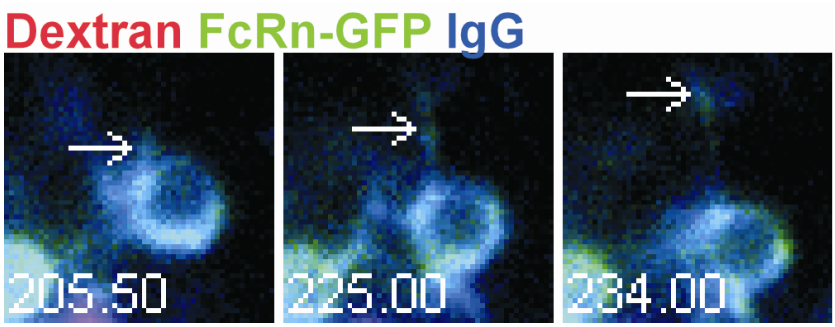

Figure 3.16

A recycling transport carrier is formed from the endosome shown in Figure 3.14. Later frames corresponding to **Figure 3.14** show that an FcRn+/IgG+ tubule (white arrows) extends (205.5 s) and leaves (234 s) the 'donor' endosome after the same endosome has interacted with a lysosome (**Figure 3.14**). Individual images are presented with the time (in seconds) at which each image was acquired (first image is arbitrarily set to time 0).

3.5 Bifurcation of LAMP-1 and FcRn trafficking pathways at the endo-lysosomal transition

LAMP-1 is colocalized with FcRn on the limiting membrane of late endosomes but, in contrast to FcRn, can also be clearly seen on this membrane of lysosomes (**Figure 3.6**). For comparative purposes, the behavior of LAMP-1 during late endosomal-lysosomal fusion events was therefore analyzed. These studies indicated that late endosomes (weakly LAMP-1+, FcRn+ and M6PR+) can interact with lysosomes (strongly LAMP-1+, M6PR-) to transfer LAMP-1 through processes that involve tubular extensions from the late endosomes. In **Figure 3.17**, a tubule can be seen extending from the lower part of the late endosomes at 0 s. This tubule then appears to form a vesicular compartment that moves around the perimeter of the late endosome prior to extending as a tubule at 39 s to fuse with the lysosome to transfer LAMP-1 (40.5-43.5 s). This transfer event is followed by separation from the late endosome. The intensity changes for GFP fluorescence in both the donor endosome (decrease in intensity) and the acceptor lysosome (increase in intensity) for this transfer event are presented in **Figure 3.18**. Due to the limited resolution of fluorescence microscopy, it is impossible to conclusively rule out an alternative, less likely interpretation that this moving structure is a separated, small compartment that contacts and moves around the perimeter of the late endosome and subsequently bridges the late endosome and the lysosome.

LAMP-1 can also migrate from a lysosome to a (late) endosome (**Figure 3.19**). In the example shown, transfers occur in stepwise fashion via two distinct tubules (12-18 and

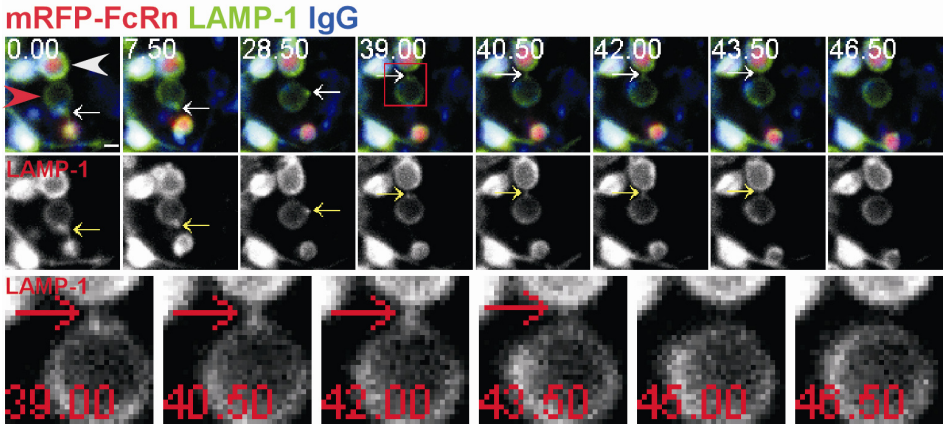

Figure 3.17

A transfer event of LAMP-1 involving a tubule from a late endosome to a lysosome. HMEC-1 cells were co-transfected with LAMP-1-GFP, mRFP-FcRn (human), and human β2m. Cells were incubated with Atto 647N-labeled IgG for 4.5 hours. Individual images are presented with the time (in seconds) at which each image was acquired (first image is arbitrarily set to time 0). The event of interest is indicated by white arrows. The boxed region at 39 seconds are presented as cropped, single color (LAMP-1) images in the lower row(s), with red arrows indicating the same events. Images shown are individual frames of Movie 3.6. Scale bar = 1 μm. A tubule (white arrows) extends (0 s) from the lower part of a late endosome (red arrowhead), forms a vesicular compartment on the limiting membrane (7.5 s), moves around the perimeter of the late endosome, extends a tubule (39 s) and contacts (40.5 s) the limiting membrane of a lysosome (LAMP-1+ limiting membrane; mRFP-FcRn+/IgG+ intraluminal space; white arrowhead), transfers LAMP-1 (40.5-43.5 s) and separates from the late endosome at 43.5 s. The LAMP-1 single color data is presented in the middle row, with the yellow arrows indicating the same tubulovesicular compartment.

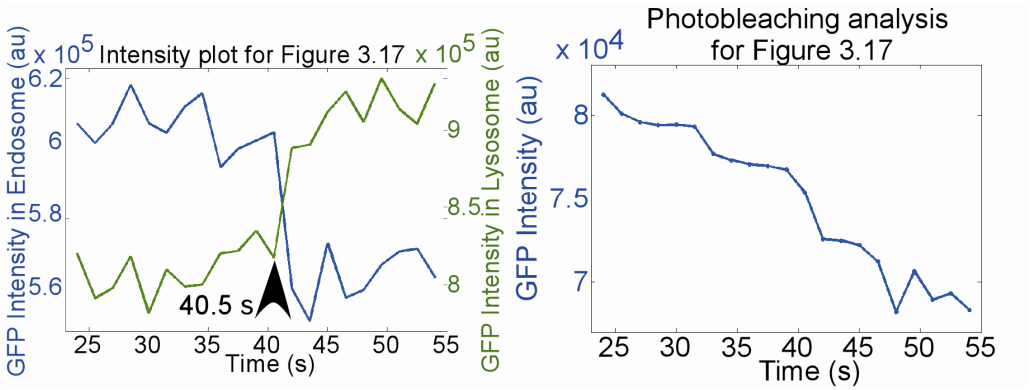

Figure 3.18

Photobleaching analysis and fluorescence intensity plot for Figure 3.17. The mean GFP intensity decay (≈ 12,000 units) during the transfer event shown in **Figure 3.17** is significantly less than the measured GFP intensity decrease (≈ 50,000 units) of the 'donor' compartment. The photobleaching analysis indicates that the intensity decrease is not only due to photobleaching.

24-25.5 s). Each of these tubules extends, merges with the limiting membrane of the recipient late endosome and separates from the donor lysosome prior to the delivery of the next tubule. Subsequently, LAMP-1 appears to diffuse into the limiting membrane of the late endosome, although other interpretations are possible such as that this LAMP-1+ tubulovesicular compartment moves rapidly out of the focal plane. The intensity changes for GFP fluorescence in the donor and acceptor compartments are shown in **Figure 3.20**. This demonstrates that bidirectional movement between the limiting membranes of late endosomes and lysosomes can occur. In all LAMP-1 transfer events (n= 6 from 4 different cells), tubular extensions were observed but neither FcRn nor IgG transfer was detected. Taken together with the distinct distribution of LAMP-1 and FcRn in lysosomes, this indicates that the transfer and internalization of FcRn into the interior of these organelles is a selective process.

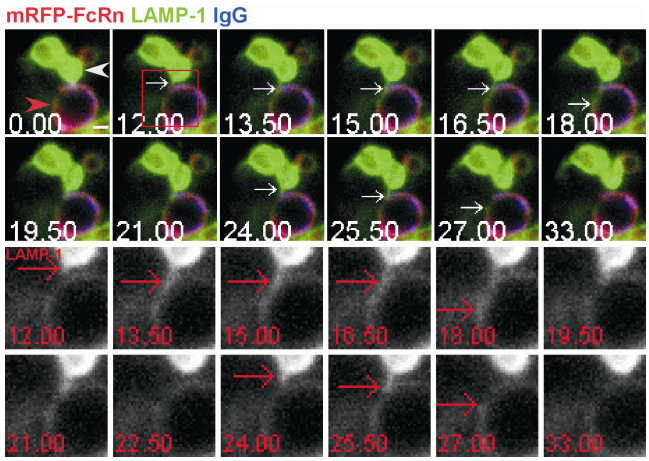

Figure 3.19

Two transfer events of LAMP-1 involving two tubules from a lysosome to a late endosome. HMEC-1 cells were co-transfected with LAMP-1-GFP, mRFP-FcRn (human), and human β2m. Cells were incubated with Atto 647N-labeled IgG for 3 hours. Individual images are presented with the time (in seconds) at which each image was acquired (first image is arbitrarily set to time 0). Events of interest are indicated by white arrows. The boxed region at 12 seconds are presented as cropped, single color (LAMP-1) images in the lower row(s), with red arrows indicating the same events. Images shown are individual frames of Movie 3.7. Scale bar = 1 μm. Two different tubules extend sequentially (starting at 12 s) from a lysosome (white arrowhead) to a late endosome (red arrowhead) and transfer LAMP-1 over two time windows (12-18 and 24-25.5 s), as indicated by white arrows. Subsequently, the LAMP-1 appears to diffuse into the limiting membrane of the late endosome. No transfer of mRFP-FcRn could be detected.

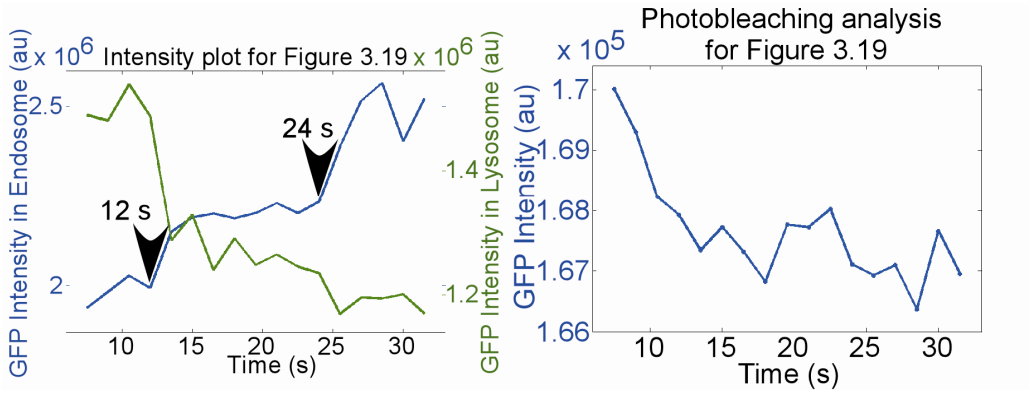

Figure 3.20

Photobleaching analysis and fluorescence intensity plots for Figure 3.19. The mean GFP intensity decay (≈ 4,000 units) during the transfer events shown in **Figure 3.19** is significantly less than the measured GFP intensity decrease (≈ 500,000 units) of the 'donor' compartment. The photobleaching analysis indicates that the intensity decrease is not only due to photobleaching.

3.6 Persistence of Rab5 on fusion-competent, late endosomes

Recent studies have shown that as early endosomes mature to form late endosomes, the Rab GTPase, Rab5, is gradually replaced by Rab7 (Rink et al., 2005). The observation that endosomal-lysosomal transfer events invariably involve FcRn+ endosomes, from which FcRn can still recycle (**Figure 3.14**, **Figure 3.16**, and data not shown), prompted me to characterize these compartments further. The Rab associations with endosomal compartments as they mature were therefore analyzed, with the overall aim of characterizing the endosomes that are 'competent' to transfer their contents to lysosomes.

Cotransfection of Rab5-fluorescent protein (FP) with FcRn-FP constructs demonstrated that Rab5, consistent with its known function in earlier studies (Christoforidis et al., 1999; Simonsen et al., 1998), can be detected on FcRn+ endosomes. Rab5+/FcRn+ compartments can transfer FcRn to lysosomes in tubule-mediated processes such as that shown in **Figure 3.21**. The tubule extends, contacts, and fuses with the lysosome and separates from the late endosome over a period of 12 s, with detectable transfer of mRFP-FcRn occurring over a period of 3 s (12-15 s) (**Figure 3.21**; The intensity changes for mRFP fluorescence in the interacting compartments and the photobleaching analysis for mRFP are shown in **Figure 3.22**). Significantly, transfer of FcRn to lysosomes occurred without detectable transfer of Rab5 (**Figure 3.21**). To exclude the possibility that Rab5 overexpression might result in mistargeting to late endosomes, Rab5 distribution in untransfected cells was analyzed using anti-Rab5 and anti-LAMP-1/anti-EEA1

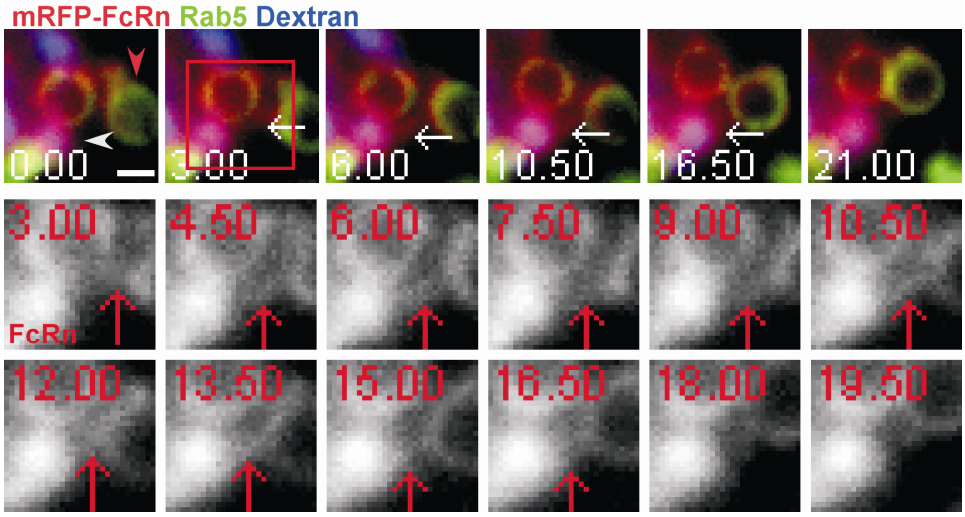

Figure 3.21

Rab5 is associated with a late endosome interacting with a lysosome. HMEC-1 cells were co-transfected with GFP-Rab5, mRFP-FcRn (human) and human β2m. Cells were pulsed with Alexa 647-labeled dextran for 2 hours and chased for 2 hours. Individual images are presented with the time (in seconds) at which each image was acquired (first image is arbitrarily set to time 0). Images shown are individual frames of Movie 3.8. Scale bar = 1 μm. A FcRn+/Rab5- tubule, as indicated by white arrows, extends (3 s) from an endosome (mRFP-FcRn+/Rab5+ limiting membrane; red arrowhead), contacts a lysosome (mRFP-FcRn+/dextran+ intraluminal space; white arrowhead) between 4.5 and 6 seconds and transfers mRFP-FcRn over a period of 3 s (12-15 s). The boxed region at 3 seconds is subsequently presented as cropped, single color (mRFP-FcRn) images in the lower two rows.

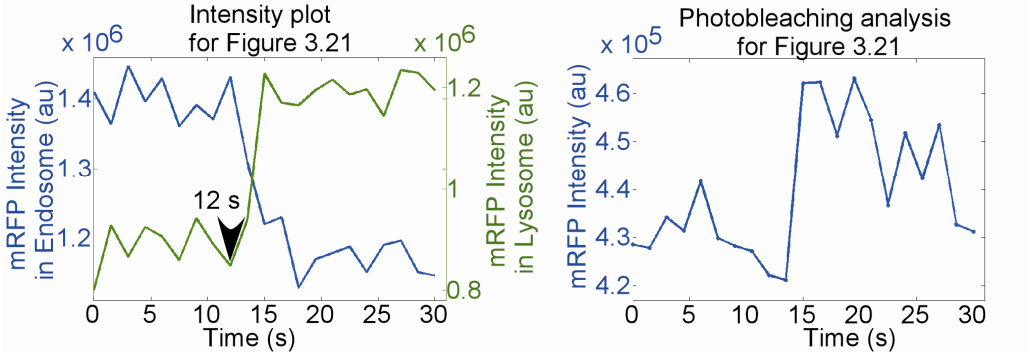

Figure 3.22

Photobleaching analysis and fluorescence intensity plots for Figure 3.21. The mean mRFP decay (≈ 0 unit) during the transfer event shown in **Figure 3.21** is significantly less than the measured mRFP intensity decrease (≈ 250,000 units) of the 'donor' endosome, indicating that the intensity decrease is not due to photobleaching.

antibodies. Rab5 was consistently observed associated with LAMP-1+ late endosomes but not LAMP-1+ lysosomes within cells (**Figure 3.23**; 58% (n=88) of Rab5+ compartments are LAMP-1+), indicating that Rab5 is not solely restricted to association with early endosomes. These late endosomes can be distinguished from lysosomes by the lower levels of LAMP-1 (**Figure 3.17**, and data not shown). In these studies, 96% of 54 late endosomes analyzed with lower LAMP-1 level are Rab5+, whereas 95% of 57 lysosomes analyzed with brighter LAMP-1 are Rab5-. The accumulation of Rab5 into domains or clusters on these compartments was frequently observed (**Figure 3.23**). This is reminiscent of the accumulation of Rab GTPases into discrete domains that precede the formation of tubulovesicular transport containers on endosomes (de Renzis et al., 2002; Sonnichsen et al., 2000; Ward et al., 2005). As expected from earlier studies (Simonsen et al., 1998), the colocalization between Rab5 and EEA1 is also extensive (**Figure 3.23**; 100% of 52 EEA1+ endosomes analyzed are Rab5+). Complete loss of Rab5 from (late) endosomes is therefore not a prerequisite for the transfer of FcRn from late endosomes to lysosomes.

Whether fusion-competent endosomes were Rab7+, and also whether transfer of Rab7 to lysosomes could be detected were also investigated. HMEC-1 cells were therefore cotransfected with GFP-Rab7 and mRFP-FcRn. **Figure 3.24** shows that Rab7 is present on both late endosomes and lysosomes, consistent with earlier observations (Bucci et al., 2000; Soldati et al., 1995). **Figure 3.25** shows the transfer of Rab7 to lysosomes. A Rab7+ tubule extends from a late endosome at 27 s, contacts a FcRn-mRFP+/dextran+

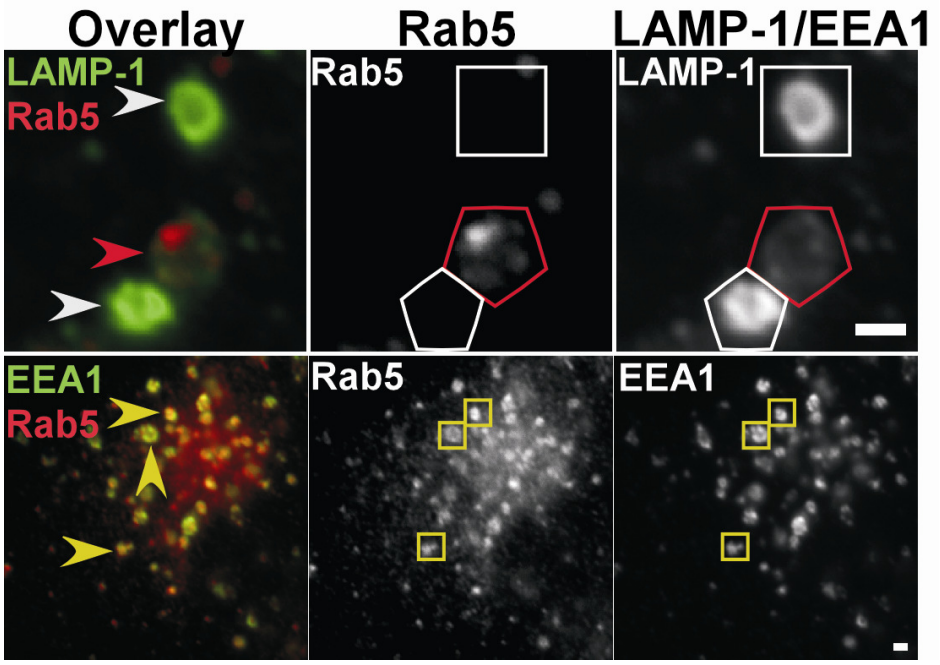

Figure 3.23

Association of Rab5 with late endosomes. HMEC-1 cells were fixed, permeabilized and stained with anti-EEA1 or LAMP-1 and anti-Rab5 antibodies. Compartments in the single color data for Rab5, EEA1 and LAMP-1 are highlighted with polygons or squares of the same colors as the arrowheads. The red arrowhead in the upper left panel indicates a LAMP-1+/Rab5+ late endosome. The accumulation of Rab5 into discrete domains or clusters on the late endosome can be observed in the Rab5 single color and overlay data. White arrowheads in the upper left panel indicate lysosomes with higher LAMP-1 levels than the late endosome. There are no detectable levels of Rab5 in the lysosomes. Yellow arrowheads in the lower left panel indicate Rab5+/EEA1+ compartments. Scale bars = 1 μm.

lysosome at 39 s and transfers Rab7 over the following 3 s. The intensity changes for GFP fluorescence in the interacting compartments and the photobleaching analysis for GFP are shown in **Figure 3.26**, respectively. Cotransfection of mRFP-Rab5 and GFP-Rab7 constructs demonstrated that Rab5+/Rab7+ endosomes can interact with lysosomes over extended periods of time (~40 s) (**Figure 3.27**). A small Rab5+ compartment, that is most likely an endosome, is also associated with this lysosome. In all cases where endosomal-lysosomal interactions were observed (n= 22 from 11 different cells), Rab7 was detectable on the endosomal compartment (**Figure 3.27**, data not shown). These data indicate that acquisition of Rab7 but not complete loss of Rab5 is necessary for late endosome-lysosome interactions. The accumulation of these Rab proteins into domains provides a mechanism whereby the late endosome can be compartmentalized into regions that have distinct intracellular fates.

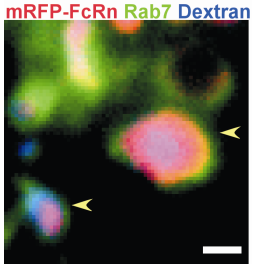

Figure 3.24

Rab7 is associated with a lysosome. HMEC-1 cells were co-transfected with GFP-Rab7, mRFP-FcRn (human) and human β2m. Cells were pulsed with Alexa 647-labeled dextran for 2 hours and chased for 5 hours. Scale bar = 1 μm. Yellow arrowheads indicate mRFP-FcRn+/dextran+ lysosomes with Rab7 on the limiting membrane.

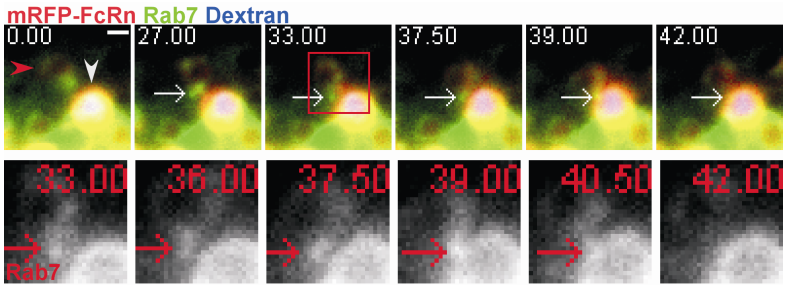

Figure 3.25

Rab7 is associated with a late endosome interacting with a lysosome. HMEC-1 cells were co-transfected with GFP-Rab7, mRFP-FcRn (human) and human β2m. Cells were pulsed with Alexa 647-labeled dextran for 2 hours and chased for 4 hours. Individual images are presented with the time (in seconds) at which each image was acquired (first image is arbitrarily set to time 0). Images are individual frames of Movie 3.9. Scale bar = 1 μm. A Rab7+ tubule, indicated by white arrows, extends (27 s) from a late endosome (mRFP-FcRn+/Rab7+ limiting membrane; red arrowhead), contacts (39 s) a lysosome (mRFP-FcRn+/dextran+ intraluminal space; white arrowhead) and transfers Rab7 over a 3 second period (39-42 s). The boxed region at 33 seconds is presented as cropped, single color (Rab7) images in the lower row.

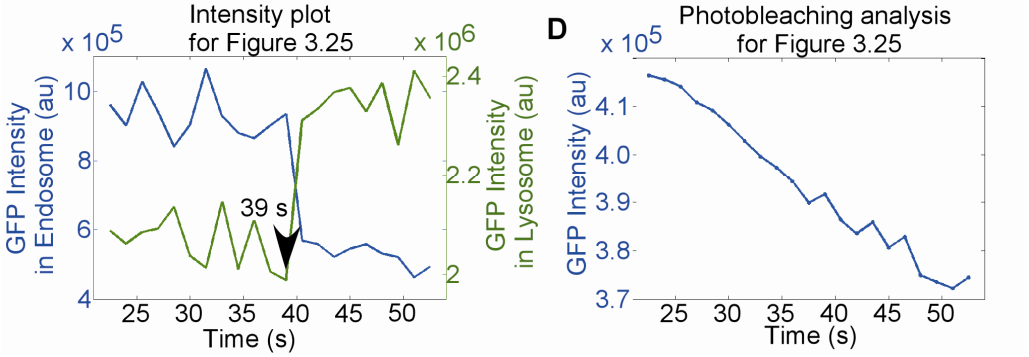

Figure 3.26

The fluorescence intensity plots and the photobleaching analysis for Figure 3.25. The mean GFP decay (≈ 50,000 units) during the transfer event shown in **Figure 3.25** is significantly less than the measured GFP intensity decrease (≈ 400,000 units) of the 'donor' endosome, indicating that the intensity decrease is not only due to photobleaching.

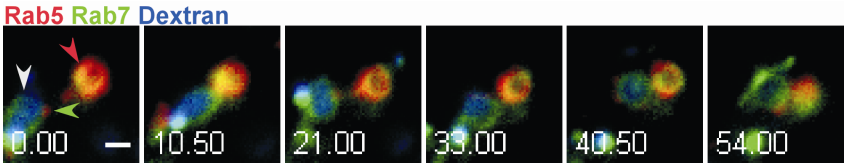

Figure 3.27

Rab5 and Rab7 are associated with a late endosome interacting with a lysosome. HMEC-1 cells were co-transfected with mRFP-Rab5 and GFP-Rab7. Cells were pulsed with Alexa 647-labeled dextran for 2 hours and chased for 6 hours. Individual images presented with the time (in seconds) at which each image was acquired (first image is arbitrarily set to time 0). Scale bar = 1 μm. A lysosome (Rab7+ limiting membrane and dextran+ intraluminal space; white arrowhead) interacts with a Rab5+/Rab7+ endosome (red arrowhead) from 10.5 s onwards. The green arrowhead indicates a small Rab5+ endosome interacting with the lysosome.

CHAPTER 4 IDENTIFYING ITINERARIES TAKEN BY TRANSPORT CARRIERS IN THE RECYCLING PATHWAY OF FcRn USING LP-MUM

4.1 Introduction

An outstanding issue in cell biology is the lack of understanding of the contribution of tubulovesicular TCs to intracellular trafficking pathways within 3D cellular environments. This is primarily due to the challenges associated with the use of microscopy techniques to track these highly motile, small compartments. Here we have used MUM, combined with localized photoactivation ('LP-MUM'), to overcome these limitations. This has resulted in several novel observations for the behavior of TCs on the recycling pathway. The experimental results are described in this Chapter. A detailed description of the set up and validation of the LP-MUM microscopy configuration is presented in Appendix A. The results described in this Chapter have been submitted for publication.

4.2 Multifocal plane imaging enables the tracking of TCs

FcRn is present on the limiting membrane of EEA1+ early/sorting endosomes of 1-2 μm in diameter, providing an identifier for these compartments (Gan et al., 2009; Ober et al., 2004b) (**Figure 4.1**). Following endocytic uptake into cells, FcRn+ TCs fuse with these sorting endosomes (Ram et al., 2008). FcRn is subsequently sorted from the

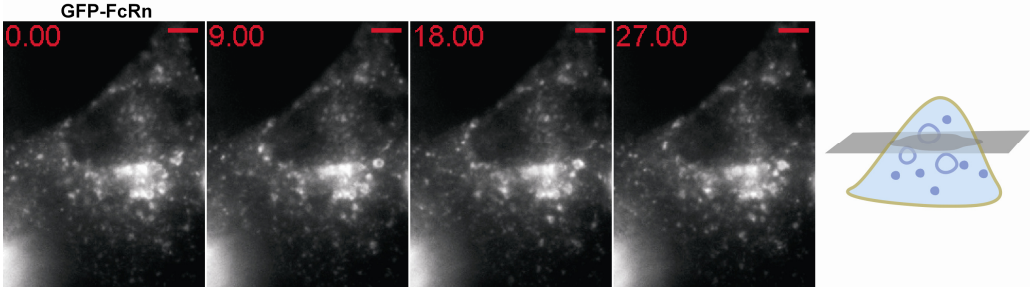

Figure 4.1

FcRn can be seen in sorting endosomes and TCs in transfected HMEC-1 cells. HMEC-1 cells were co-transfected with GFP-FcRn/human β_2m. Individual images are presented with the time (in seconds) at which each image was acquired (first image is arbitrarily set to time 0). Images are individual frames of Movie 4.1. Scale bars = 5 µm. FcRn can be seen in 1-2 µm ring-like endosomes and tubulovesicular TCs. Schematic representation is shown on the right column.

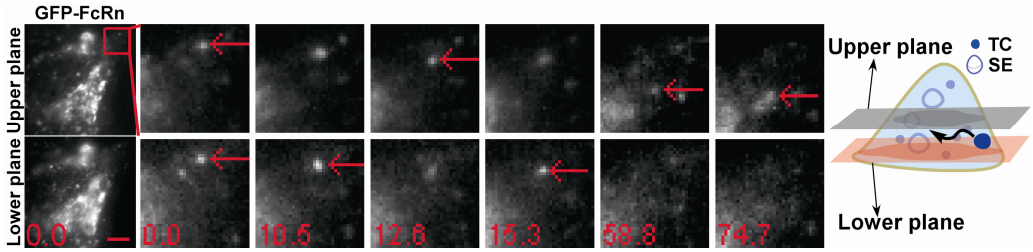

Figure 4.2

TC can be tracked with MUM. HMEC-1 cells were co-transfected with GFP-FcRn/human β_2m. Individual images are presented with the time (in seconds) at which each image was acquired (first image is arbitrarily set to time 0). Red arrows show the event of interest. Scale bar = 5 µm. The most left column shows the MUM data for a complete cell, with the boxed region expanded as cropped images for the 0 second and later images. A FcRn+ TC moves between the two focal planes. Schematic representation is shown on the right column.

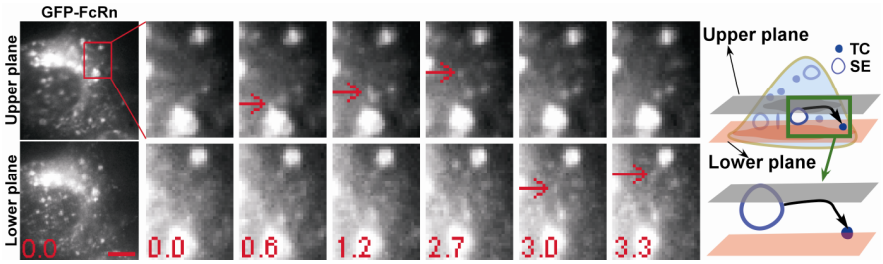

Figure 4.3

A TC left a sorting endosome can be tracked with MUM. HMEC-1 cells were co-transfected with GFP-FcRn/human β_2m. Individual images are presented with the time (in seconds) at which each image was acquired (first image is arbitrarily set to time 0). Red arrows show the event of interest. Scale bar = 5 μm. The most left column shows the MUM data for a complete cell, with the boxed region expanded as cropped images for the 0 second and later images. A FcRn+ TC leaves a sorting endosome in the upper plane at 1.2 s and moves to the lower plane at 3 s. Schematic representation is shown on the right column.

endosomes in tubulovesicular TCs that bud off from the limiting membrane (Ward et al., 2005). In Movie 4.1, the movement of large numbers of highly motile, small TCs that sometimes fuse with these sorting endosomes can be seen. The TCs frequently move in and out of the focal plane and, combined with their high density, this precludes unambiguous identification using single plane imaging. The use of MUM (Prabhat et al., 2007; Prabhat et al., 2004) can overcome these problems (**Figure 4.2**, **Figure 4.3**). In **Figure 4.2**, a TC that moves between the two focal planes can be tracked for > 1 minute. In **Figure 4.3**, a TC leaves a sorting endosome and moves from the upper to the lower focal plane (2.7-3.0 s). This Chapter is directed towards using MUM and in some cases, localized photoactivation, to characterize TCs on the endocytic recycling pathway.

The effectors analyzed in this Chapter include Rab4, Rab11 and SNX4. It was important to confirm that transfection does not affect the recycling pathway. Therefore, HMEC-1 cells were co-transfected with GFP-Rab4/mCherry-SNX4 or GFP-Rab11/mCherry-SNX4, and transferrin recycling rates were assessed using flow cytometry. **Figure 4.4** and **Figure 4.5** show that for cells co-expressing Rab proteins/SNX4 in the range used for imaging in this research project, no significant differences were observed between transfected and untransfected cells in transferrin recycling rates.

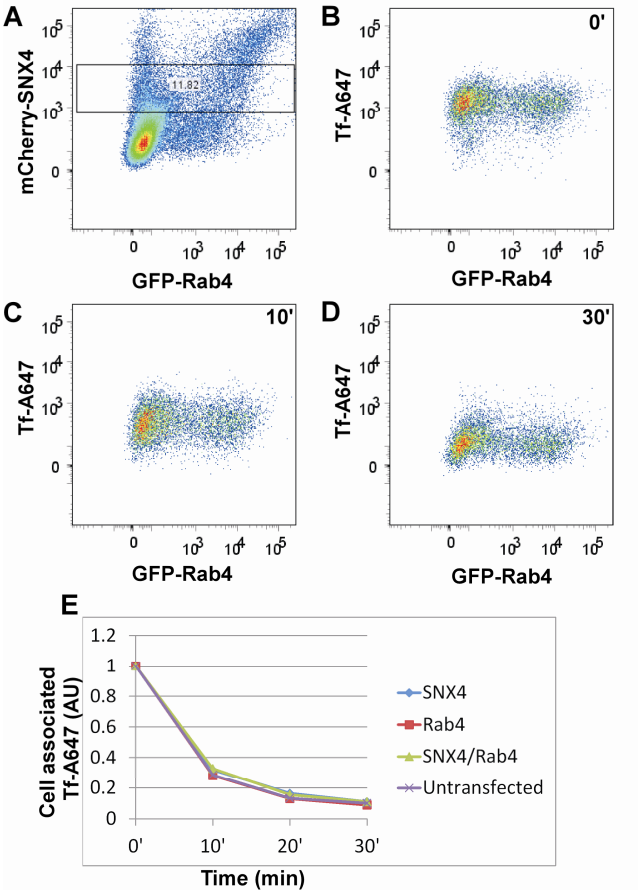

Figure 4.4

Transferrin recycling in GFP-Rab4/mCherry-SNX4 co-transfected HMEC-1 cells. HMEC-1 cells were co-transfected with GFP-Rab4 and mCherry-SNX4. Transfected cells were pulsed with 10 µg/mL Alexa 647-labeled transferrin for 30 min and then harvested by trypsinization (0' chase) or chased in medium containing 250 µg/mL holotransferrin for 10', 20' or 30' before harvesting. Cell associated transferrin levels were quantitated by flow cytometry. A, cells expressing mCherry-SNX4 at the levels used for imaging were gated. B, C, and D, the GFP-Rab4 and cell associated transferrin levels after 0' (B), 10' (C) or 30' (D) chase for the gated subpopulation that expresses mCherry-SNX4 shown in panel A. E, transferrin recycling kinetics for cell subpopulations that express mCherry-SNX4, GFP-Rab4, or mCherry-SNX4/GFP-Rab4 compared with untransfected cells.

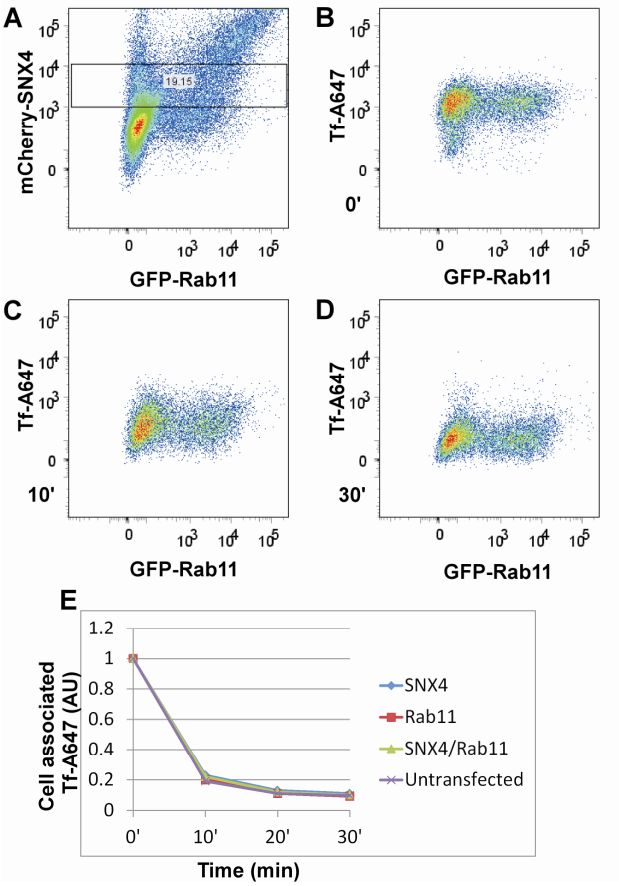

Figure 4.5

Transferrin recycling in GFP-Rab11/mCherry-SNX4 co-transfected HMEC-1 cells. HMEC-1 cells were co-transfected with GFP-Rab11 and mCherry-SNX4. Transfected cells were pulsed with 10 µg/mL Alexa 647-labeled transferrin for 30 min and then harvested by trypsinization (0' chase) or chased in medium containing 250 µg/mL holotransferrin for 10', 20' or 30' before harvesting. Cell associated transferrin levels were quantitated by flow cytometry. A, cells expressing mCherry-SNX4 at the levels used for imaging were gated. B, C, and D, the GFP-Rab11 and cell associated transferrin levels after 0' (B), 10' (C) or 30' (D) chase for the gated subpopulation that expresses mCherry-SNX4 shown in panel A. E, transferrin recycling kinetics for cell subpopulations that express mCherry-SNX4, GFP-Rab11, or mCherry-SNX4/GFP-Rab11 compared with untransfected cells.

4.3 The different itineraries taken by TCs on the recycling pathway can involve a pre-endosomal or post-endosomal sorting step, an interendosomal transfer process and a novel looping pathway

The recycling pathway involving FcRn+ TCs can be broadly defined by four distinct intracellular trafficking processes in HMEC-1 cells that form the focus of analysis in this research project. Early in the process, a pre-endosomal sorting step is observed in which TCs move from the periphery of the cell and fuse with sorting endosomes (Ram et al., 2008). Subsequent trafficking steps can be categorized as follows: a post-endosomal sorting pathway involves migration of the TC to exocytic sites at the plasma membrane (Prabhat et al., 2007). In addition, there are two other pathways in which TCs either migrate between sorting endosomes in interendosomal transfer events (Ober et al., 2004b) or segregate from a sorting endosome and then return to the same endosome (**Figure 4.6**). The latter leave and return, or 'looping', events have not been described previously.

Looping events involving TCs moving bidirectionally to and from the same sorting endosome usually occur over a relatively long time scale. As a result, to avoid loss of TC identity during imaging the use of localized photoactivation combined with MUM (LP-MUM) is necessary. **Figure 4.6** shows an example of such a looping event in HMEC-1 cells transfected with FcRn-PAGFP. FcRn-PAGFP on a sorting endosome (labeled with mRFP-Rab4) was photoactivated using a focused 405 nm laser beam with 1 second exposure. An FcRn+ TC leaves this sorting endosome, moves from the lower to upper

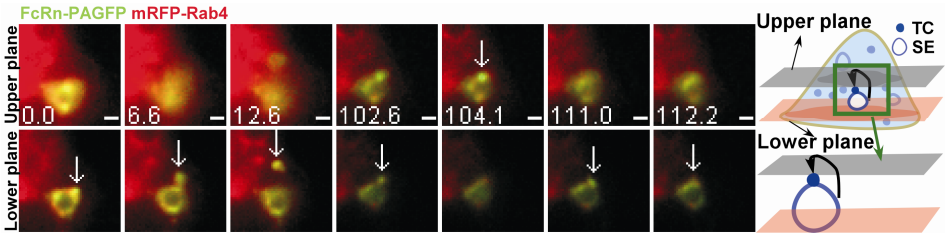

Figure 4.6

A TC involved in a looping event. HMEC-1 cells were co-transfected with FcRn-PAGFP/human β_2m/mRFP-Rab4. A 405 nm laser beam was focused onto a Rab4+ sorting endosome for ~1 s to photoactivate PAGFP. Individual images are presented with the time (in seconds) at which each image was acquired (first image is arbitrarily set to time 0). White arrows in the overlay images show the event of interest. Images are individual frames of Movie 4.2. Scale bars = 1 µm. A FcRn+/Rab4+ TC extends from a sorting endosome (0-6.6 s) in the lower plane, segregates and moves to the upper plane at 104.1 s. Subsequently this TC returns to and merges with the same sorting endosome (111.0 s). Schematic representation is shown on the right column.

focal plane (102.6-104.1 s) and returns to the lower plane and fuses with the same sorting endosome. Additional examples of these types of events, and the effectors associated with them, are described below.

4.4 TCs on the pre-endosomal sorting pathway have associated APPL1

Pre-endosomal sorting pathways of FcRn+ TCs that precede fusion with sorting endosomes were initially analyzed. The involvement of APPL1 in the early endocytic pathway of other receptors such as EGFR (Miaczynska et al., 2004) prompted me to investigate whether APPL1 is also present on FcRn+ TCs that fuse with these endosomes. HMEC-1 cells were co-transfected with GFP-APPL1 and mRFP-FcRn and imaged as live cells. FcRn+/APPL1+ TCs that merge with sorting endosomes were observed (n = 14). **Figure 4.7** shows an example of such a TC that moves from the periphery of the cell and fuses with a sorting endosome.

To investigate whether APPL1+/FcRn+ TCs are on a pathway preceding endosomal fusion and sorting rather than a later step of the recycling pathway, cells were pretreated for a relatively short time period with endocytic cargo prior to imaging. HMEC-1 cells were co-transfected with GFP-APPL1 and a mutated variant of FcRn ('FcRn-mut') (Prabhat et al., 2007) to allow endocytosed, labeled ligand (IgG) to be tracked. Transfected cells were pulsed with an Alexa 555-labeled, engineered IgG1 antibody (MST-HN) (Vaccaro et al., 2005) to label the pre-endosomal pathway. MST-HN interacts with FcRn-mut with high affinity (Kd~10 nM) at near neutral pH, resulting in receptor-

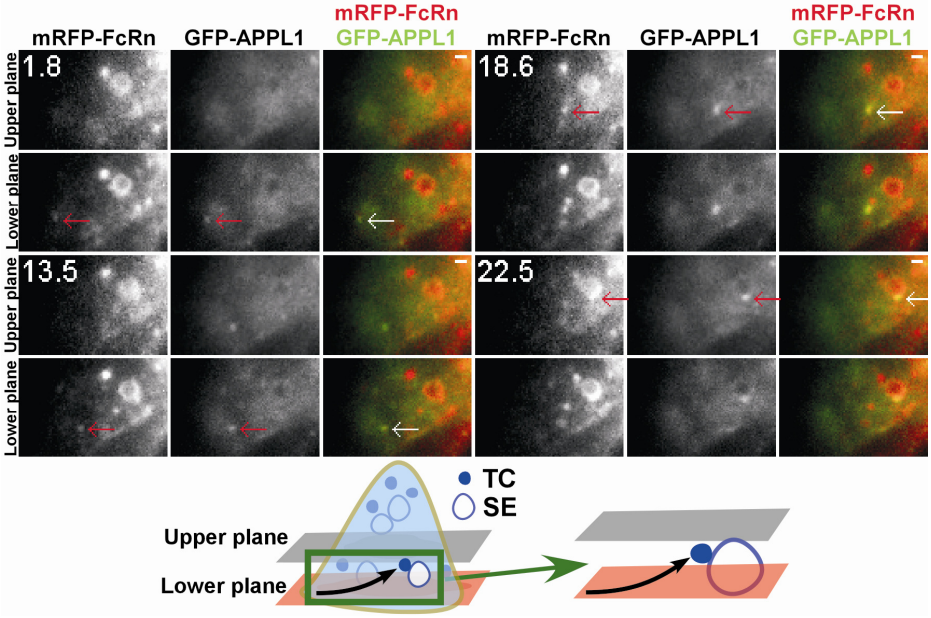

Figure 4.7

FcRn enters the cell in an APPL1+ TC. HMEC-1 cells were co-transfected with mRFP-FcRn/human β_2m/GFP-APPL1. Individual images are presented with the time (in seconds) at which each image was acquired (first image is arbitrarily set to time 0). White arrows in the overlay images show the event of interest that are also indicated in the single color data by red arrows. Images are individual frames of Movie 4.3. Scale bars = 1 µm. A GFP-APPL1+/mRFP-FcRn+ TC appears near the edge of the cell (1.8 s), moves between the two focal planes and merges with a sorting endosome (22.5 s). Schematic representation is shown on the bottom row.

mediated uptake of ligand into cells. All MST-HN+ TCs that merge with sorting endosomes within 10 minutes of MST-HN addition have associated APPL1 (n = 6). For example, **Figure 4.8** shows data obtained using a two plane MUM configuration. In the early stages of the movie (4.8-25.8 s), an MST-HN+/APPL1+ TC can be clearly seen. This TC migrates from the lower plane to the upper plane (27.6 s) and subsequently fuses with a sorting endosome. Collectively, the data demonstrate that APPL1 is associated with FcRn+ TCs preceding endosomal fusion and sorting.

4.5 APPL1 is undetectable or rapidly lost from sorting endosomes following TC fusion

Although APPL1+ TCs fuse with sorting endosomes (**Figure 4.7**, **Figure 4.8**), APPL1 could not be detected on the majority of these 'acceptor' compartments. This suggests that APPL1 is lost during fusion events involving APPL1+ TCs. In rare cases (8%; n = 36) when APPL1 is detectable on the sorting endosome, the signal intensity decreases more rapidly than the photobleaching rate (**Figure 4.9**, **Figure 4.10**). APPL1 therefore dissociates from sorting endosomes, consistent with earlier studies indicating that this protein is displaced by EEA1 through competition for binding to Rab5 (Zoncu et al., 2009). In addition, immunofluorescence analyses using anti-APPL1 and anti-EEA1 antibodies demonstrated that 85% of APPL1+ TCs (n = 69) have detectable levels of EEA1, and APPL1+/EEA1- TCs are in general located closer to the cell periphery relative to their EEA1+ counterparts (**Figure 4.11**). This is consistent with the concept

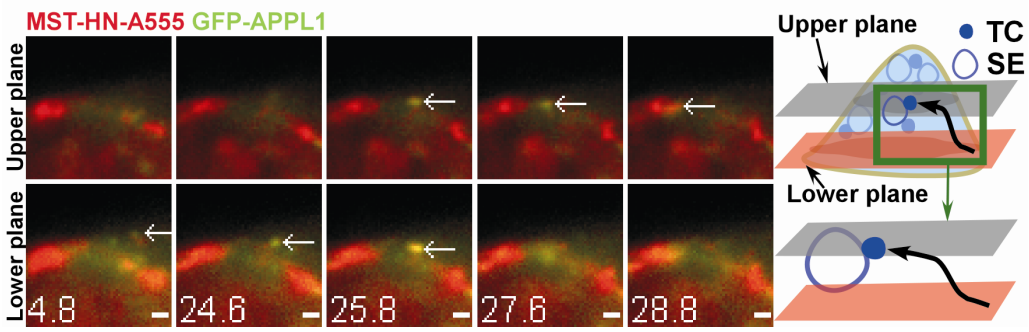

Figure 4.8

MST-HN enters a sorting endosome in an APPL1+ TC. HMEC-1 cells were co-transfected with FcRn/human β_2m/GFP-APPL1. Transfected cells were incubated with 5 µg/mL Alexa-555-labeled MST-HN in pH 7.4 Ham's medium for 2 min before imaging. Individual images are presented with the time (in seconds) at which each image was acquired (first image is arbitrarily set to time 0). White arrows in the overlay images show the event of interest. Images are individual frames of Movie 4.4. Scale bars = 1 µm. An APPL1+/MST-HN+ TC appears on the lower plane (4.8 s), moves to the upper plane (25.8 s) and merges with a sorting endosome (28.8 s). Schematic representation is shown on the right column.

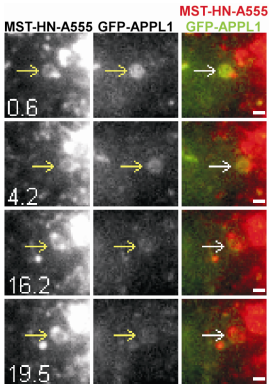

Figure 4.9

APPL1 is lost rapidly from a sorting endosome. HMEC-1 cells were co-transfected with FcRn/human β_2m/GFP-APPL1. Transfected cells were incubated with 5 µg/mL Alexa-555-labeled MST-HN in pH 7.4 Ham's medium for 2 min before imaging. Individual images are presented with the time (in seconds) at which each image was acquired (first image is arbitrarily set to time 0). White arrows in the overlay images show the event of interest that are also indicated in the single color data by yellow arrows. Scale bars = 1 µm. An APPL1+/MST-HN+ sorting endosome loses GFP-APPL1 fluorescence over ~20 s.

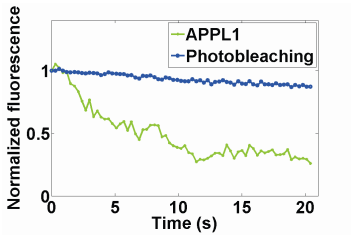

Figure 4.10

Photobleaching analysis. The average photobleaching rate of GFP-APPL1 signal in the same cell is lower than the rate of decrease of GFP-APPL1 in the sorting endosome shown in **Figure 4.9**.

that APPL1+ TCs acquire EEA1 as they move away from the plasma membrane (Zoncu et al., 2009).

4.6 Analyses of the distribution of SNX4, Rab4 and Rab11 in sorting endosomes and TCs

In previous studies SNX4, Rab4 and Rab11 have been associated with endosomal sorting and recycling (McCaffrey et al., 2001; Pagano et al., 2004; Sonnichsen et al., 2000; Traer et al., 2007). Towards analyzing the trafficking pathways of TCs following their segregation from sorting endosomes, the distribution of these effector proteins in sorting endosomes and TCs in HMEC-1 cells was next investigated. SNX4 and Rab4 are almost completely colocalized (**Figure 4.12**), allowing these proteins to be used interchangeably in our analyses. By contrast, Rab11 is less extensively colocalized with SNX4/Rab4 in TCs (**Figure 4.13**), although SNX4/Rab4 and Rab11 are present on all sorting endosomes.

4.7 SNX4/Rab4 and Rab11 can associate with APPL1+ TCs

Analyses of the distribution of SNX4 on TCs led to the unexpected observation that this sorting nexin can be present at the pre-endosomal sorting step involving APPL1+ TCs. Specifically, analyses of HMEC-1 cells transfected with GFP-APPL1, mCherry-SNX4 and FcRn-mut (stop) followed by pulsing with Atto-647 labeled IgG1 mutant, MST-HN (Vaccaro et al., 2005), to label FcRn indicated that 50% of APPL1+ TCs have associated

SNX4 (**Figure 4.14**). Further, live cell imaging of HMEC-1 cells transfected with mCherry-SNX4 and GFP-APPL1 demonstrated that APPL1+/SNX4+ TCs fuse with sorting endosomes (**Figure 4.15**). All APPL1+ TCs (n = 7) that fuse with sorting endosomes have detectable levels of SNX4 (**Figure 4.15**, data not shown), suggesting that the presence of SNX4 is a marker of fusion competent TCs.

Consistent with the observation that SNX4 is associated with a subset of APPL1+ TCs and extensively colocalized with Rab4 (**Figure 4.12**), staining of mRFP-Rab4 transfected cells with anti-APPL1 antibody demonstrated that 50% (n = 57) of APPL1+ TCs are also Rab4+ (**Figure 4.16**). In addition, whether Rab11, which is associated with endosomal sorting on the exocytic pathway in HMEC-1 cells (Ward et al., 2005), colocalizes with APPL1 was investigated. To assess overlap between APPL1, SNX4/Rab4 and Rab11, HMEC-1 cells were transfected with GFP-Rab11, mCherry-SNX4 and stained with an anti-APPL1 antibody following fixation. These cells were also co-transfected with FcRn-stop (containing FcRn-mut that has high affinity for IgG) to allow localization of FcRn by pulsing with labeled IgG1 mutant, MST-HN (**Figure 4.17**). A relatively low proportion (7%; n = 69) of FcRn+/APPL1+ TCs have associated SNX4/Rab4 and Rab11. Further, 43% of APPL1+/FcRn+ TCs have associated SNX4/Rab4 (with no detectable Rab11), whereas 14% of APPL1+/FcRn+ TCs have associated Rab11 (with no detectable SNX4/Rab4). Thus, Rab4 and Rab11 can unexpectedly associate with APPL1+/FcRn+ TCs at the pre-endosomal sorting stage of the recycling pathway, although Rab4 association is more common than that of Rab11. Collectively, pre-endosomal TCs have

associated APPL1, with the possible presence of SNX4/Rab4 and Rab11 for partially overlapping subsets of these TCs.

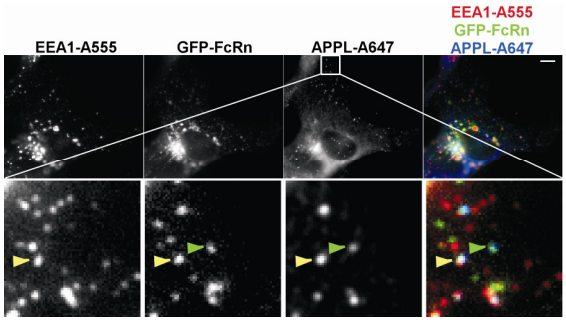

Figure 4.11

FcRn can be detected in APPL1+ TCs. HMEC-1 cells were co-transfected with GFP-FcRn and human β_2m. Transfected cells were fixed and stained with anti APPL and EEA1 antibodies. Scale bar = 5 µm. The boxed region at the edge of the cell in the upper row is presented as cropped images in the lower row. The yellow arrowheads indicate an example of a FcRn+/APPL+/EEA1+ TC and the green arrowheads indicate an example of a FcRn+/APPL+/EEA1- TC.

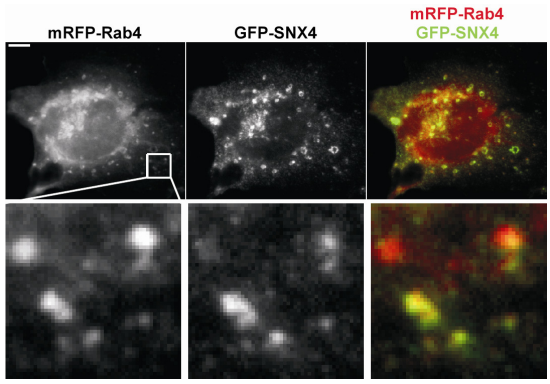

Figure 4.12

Rab4 extensively colocalizes with SNX4. HMEC-1 cells were co-transfected with GFP-SNX4/mRFP-Rab4. Transfected cells were fixed. The boxed region in the upper row is presented as cropped images in the lower row. Scale bar = 5 µm. Rab4 and SNX4 colocalized extensively with each other.

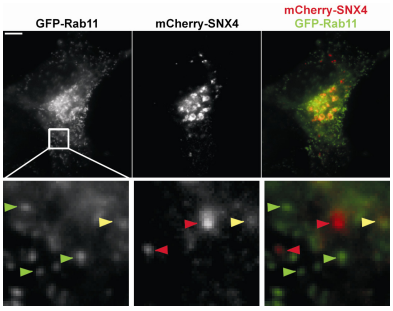

Figure 4.13

Rab11 is partially colocalized with SNX4. HMEC-1 cells were co-transfected with GFP-Rab11/mCherry-SNX4. Transfected cells were fixed. The boxed region in the upper row is presented as cropped images in the lower row. Scale bar = 5 µm. The red, green or yellow arrows indicate examples of SNX4+, Rab11+, or SNX4+/Rab11+ TCs, respectively.

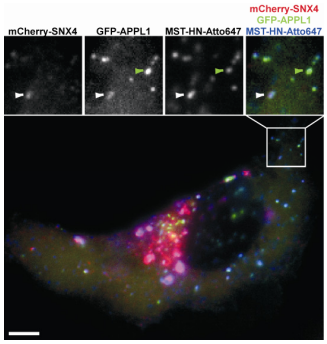

Figure 4.14

SNX4 colocalizes with APPL1 in TCs. HMEC-1 cells were co-transfected with FcRn/human β_2m/GFP-APPL1/mCherry-SNX4. Scale bar = 5 µm. Transfected cells were incubated with 2.5 µg/mL Atto-647-labeled MST-HN in pH 7.4 Ham's medium for 30 min. The boxed region in the lower row is presented as cropped images in the upper row. The green arrowheads indicate an example of a MST-HN+/APPL1+/SNX4- TC and the white arrowheads indicate an example of a MST-HN+/APPL1+/SNX4+ TC.

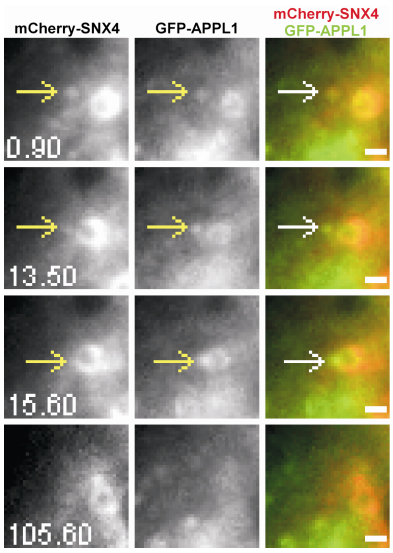

Figure 4.15

A SNX4+/APPL1+ TC merges with a sorting endosome. HMEC-1 cells were co-transfected with mCherry-SNX4/GFP-APPL1. Scale bars = 1 µm. Individual images are presented with the time (in seconds) at which each image was acquired (first image is arbitrarily set to time 0). White arrows in the overlay images show the event of interest that is also indicated in the single color data by yellow arrows. A SNX4+/APPL1+ TC merges with a SNX4+/APPL1+ sorting endosome (15.6 s).

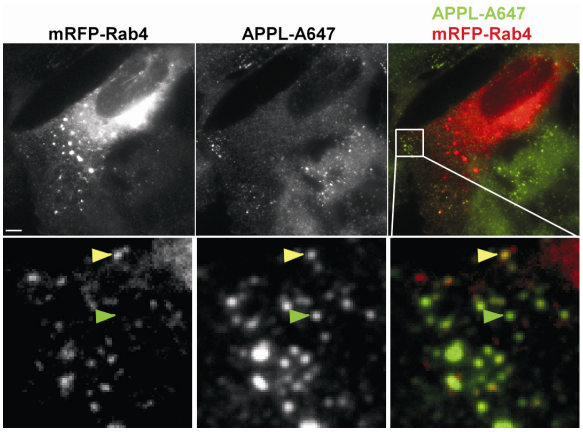

Figure 4.16

Rab4 can be seen in APPL1+ TCs. HMEC-1 cells were co-transfected with mRFP-Rab4. Transfected cells were fixed and stained with anti APPL antibody. The boxed region in the upper row is presented as cropped images in the lower row. Scale bar = 5 µm. The yellow arrowheads indicate an example of an APPL+/Rab4+ TC and green arrowheads indicate an example of an APPL+/Rab4- TC.

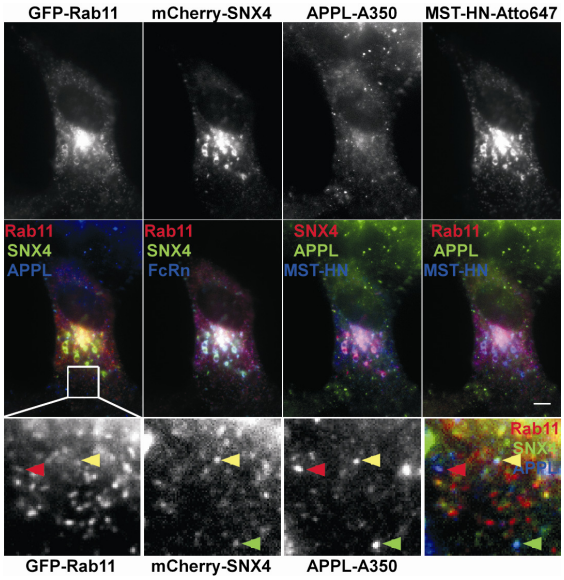

Figure 4.17

Distributions of SNX4, Rab4 and Rab11 in sorting endosomes and TCs. HMEC-1 cells were co-transfected with FcRn/human β_2m/GFP-Rab11/mCherry-SNX4. Transfected cells were incubated with 5 µg/mL MST-HN-Atto 647 in pH 7.4 Ham's medium for 30 min. Cells were then fixed and stained with anti APPL antibody. The upper (middle) row shows the single color (overlay) images. The boxed region in the middle row is presented as cropped images in the lower row. Scale bar = 5 µm. The red, green or yellow arrowheads indicate examples of MST-HN+ TCs that are APPL+/Rab11+, APPL1+/SNX4+ or APPL+/SNX+/Rab11+, respectively.

4.8 Interendosomal TCs have associated SNX4/Rab4 without detectable levels of APPL1 or Rab11

Whilst analyzing APPL1 associations with TCs, I also observed endosomal fusion of FcRn+ TCs without detectable levels of APPL1. Collectively with our earlier observations that TCs can migrate between endosomes (Ober et al., 2004b), this prompted me to further analyze these interendosomal transfer events. Given the previously identified role of SNX4 in endosomal sorting (Cullen, 2008; Traer et al., 2007), whether TCs involved in interendosomal transfer have associated SNX4 was first investigated by co-transfecting HMEC-1 cells with GFP-SNX4 and mRFP-FcRn. SNX4+/FcRn+ TCs can fuse with other sorting endosomes of similar size and morphology (n = 5). In **Figure 4.18**, a representative event of this type is shown. A SNX4+/FcRn+ TC leaves a sorting endosome in the upper plane, migrates to the lower plane (6 s) and fuses with a second endosome. By contrast with SNX4, the analysis of cells co-transfected with GFP-Rab11 and mCherry-SNX4 indicated that Rab11 does not associate with interendosomal TCs (n = 11). In the example shown (**Figure 4.19**), a SNX4+ TC leaves a sorting endosome and moves in the same plane to fuse with a second sorting endosome.

Consistent with the extensive colocalization of Rab4 and SNX4 (**Figure 4.12**), I also observed interendosomal transfer events involving SNX4+/Rab4+ TCs in cells transfected with PAGFP-Rab4 and mCherry-SNX4 followed by local photoactivation of

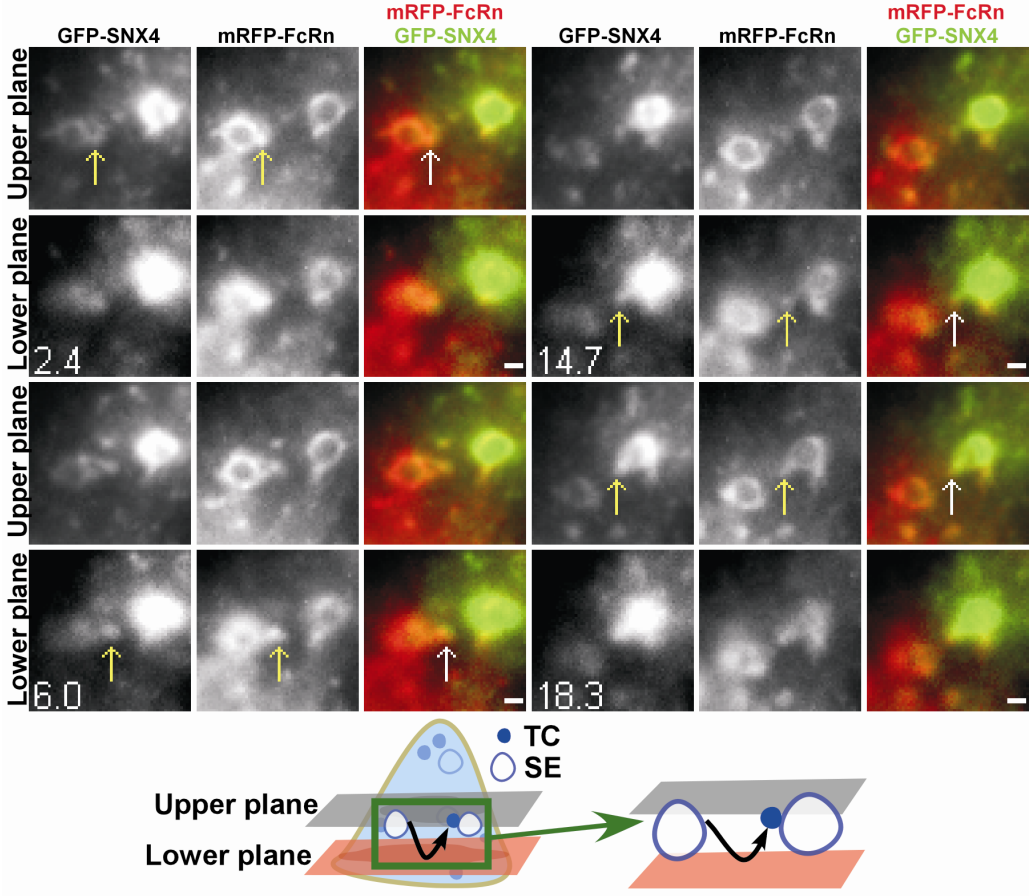

Figure 4.18

A FcRn+/SNX4+ interendosomal TC. HMEC-1 cells were co-transfected with GFP-SNX4/human β_2m/mRFP-FcRn. Individual images are presented with the time (in seconds) at which each image was acquired (first image is arbitrarily set to time 0). White arrows in the overlay images show the event of interest that are also indicated in the single color data by yellow arrows. Images are individual frames of Movie 4.5. Scale bars = 1 µm. A FcRn+/SNX4+ TC extends from a sorting endosome (2.4-6 s), segregates and moves between the two focal planes. This TC merges with another sorting endosome (18.3 s). Schematic representation is shown on the bottom row.

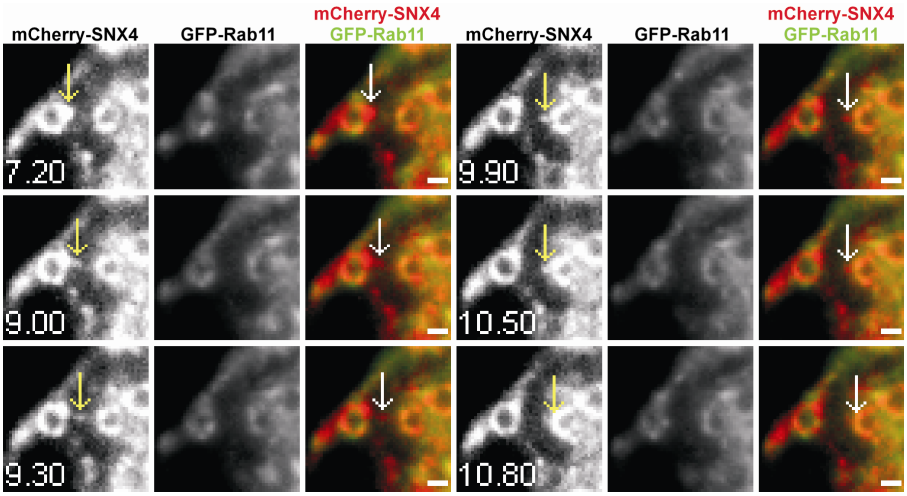

Figure 4.19

An interendosomal TC that does not have associated Rab11. HMEC-1 cells were co-transfected with mCherry-SNX4/GFP-Rab11. Individual images are presented with the time (in seconds) at which each image was acquired (first image is arbitrarily set to time 0). White arrows in the overlay images show the event of interest that are also indicated in the single color data by yellow arrows. Scale bars = 1 µm. A SNX4+/Rab11- TC extends from a sorting endosome (7.2-9.0 s), segregates and subsequently merges with another sorting endosome (10.50 s).

PAGFP-Rab4 on individual sorting endosomes (n = 9 events). In **Figure 4.20**, a SNX4+/Rab4+ TC leaves a sorting endosome and fuses with a proximal sorting endosome within the same focal plane. A second TC also leaves this endosome in the lower focal plane, moves to the upper focal plane (64.8 s), migrates back and forth (66.6 s) and returns to fuse with the second endosome (**Figure 4.21**). LP-MUM experiments carried out using cells transfected with FcRn-PAGFP and mRFP-Rab4 resulted in the observation of transfer of Rab4+/FcRn+ TCs between sorting endosomes (**Figure 4.22**). In addition, when multiple interendosomal transfer events were seen from an individual sorting endosome (four different endosomes, two transfer events per endosome), the transfer was unidirectional. Despite the presence of Rab11 on donor and acceptor endosomes, the migrating TCs do not have detectable levels of Rab11 (n = 15; **Figure 4.19**). Consistent with current and earlier studies of APPL1 (Miaczynska et al., 2004; Zoncu et al., 2009), these TCs also do not have associated APPL1 (n = 5). Interendosomal TCs are therefore SNX4/Rab4+, with undetectable levels of Rab11 and APPL1.

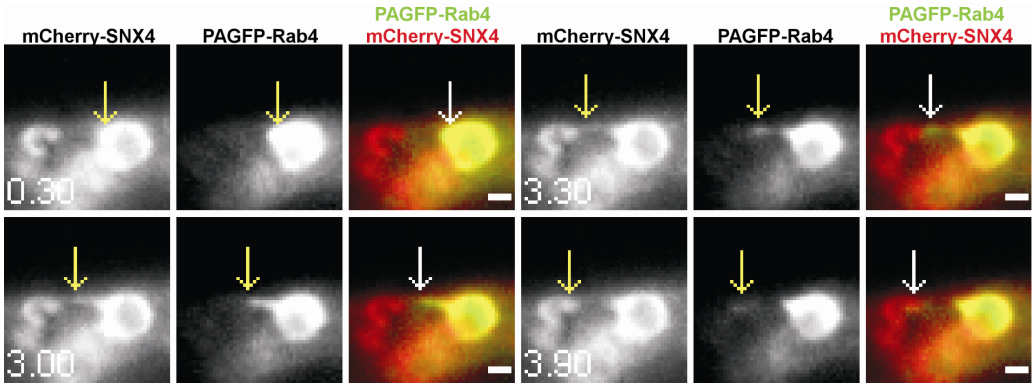

Figure 4.20

A SNX4+/Rab4+ interendosomal TC. HMEC-1 cells were co-transfected with mCherry-SNX4/PAGFP-Rab4. A 405 nm laser beam was focused onto a SNX4+ sorting endosome for ~1 s to photoactivate PAGFP. Individual images are presented with the time (in seconds) at which each image was acquired (first image is arbitrarily set to time 0). White arrows in the overlay images show the event of interest that are also indicated in the single color data by yellow arrows. Scale bars = 1 µm. A SNX4+/Rab4+ TC extends from a sorting endosome (0.3-3.3 s), segregates and subsequently merges with another sorting endosome (3.9 s).

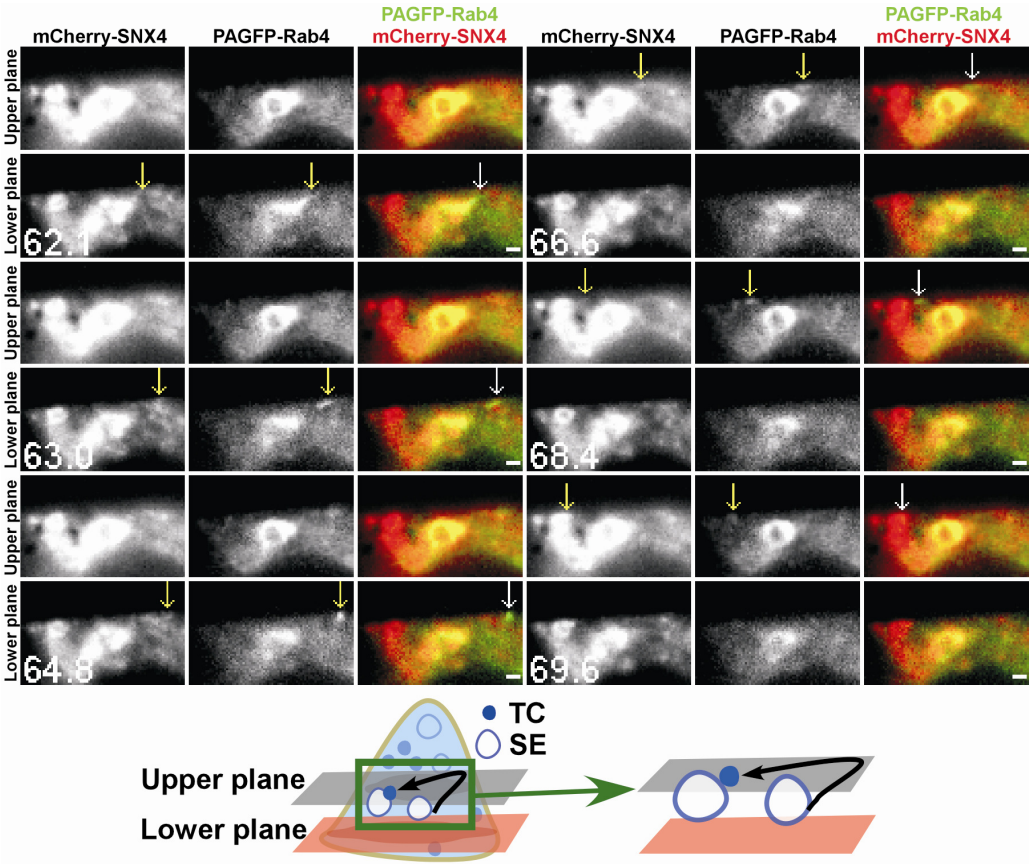

Figure 4.21

A SNX4+/Rab4+ interendosomal TC. HMEC-1 cells were co-transfected with mCherry-SNX4/PAGFP-Rab4. A 405 nm laser beam was focused onto a SNX4+ sorting endosome for ~1 s to photoactivate PAGFP. Individual images are presented with the time (in seconds) at which each image was acquired (first image is arbitrarily set to time 0). White arrows in the overlay images show the event of interest that are also indicated in the single color data by yellow arrows. Images are individual frames of Movie 4.6. Scale bars = 1 µm. A second SNX4+/Rab4+ TC leaves the same 'donor' sorting endosome as in **Figure 4.20** in the lower plane (62.1 s), moves rightwards at 64.8 s, changes direction and moves leftwards at 66.6 s. it merges with the 'acceptor' endosome in the upper plane (69.6 s). Schematic representation is shown on the bottom row.

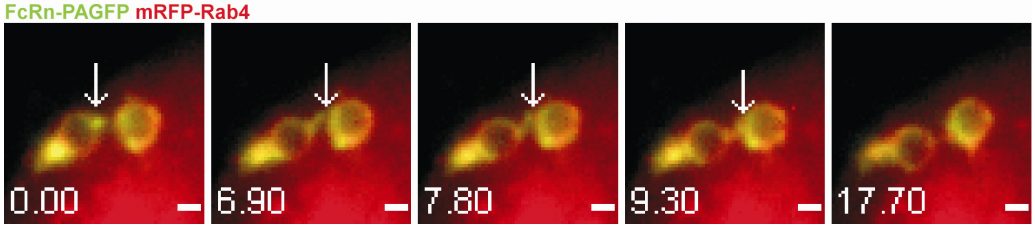

Figure 4.22

An interendosomal TC that has associated Rab4. HMEC-1 cells were co-transfected with mRFP-Rab4/human β_2m/FcRn-PAGFP. A 405 nm laser beam was focused onto Rab4+ sorting endosomes for ~1 s to photoactivate PAGFP. Individual images are presented with the time (in seconds) at which each image was acquired (first image is arbitrarily set to time 0). White arrows in the overlay images show the event of interest. Scale bars = 1 µm. A FcRn+/Rab4+ TC extends from one sorting endosome at 0 s, merges with the second sorting endosome (6.9-7.8 s) and subsequently segregates from the original endosome.

4.9 TCs involved in looping events are associated with both SNX4/Rab4 and Rab11

A novel class of looping events involving the segregation of TCs from sorting endosomes and their subsequent return to the same endosome was observed in cells transfected with different combinations of Rab4, Rab11, SNX4 and FcRn (PAGFP-Rab11/mCherry-SNX4, FcRn-PAGFP/mRFP-Rab4, FcRn-PAGFP/mCherry-SNX4, mRFP-FcRn/PAGFP-Rab11 or PAGFP-Rab4/mCherry-SNX4; n = 19 events for all transfection combinations). Representative examples of these processes are shown in **Figure 4.6**, **Figure 4.23** and **Figure 4.24**. Looping events are frequently of relatively long duration, accounting for their difficulty in detection in earlier studies using conventional imaging modalities. In the majority (89%, n = 19) of looping events analyzed, the TC segregates from the endosome, moves towards the cell periphery, pauses and then reverses direction to return and fuse with the originating endosome. In multiple cases looping TCs migrate between different focal planes (e.g. **Figure 4.6** and **Figure 4.23**), necessitating the use of MUM for unambiguous tracking. Further, in PAGFP-Rab11/mCherry-SNX4 transfected cells, all TCs of this type have associated Rab11 and SNX4/Rab4 (n = 6 events), indicating that looping TCs can be distinguished from interendosomal transfer TCs by the presence of Rab11**.**

Although for technical reasons it was not possible to track looping events in APPL1-GFP transfected cells, several observations indicate that APPL1 is not present on looping TCs. First, in GFP-APPL1 transfected cells, APPL1 is not associated with any TCs that segregate from sorting endosomes. This is consistent with the low or undetectable levels

of APPL1 on these endosomes. Second, in GFP-APPL1 transfected cells pulsed with MST-HN for short periods to label the early stages in endocytic recycling, the majority (90%, n = 119) of APPL1+ TCs have associated MST-HN, suggesting that APPL1 is predominantly associated with pre-endosomal TCs (data not shown). Further, the low percentage (10%) of APPL1+ TCs that do not contain MST-HN are also SNX4-.

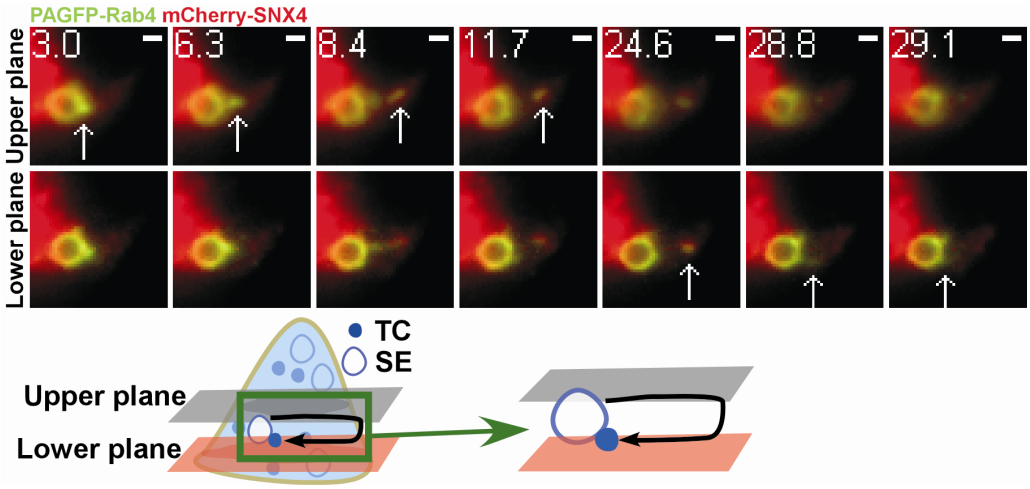

Figure 4.23

A SNX4+/Rab4+ TC involved in a looping event. HMEC-1 cells were co-transfected with PAGFP-Rab4/mCherry-SNX4. A 405 nm laser beam was focused onto a SNX4+ sorting endosome for ~1 s to photoactivate PAGFP. Individual images are presented with the time (in seconds) at which each image was acquired (first image is arbitrarily set to time 0). White arrows in the overlay images show the event of interest. Images are individual frames of Movie 4.7. Scale bars = 1 µm. A SNX4+/Rab4+ TC extends from a sorting endosome (3-6.3 s) in the upper plane, segregates and subsequently moves to the lower plane at 24.6 s. This TC returns and merges with the same endosome (29.1 s). Schematic representation is shown on the bottom row.

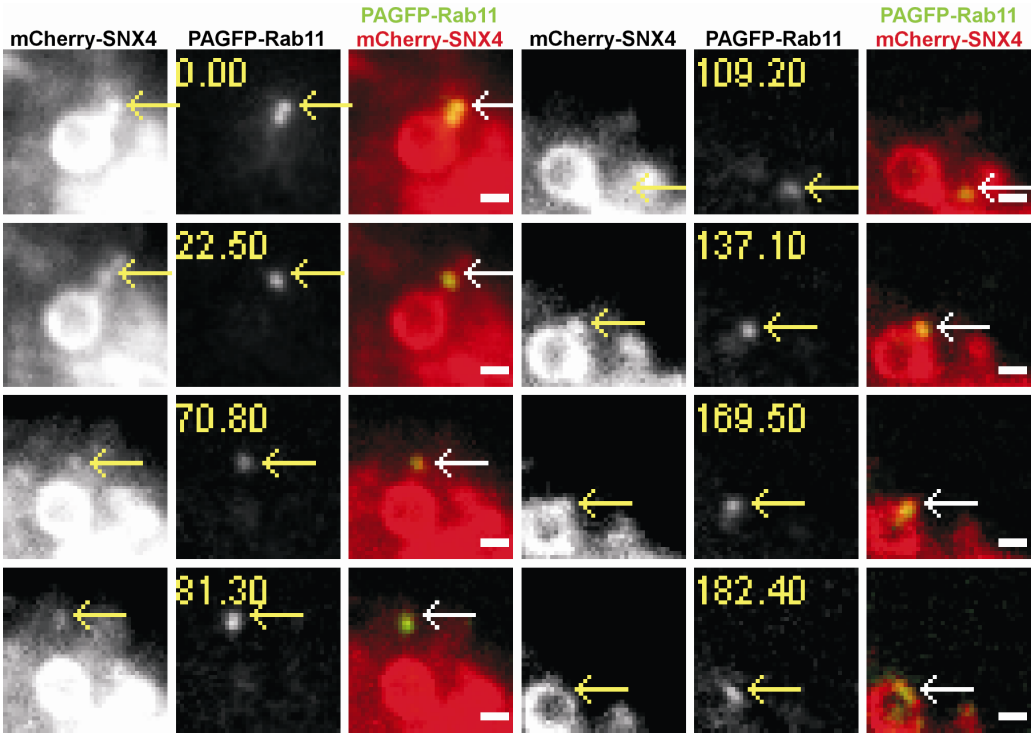

Figure 4.24

A SNX4+/Rab11+ TC involved in a looping event. HMEC-1 cells were co-transfected with mCherry-SNX4/PAGFP-Rab11. A 405 nm laser beam was focused onto a SNX4+ sorting endosome for ~1 s to photoactivate PAGFP. Individual images are presented with the time (in seconds) at which each image was acquired (first image is arbitrarily set to time 0). White arrows in the overlay images show the event of interest that are also indicated in the single color data by yellow arrows. Images are individual frames of Movie 4.8. Scale bars = 1 µm. A SNX4+/Rab11+ TC extends from a sorting endosome (0 s), segregates and subsequently returns and merges with the same endosome at (137.1-182.4) s.

4.10 Post-endosomal sorting TCs are associated with Rab11 without detectable levels of SNX4/Rab4

In experiments with SNX4 or Rab4 transfected cells, a subset of FcRn+ TCs segregate from sorting endosomes that are not involved in interendosomal transfer or looping events. These TCs do not contain detectable levels of SNX4/Rab4 (n = 4 for SNX4- TCs and n = 3 for Rab4- TCs; data not shown). Collectively with our earlier observations that Rab11 is associated with exocytic events involving FcRn (Ward et al., 2005), this suggested that such TCs might be on the post-endosomal sorting pathway leading to exocytosis. The fate of Rab11+ TCs was therefore investigated using LP-MUM, which proved to be essential for the analysis of the behavior of Rab11+ TCs due to the high background haze of Rab11-associated fluorescence. By contrast with the properties of Rab4+ TCs, imaging of cells following co-transfection with PAGFP-Rab11 and mRFP-FcRn resulted in the observation of Rab11+/FcRn+ TCs leaving sorting endosomes and frequently moving to the cell periphery. In **Figure 4.25**, the TC moves from the upper plane to the lower plane (i.e. near the cover glass). Similarly, in mCherry-SNX4/PAGFP-Rab11 transfected cells, Rab11+ TCs with undetectable levels of SNX4 can be seen leaving endosomes and migrating from the upper plane to the cell periphery in the lower plane (7.2-20.1 s) (**Figure 4.26**). Within the time frame of imaging, none of these Rab11+/FcRn+ TCs (n = 5; n = 6 for Rab11+/SNX4- TCs) are involved in interendosomal transfer or looping events. Instead, the TCs migrate towards the plasma membrane. Collectively, Rab11, but not SNX4/Rab4, is associated with post-endosomal

sorting TCs. Combined with our earlier TIRFM analyses (Ward et al., 2005), these TCs most likely lead to exocytosis of FcRn.

We have previously used TIRFM to demonstrate that, by contrast with Rab11, Rab4 is not associated with exocytic events (Ward et al., 2005). The extensive colocalization of Rab4 and SNX4 with each other (**Figure 4.12**) indicated that SNX4 would also not be associated with exocytic processes. This was confirmed by TIRFM analyses of HMEC-1 cells co-transfected with mCherry-SNX4 and GFP-FcRn. In all exocytic events involving FcRn (n = 14), we could not detect SNX4 (**Figure 4.27**, **Figure 4.29**). Analogous analyses of cells co-transfected with mRFP-APPL1 and FcRn tagged with ecliptic pHluorin (Prabhat et al., 2007), a pH-sensitive variant of GFP (Miesenbock et al., 1998), demonstrated that exocytic events involving FcRn do not have detectable levels of APPL1 (**Figure 4.28**, **Figure 4.29**). This is consistent with a role for APPL1 TCs in pre-endosomal sorting pathways (**Figure 4.7**, **Figure 4.8**, (Miaczynska et al., 2004; Zoncu et al., 2009)).

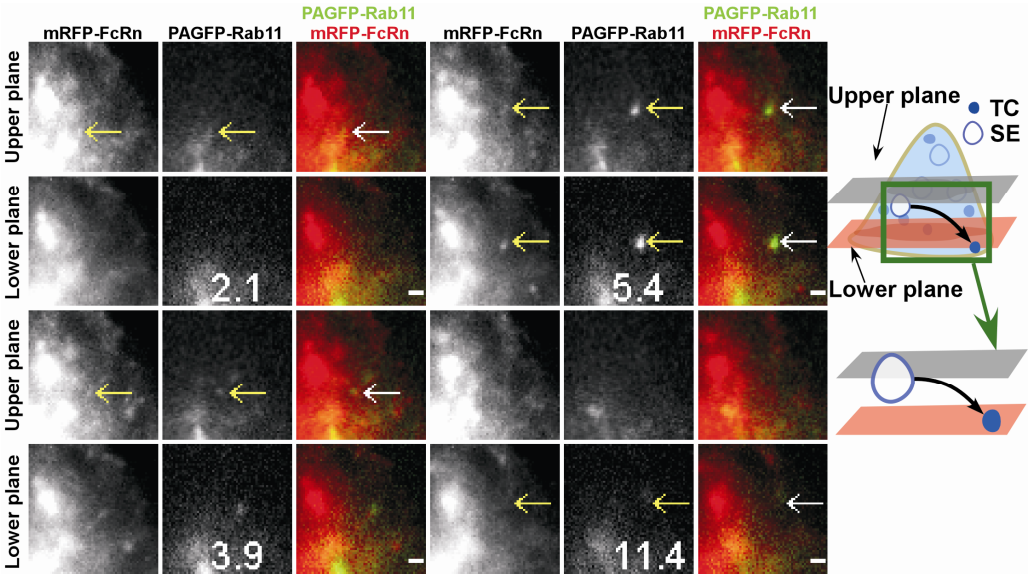

Figure 4.25

A FcRn+/Rab11+ TC leaves a sorting endosome and moves to the cell periphery. HMEC-1 cells were co-transfected with mRFP-FcRn/human β_2m/PAGFP-Rab11. A 405 nm laser beam was focused onto an FcRn+ sorting endosome for ~1 s to photoactivate PAGFP. Individual images are presented with the time (in seconds) at which each image was acquired (first image is arbitrarily set to time 0). White arrows in the overlay images show the event of interest that are also indicated in the single color data by yellow arrows. Images are individual frames of Movie 4.9. Scale bars = 1 µm. A FcRn+/Rab11+ TC extends from a sorting endosome (2.1 s), segregates and subsequently moves to the lower plane (5.4 s). This TC disappears from the lower plane (11.4 s). Schematic representation is shown on the right column.

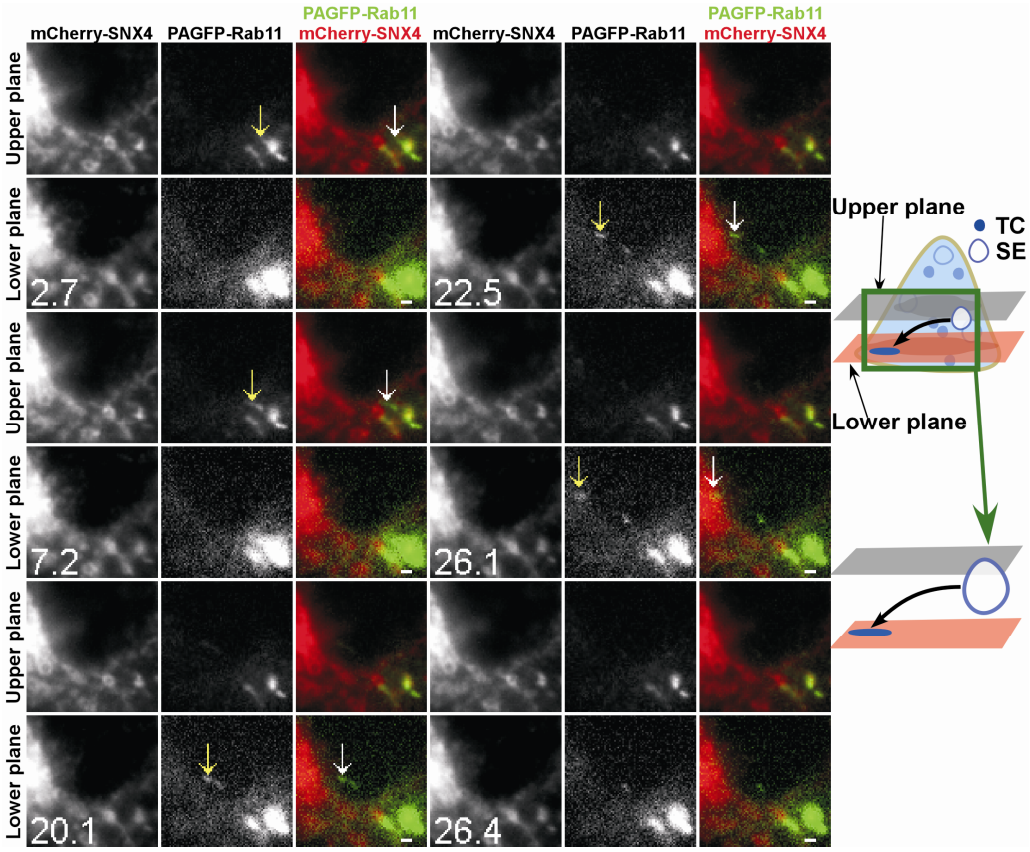

Figure 4.26

A SNX4-/Rab11+ TC leaves a sorting endosome and moves to the cell periphery. HMEC-1 cells were co-transfected with PAGFP-Rab11/mCherry-SNX4. A 405 nm laser beam was focused onto a SNX4+ sorting endosome for ~1 s to photoactivate PAGFP. Individual images are presented with the time (in seconds) at which each image was acquired (first image is arbitrarily set to time 0). White arrows in the overlay images show the events of interest that are also indicated in the single color data by yellow arrows. Images are individual frames of Movie 4.10. Scale bars = 1 µm. A SNX4-/Rab11+ TC extends from a sorting endosome (2.7 s), segregates and subsequently moves to the lower plane (20.1 s). This TC disappears from the lower plane (26.1 s). Schematic representation is shown on the right column.

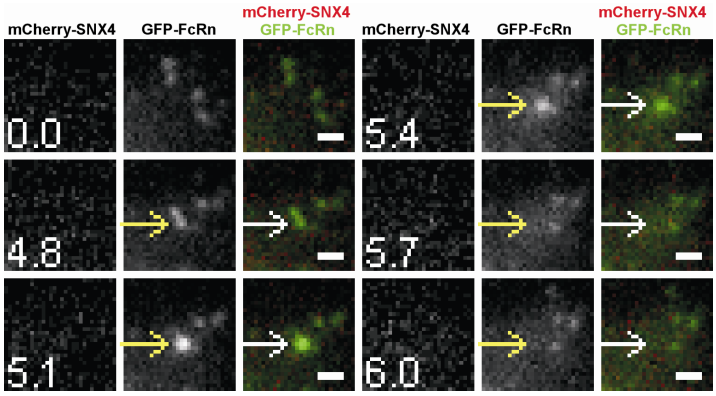

Figure 4.27

A FcRn exocytosis event without associated SNX4. HMEC-1 cells were co-transfected with mCherry-SNX4/GFP-FcRn. Individual images are presented with the time (in seconds) at which each image was acquired (first image is arbitrarily set to time 0). White arrows in the overlay images show the event of interest that is also indicated in the single color data by yellow arrows. Scale bars = 1 µm. TIRFM images show an exocytic event involving FcRn without detectable levels of APPL1 (4.8-5.7 s). The core/annulus intensity plots of the changes in fluorescence intensity for the exocytic event are displayed in **Figure 4.29**.

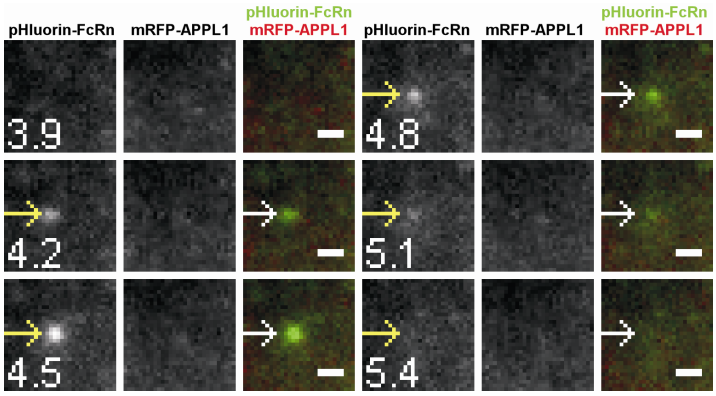

Figure 4.28

A FcRn exocytosis event without associated APPL1. HMEC-1 cells were co-transfected with mRFP-APPL1/pHluorin-FcRn. Individual images are presented with the time (in seconds) at which each image was acquired (first image is arbitrarily set to time 0). White arrows in the overlay images show the event of interest that is also indicated in the single color data by yellow arrows. Scale bars = 1 µm. TIRFM images show an exocytic event involving FcRn without detectable levels of SNX4 (4.2-5.1 s). The core/annulus intensity plots of the changes in fluorescence intensity for the exocytic event are displayed in **Figure 4.29**.

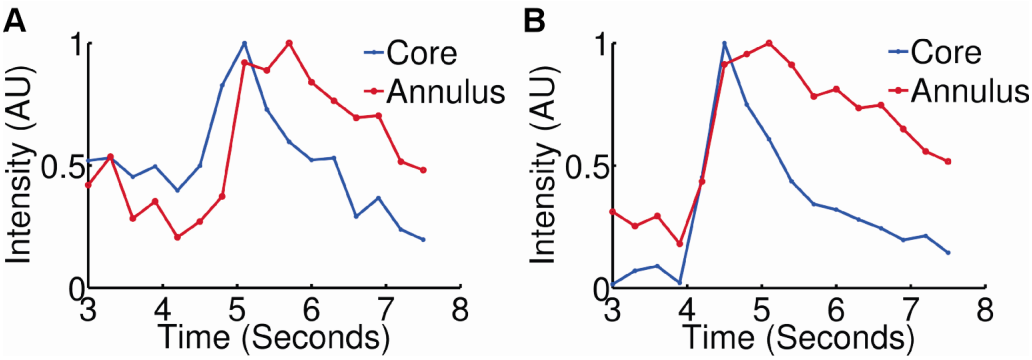

Figure 4.29

The core/annulus intensity plots of the changes in fluorescence intensity for the exocytic events displayed in Figure 4.27 (A) and Figure 4.28 (B), respectively.

CHAPTER 5 CONCLUSIONS AND FUTURE DIRECTIONS

5.1 Overview

In this research project, the intracellular trafficking pathways of FcRn were investigated using advanced fluorescence microscopy. The analyses presented in CHAPTER 3 and CHAPTER 4 have led to novel observations for the lysosomal delivery and the recycling pathways of FcRn. These results are discussed and two models for these pathways are proposed in this Chapter.

5.2 A novel lysosomal delivery pathway

Despite the central role that lysosomes play in cellular homeostasis, how membrane receptors are delivered from the endocytic pathway for degradation remains an area of active investigation (Luzio et al., 2007). In this research project the intracellular trafficking processes that lead to the transfer of the Fc receptor, FcRn, from late endosomes to lysosomes have been analyzed. In contrast to previously described receptors (Piper and Katzmann, 2007), data shown in CHAPTER 3 demonstrate that FcRn does not enter ILVs in late endosomes prior to lysosomal delivery. The pathway that this receptor takes in transit to lysosomes is therefore distinct to the ubiquitin-dependent and -independent processes for ILV entry (Katzmann et al., 2001; McNatt et al., 2007; Piper and Katzmann, 2007; Reggiori and Pelham, 2001; Urbanowski and Piper,

2001). In this context, the lysine residue in the cytosolic tail of human FcRn is not conserved in mouse FcRn (Ahouse et al., 1993; Story et al., 1994), and the similar behavior of mouse and human FcRn therefore indicate that the trafficking of this receptor is ubiquitin-independent. These analyses also demonstrate that FcRn delivery to lysosomes occurs via fusion processes that usually involve tubular transport or organellar interactions that resemble kiss-and-linger (Bright et al., 2005; Gandhi and Stevens, 2003; Ryan, 2003; Storrie and Desjardins, 1996), rather than complete merging of the participating organelles.

These data are consistent with the following model that encompasses several novel features for the lysosomal delivery of membrane receptors (**Figure 5.1**). The receptor is present on the membrane of Rab5+ early endosomes that mature into Rab5+/Rab7+ late endosomes. Recycling/transcytotic receptors such as FcRn that remain on the limiting membrane can segregate from these endosomes into the recycling/transcytotic pathway, or enter lysosomes via processes that usually employ tubular connections or resemble kiss-and-linger events (Bright et al., 2005; Gandhi and Stevens, 2003; Ryan, 2003; Storrie and Desjardins, 1996) but do not involve 'backflow' of lysosomal contents. This functional plasticity of endosomes is congruent with the formation of membrane domains that are characterized by distinct compositions of Rab GTPases and lipids (Pfeffer, 2003; Sonnichsen et al., 2000; Ward et al., 2005). Transfer can be mediated by an extension of a tubule from one compartment to another, or by direct contact of the two compartments. By contrast, complete fusion of late endosomes and lysosomes is rarely observed. Transfer by tubular extensions would be expected to limit content mixing, and might be

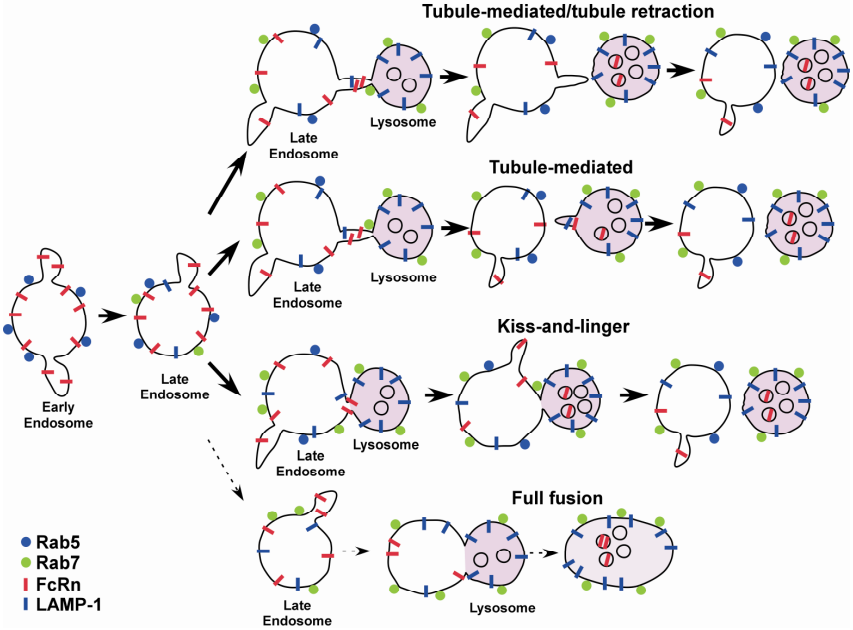

Figure 5.1

A model for the transfer of FcRn from late endosomes to lysosomes. Rab5+/FcRn+ early endosomes can mature to Rab5+/Rab7+ late endosomes. The receptors remain on the limiting membrane of late endosomes and can either enter the recycling/transcytotic pathways or lysosomes. Transfer of FcRn from the limiting membrane of late endosomes to lysosomes can occur via several different processes as indicated. FcRn transfer to lysosomes is rapidly followed by internalization into the intraluminal space of lysosomes, whereas LAMP-1 persists on the limiting membrane. The lower frequency of full fusion events relative to the other types of processes is indicated by a dotted arrow.

analogous to the exocytic processes that involve direct endosomal-plasma membrane connections that we have described previously (Prabhat et al., 2007). Interestingly, tubules can either retract to, or separate from, their donor organelle following or during transfer of material to lysosomes. Movement of the Fc receptor, FcRn, from the late endosome to the lysosome is rapidly followed by internalization into the intraluminal space, via a process that might resemble ILV internalization in MVBs/late endosomes (Piper and Katzmann, 2007). By contrast, proteins such as LAMP-1 migrate in a bidirectional fashion between the limiting membranes of late endosomes and lysosomes. The model also incorporates features concerning the behavior of the Rab GTPases, Rab5 and Rab7. Although Rab7 acquisition appears to be a prerequisite for a late endosome to reach a state of fusion competence with lysosomes, complete loss of Rab5 is unexpectedly not.

The dominance of selective transfer processes such as via tubular connections, rather than complete fusion, during lysosomal delivery has several important consequences: first, it provides a mechanism for the exclusion of Rab5 transfer to lysosomes, which, if it occurred, could promote (early) endosomal-lysosomal fusion (Christoforidis et al., 1999; Simonsen et al., 1998) with concomitant degradation of endosomal contents. Second, in a more general sense, tubular transfer and kiss-and-linger type modes allow late endosomes to retain functional plasticity so that receptors on the limiting membrane can be selectively recycled or degraded. By extending the window of time during which recycling can occur, this might improve the fidelity of this process. Third, these transfer

modes remove the necessity for organelle retrieval from hybrid compartments (Bright et al., 2005; Luzio et al., 2007).

FcRn transfer to lysosomes occurs without detectable 'backflow' of lysosomal contents such as dextran to late endosomes. The involvement of tubular extensions with large surface area to volume ratios could regulate this. In this context, size selective transfer of dextran between compartments on the endocytic, phagocytic and exocytic pathways has been shown to occur in several distinct cell types (Berthiaume et al., 1995; Duclos et al., 2003; Jaiswal et al., 2004; Wang and Goren, 1987). Constriction of the tubule could also occur in the vicinity of the truncation point with the donor organelle for tubules that separate, or closer to their 'fusing' end for tubules that retract back to their donor organelle. Such processes might also, for example, play a role in limiting endosomal release in exocytic pathways where tubular connections undergo exocytosis whilst retaining endosomal connectivity (Prabhat et al., 2007).

A study that is complementary to these analyses has described the processes that are involved in the transfer of the lumenal content of late endosomes to lysosomes in rat kidney fibroblast cells (Bright et al., 2005). Full fusion events between late endosomes and lysosomes were observed relatively frequently, and transfer of dextran between organelles occurred during kiss-and-run/kiss-and-linger events. These differences in mechanisms for membrane receptor and luminal content transfer suggest that late endosomes might have specific stages of maturation that are active in the transfer of these distinct constituents. Consistent with this, others have shown that not all endosomes or

late endosomes/MVBs in a given cell are functionally equivalent (Rink et al., 2005; White et al., 2006).

Following transfer from the limiting membrane of late endosomes, FcRn enters the intraluminal space of the lysosome. This contrasts with the behavior of the lysosomal membrane protein, LAMP-1, which migrates bidirectionally between the limiting membranes of late endosomes and lysosomes without detectable levels of FcRn. This suggests that the transfer and/or entry of FcRn into the lysosomal lumen is driven by a selective process that has not, to our knowledge, been described. Such a process could also be relevant for other, as yet unidentified, membrane receptors that do not enter ILVs in late endosomes (or MVBs) via ubiquitin-dependent or -independent processes (Katzmann et al., 2001; McNatt et al., 2007; Piper and Katzmann, 2007; Reggiori and Pelham, 2001; Urbanowski and Piper, 2001). The question therefore arises as to why distinct lysosomal entry pathways exist for different endocytic receptors. This could be related to a fundamental difference between the pathways taken on the constitutive vs. stimulated degradative pathways; stimulated pathways necessitate the degradation of essentially all relevant receptor cargo whereas constitutive breakdown only applies to a fraction of the receptor load in late endosomes. In addition, ILV entry into MVBs is known to extinguish signaling of receptors such as EGFR (Katzmann et al., 2002), and a process that shortens the period of signaling activity post-internalization might be advantageous.

Recent studies have reported that early endosomal maturation to late endosomes is accompanied by gradual replacement of Rab5 by Rab7 (Rink et al., 2005). Based on these analyses, a model in which all Rab5 is lost from late endosomes before they are competent to fuse with lysosomes has been proposed (Rink et al., 2005). Data shown in CHAPTER 3 demonstrate that Rab5 can persist on the membrane of late endosomes during their interactions with lysosomes. In this context, others have shown that this Rab is involved in trafficking at late stages of the endolysosomal pathway (Duclos et al., 2003). Further, although the lysosomes in HMEC-1 cells are Rab7+, they lack Rab5, which is consistent with multiple earlier studies (Bucci et al., 2000; Christoforidis et al., 1999; Simonsen et al., 1998; Soldati et al., 1995). In combination with the propensity of Rabs to form discrete domains on endosomes (Sonnichsen et al., 2000), this is congruent with the selective transfer of membrane (associated) proteins to lysosomes during late endosomal-lysosomal interactions.

Although not a central focus of this research project, these analyses bear some relevance to the intracellular fate of engineered IgGs, which in turn impacts *in vivo* behavior. The IgG that is used in this research project is an engineered variant of human IgG1 that, relative to wild type IgG1, binds to FcRn with enhanced affinity in the pH range 6.0-7.4 (Vaccaro et al., 2005). IgGs of this class have short *in vivo* half-lives (Dall'Acqua et al., 2002). This research project shows that this IgG, which remains tightly associated with FcRn and is not released during exocytic events (Ober et al., 2004a; Vaccaro et al., 2005), accumulates in lysosomes following several hours of uptake into FcRn+ cells. This degradative fate provides a molecular explanation for the reduced whole body

persistence. By contrast, wild type IgGs that bind to FcRn at pH 6.0 but not detectably at near neutral pH are salvaged from lysosomal degradation in FcRn expressing cells by recycling/transcytosis followed by exocytic release (Ober et al., 2004a; Ober et al., 2004b). Consequently, such IgGs have relatively long *in vivo* half-lives.

In summary, pathways by which the Fc receptor, FcRn, undergoes constitutive degradation have been elucidated. These analyses reveal several novel aspects of endosomal/lysosomal trafficking and have led to a model that could be generally relevant to other membrane receptors. These studies demonstrate that late endosomal contents are not irreversibly destined for lysosomal degradation, with the dominant mechanism of lysosomal delivery involving selective transfer by tubular extensions or kiss-and-linger like processes. Following transfer from the limiting membrane of late endosomes to lysosomes, FcRn accumulates in the intraluminal space of these compartments in a pathway that distinguishes it from other previously characterized receptors that enter ILVs in late endosomes/MVBs prior to lysosomal delivery. These studies are of relevance to understanding the processes that regulate the degradation of membrane receptors within cells.

5.3 Identifying itineraries taken by TCs in the recycling pathway of FcRn with LP-MUM

Receptor recycling represents an essential component of normal cell physiology. This pathway also provides multiple opportunities for drug targeting and delivery. However,

despite extensive analyses, there is a limited understanding concerning the recycling process. A major barrier to the definition of the components constituting this pathway has been the difficulty in characterizing the contributions of tubulovesicular TCs. Specifically, the itineraries taken by TCs and how their effector associations demarcate TCs at different trafficking steps have to date been elusive. The analysis of TCs is complicated by their formation of a complex, highly dynamic interconnected network within cells. Although significant advances have recently been made in fluorescence microscopy, it has proved extremely challenging to track these TCs at high spatial and temporal resolution in three dimensions. In this research project MUM (Prabhat et al., 2007; Prabhat et al., 2004; Ram et al., 2008), combined with localized photoactivation, have been applied to overcome these limitations. This has enabled the characterization of the pathways and effector associations of the TCs that participate in the intracellular recycling pathway involving the Fc receptor, FcRn. Such studies not only have relevance to understanding the recycling process for which FcRn is a representative receptor, but also provide a framework for the global analyses of TCs in cells.

These studies have resulted in the identification of several discrete pathway components that involve TCs and constitute recycling. Importantly, the TCs participating in these components can be distinguished from each other based on associations with the different effectors, APPL1, Rab4 and Rab11 (**Figure 5.2**). The pre-endosomal sorting step involves APPL1+ TCs that fuse with endosomes prior to subsequent trafficking steps. These TCs can also have associated Rab4 and/or Rab11. Following the fusion of APPL1+ TCs with sorting endosomes, the recycling pathway can be categorized into

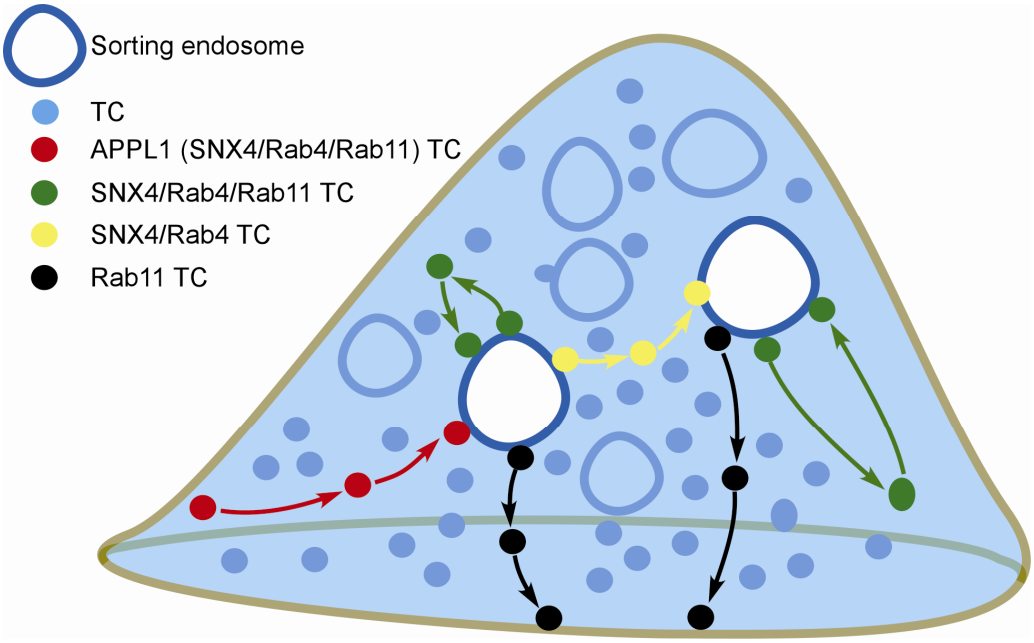

Figure 5.2

A model for itineraries of TCs in the recycling pathway. Four itineraries of TCs were observed in the FcRn recycling pathway. The pre-endosomal TCs that deliver receptors to sorting endosomes from the plasma membrane are APPL1+. These TCs also can have associated Rab4/SNX4 and/or Rab11. The interendosomal TCs are Rab4+/SNX4+ but Rab11-. The post-endosomal TCs are Rab11+ but Rab4-/SNX4-. TCs that are involved in looping events are Rab11+ and SNX4+/Rab4+.

interendosomal transfer, looping or post-endosomal sorting processes. These three possible components are distinguishable based on the following Rab4/Rab11 associations: TCs involved in interendosomal transfer are Rab4+ without detectable levels of Rab11, whereas Rab4+/Rab11+ TCs traffick to and from the same sorting endosome in looping events. By contrast with the pathways involving transport to and from endosomes, the post-endosomal sorting component of recycling is characterized by the segregation of Rab11+ (Rab4-) TCs from sorting endosomes followed by their migration to the cell periphery. SNX4 and Rab4 are extensively colocalized, indicating that Rab4 can be used as a surrogate marker for SNX4 and vice versa.

At the pre-endosomal sorting step, APPL1 can be used as a marker of FcRn+ TCs that fuse with sorting endosomes. In earlier studies, APPL1+ endosomes and macropinosomes have been shown to transport signaling receptors within cells following internalization by clathrin or non-clathrin-mediated pathways (Miaczynska et al., 2004; Zoncu et al., 2009). Here the role of APPL1+ TCs has been extended to the transport of receptors that have no known signaling activity. The effector EEA1 is known to compete for APPL1 binding to Rab5 on APPL1+ compartments (Zoncu et al., 2009). Consistently, data shown in **Figure 4.9** indicates that APPL1 is either undetectable or rapidly lost from larger EEA1+ sorting endosomes.

Interestingly, SNX4 can also be associated with a subset of APPL1+ TCs. This is unexpected since earlier studies demonstrated that SNX4 is involved in the tubulation of sorting endosomes followed by transport of SNX4+ TCs to recycling endosomes (Traer

et al., 2007), rather than the pre-endosomal sorting step. Significantly, all fusion events of APPL1+ TCs with sorting endosomes have associated SNX4, suggesting that this effector accumulates on the TCs as they mature. Rab4, which is extensively colocalized with SNX4, and Rab11, are also present on a subset (50%) of APPL1+ TCs. A relatively small subset (7%) of APPL1+ TCs have detectable levels of both SNX4/Rab4 and Rab11. Thus, although TCs that fuse with endosomes prior to endosomal sorting can be uniquely identified by the presence of APPL1, these TCs can also have associated SNX4/Rab4 and/or Rab11.

A fundamental question in cell biology is how do early/sorting endosomes form? Longstanding models involving the delivery of internalizing receptors via vesicular transport to sorting endosomes (Gruenberg, 2001) have recently been challenged by the observation of homotypic fusion of incoming vesicles followed by their maturation to generate larger early/sorting endosomes (Zoncu et al., 2009). In another study (Rink et al., 2005), the early to late endosome transition has been shown to involve a maturation process designated Rab conversion that also included homotypic fusion of early endosomes. Data shown in CHAPTER 4 indicate that APPL1+ TCs formed early on the endocytic pathway fuse with larger, more static sorting endosomes, providing support for vesicular transport models in this component of the endosomal recycling pathway. Nevertheless, our earlier studies (Gan et al., 2009) are consistent with the maturation of sorting endosomes to late endosomes, indicating that both vesicular transport and maturation models are relevant to the recycling pathway.

By contrast with pre-endosomal sorting TCs, carriers that are involved in post-endosomal sorting, looping to and from the same sorting endosome or interendosomal transfer do not have detectable levels of APPL1. This is congruent with the rapid loss or absence of APPL1 from sorting endosomes (this study, (Miaczynska et al., 2004; Zoncu et al., 2009)). The presence of SNX4/Rab4 on interendosomal transfer, looping TCs and fusing APPL1+ TCs suggests that these effectors mark TCs 'competent' to fuse with either the same or other sorting endosomes. Prior reports demonstrating Rab4-syntaxin 4 or 13 associations (Hoogenraad et al., 2010; Li et al., 2001) indicate that these SNARE proteins could be involved in fusion with sorting endosomes. In support of this concept, post-endosomal sorting Rab11+ TCs do not have detectable levels of SNX4/Rab4 and leave sorting endosomes prior to fusion with a different acceptor, namely the plasma membrane.

The question arises concerning the function of looping events involving the apparently futile cycling of TCs to and from the same endosome in processes that can take several minutes to complete? These events could represent erroneous or poorly targeted sorting steps that require subsequent editing by addition/removal of effectors following return to the parent endosome. Consequently, looping TCs go through iterative cycles of sorting that are energetically costly. Such processes could be analogous to enzymatic proofreading and improve the fidelity of trafficking.

Looping TCs could accumulate other, as yet undefined, effector(s) as they migrate through the cytosol, resulting in a change in composition of the parent endosome. This

could also account for the frequent pauses and turnarounds that are observed for nearly all of these TCs. The behavior of looping TCs suggests the involvement of different motor proteins such as kinesins and dyneins that oppose each others' motion (Schuster et al., 2011b). These motor proteins are associated with movement on microtubules in the minus end direction towards the center of the cell (dynein) or plus end direction towards the cell periphery (kinesin) (Schuster et al., 2011b). Both Rab4 and Rab11 can associate with dynein and/or kinesin (Bielli et al., 2001; Horgan et al., 2010; Imamura et al., 2003; Schonteich et al., 2008), and SNX4 has been shown to bind to dynein indirectly through KIBRA (Traer et al., 2007). It is therefore tempting to speculate that SNX4+/Rab4+/Rab11+ looping TCs initially move towards the cell periphery due to a dominance of kinesin-directed motion. These TCs then stop for 10-50 seconds as more dynein loads onto SNX4/Rab4/Rab11, driven by the increase in concentration of dynein towards the peripheral region of the cell (Schuster et al., 2011a). An increase in dynein loading would result in retrograde, minus end-directed motion towards the donor endosome, consistent with the ability of dynein to override kinesin-mediated directionality (Schuster et al., 2011b; Yao et al., 2012).

These analyses are consistent with the previously ascribed roles of Rab4 and Rab11 in the regulation of receptor recycling rates (McCaffrey et al., 2001; Pagano et al., 2004; Schonteich et al., 2008; Ullrich et al., 1996; van der Sluijs et al., 1992). In both our this and earlier analyses, Rab11 is associated with post-endosomal TCs that directly recycle from sorting endosomes to the plasma membrane (Ward et al., 2005). By contrast, SNX4/Rab4+ TCs (with or without associated Rab11) migrate to other, or even the same,

sorting endosomes in cells. In addition, SNX4 could not be detected using TIRFM during exocytic events involving FcRn+ TCs. Since SNX4 and Rab4 are almost completely colocalized within cells, this is congruent with our earlier analyses in which we could not detect Rab4 associations with exocytic events involving FcRn (Ward et al., 2005).

In summary, using MUM in combination with localized photoactivation, the spatiotemporal dynamics of the TCs involved in different steps of the recycling pathway of FcRn have been characterized. Importantly, this research project has resulted in the identification of different combinations of APPL1, SNX4/Rab4 and Rab11 on tubulovesicular TCs as markers of distinct trafficking components. Importantly, the fusion of incoming APPL1+ TCs with more static sorting endosomes was observed, providing support for vesicular transport models in this early part of the recycling pathway. These data also reveal a novel process involving looping TCs that migrate to and from the same endosome. The approaches described herein should have broad applicability to the analysis of other subcellular trafficking processes that are almost invariably three dimensional in nature and suffer from the crowdedness of TCs, other membranous compartments and cytosolic proteins. Finally, I expect that the observations in this research project could have relevance to multiple other receptors and cargo on endolysosomal/recycling pathways.

5.4 Future directions

The model shown in **Figure 5.2** describes pathway components involved in recycling which forms a basis for further analyses. For example, the connectivity between the different steps to form a complete recycling circuit for FcRn (or any receptor) remains uncertain. For example, does cargo in all TCs undergo interendosomal transfer and/or looping before being sorted into TCs destined for exocytosis? Can a recycling receptor undergo multiple interendosomal transfer events? These questions also relate to defining the trafficking components in spatiotemporal terms that constitute the fast and slow recycling pathways (Grant and Donaldson, 2009; Hopkins and Trowbridge, 1983; Maxfield and McGraw, 2004; Sheff et al., 1999). For example, looping and interendosomal transfer events could contribute to the slow recycling pathway. To address these issues, it will be necessary to carry out single molecule tracking studies for complete cycles of the recycling pathway in three dimensions, which has to date not been achieved due to the enormous technical challenges that this presents.

The relatively high mobility, density and small size of TCs have limited their analysis using fluorescence microscopy. The application of MUM combined with local photoactivation enables TC behavior on the recycling pathway to be characterized in three dimensions. In this research project two focal planes can be imaged simultaneously for two color channels. In future the LP-MUM setup can be improved further for more focal planes and/or color channels by using optical filters of high quality. More photoactivatable fluorescent proteins have been developed recently (Subach et al., 2010).

These new PA-FPs are brighter, more stable and offer more choices with different emission wavelengths.

Although it is still challenging, sophisticated algorithms can be used to detect the events of interest automatically to enhance the throughput of analyzing TCs in the intracellular trafficking pathways.

Having identified four itineraries of TC in the FcRn recycling pathway, we can study further with the LP-MUM how the movement of the TCs is regulated by molecular motors such as dynein and kinesin, how the Rab GTPases interact with molecular motors and how the movement is related to actin and microtubule networks.

The approaches described herein can have broad applicability to the study of other subcellular trafficking processes that are almost invariably three dimensional in nature and suffer from the crowdedness of TCs, other membranous compartments and cytosolic proteins, such as the cell secretion pathway or retrograde transport from endosomes to the *trans*-Golgi network.

APPENDIX A THE DESIGN AND VALIDATION OF LOCALIZED PHOTOACTIVATION-MULTIFOCAL PLANE MICROSCOPY

Introduction

Conventional live cell microscopy generates images from a single focal plane at a time within cells. However, cellular compartments or proteins of interest move within the three dimensional space of a cell. Therefore, when imaging these compartments with conventional live cell microscopy, one of the problems is that the compartments/proteins frequently move out of the focal plane and disappear from the field of view. Focusing devices, such as piezos can be used to image different focal planes sequentially. However the frame rates are relative slow. Also, since the images from different focal planes are acquired sequentially, events of interest occurring in other planes can be missed. Another problem faced in live cell imaging is that cellular compartments of interest can be very dense and motile. Therefore, a single compartment tracked within a field of view with dense, similar structures and background haze can lose its identity easily. To overcome the first problem, MUM has been developed in our laboratory to image different focal planes within cells simultaneously (Prabhat et al., 2004). In this research project a localized photoactivation technique in combination with MUM (LP-MUM) has been developed to facilitate the tracking of motile compartments in three dimensions. The design and development of the LP-MUM imaging station are presented in this chapter.

Localized photoactivation

In order to locally activate photoswitchable fluorescent proteins such as PA-GFP in an individual cellular compartment, such as a sorting endosome of 1-2 µm in diameter in HMEC-1 cells, a smaller focal volume is desired for the 405 nm activation light beam. It is difficult to obtain such a small focal volume using conventional wide field illumination. Hence a DCS-120 confocal scan head from Becker & Hickl GmbH was used to produce a focal spot. To combine the confocal photoactivation light path and wide field excitation, a dual microscope body/dual objective configuration using two Zeiss Axio Observer.A1 inverted microscope bodies was therefore designed (**Figure 6.1**). The transmitted light illuminator carrier was detached from each microscope body. The stage and the binocular section of the binocular tube were removed from one microscope body. This microscope body was oriented in an upside down position and mounted on the top of the other one through linear translation stages (Ram et al., 2009). The confocal scan head was mounted on the left sideport of the microscope on the top. The 405 nm laser beam from a BDL-405-SMC 405 nm laser (Becker-Hickl) was introduced to the scan head through an optical fiber. A Carl Zeiss ACHROPLAN 63x/0.95 W water-dipping objective lens was mounted on the top microscope body and spacers were used to make sure that the tip of the objective can reach the sample placed on the stage of the bottom microscope. The 405 nm laser beam passes through the pinhole in the scan head and the water dipping objective lens so it forms a small focal volume within the sample to photoactivate individual compartments from the top of the sample. The location of the focal point of the 405 nm laser is adjustable through the linear translation stages (X, Y

directions) and the focusing knob of the top microscope body (Z direction). The samples are excited by lasers of different wavelengths through the opposing, bottom objective, a Zeiss 1.45 NA 100x αPlan-Fluar oil immersion objective lens that was mounted in the bottom microscope. The fluorescent signal emitted from the sample is collected by the bottom objective and guided into the cameras.

This design allows us to simultaneously photoactivate the photoswitchable fluorescent proteins, excite the samples and collect the data. The target endosomes can be moving during localized photoactivation. Hence a successful photoactivation requires rapidly switching on the 405 nm laser. Our dual microscope design facilitates the rapid photoactivation of fluorescent proteins within cells.

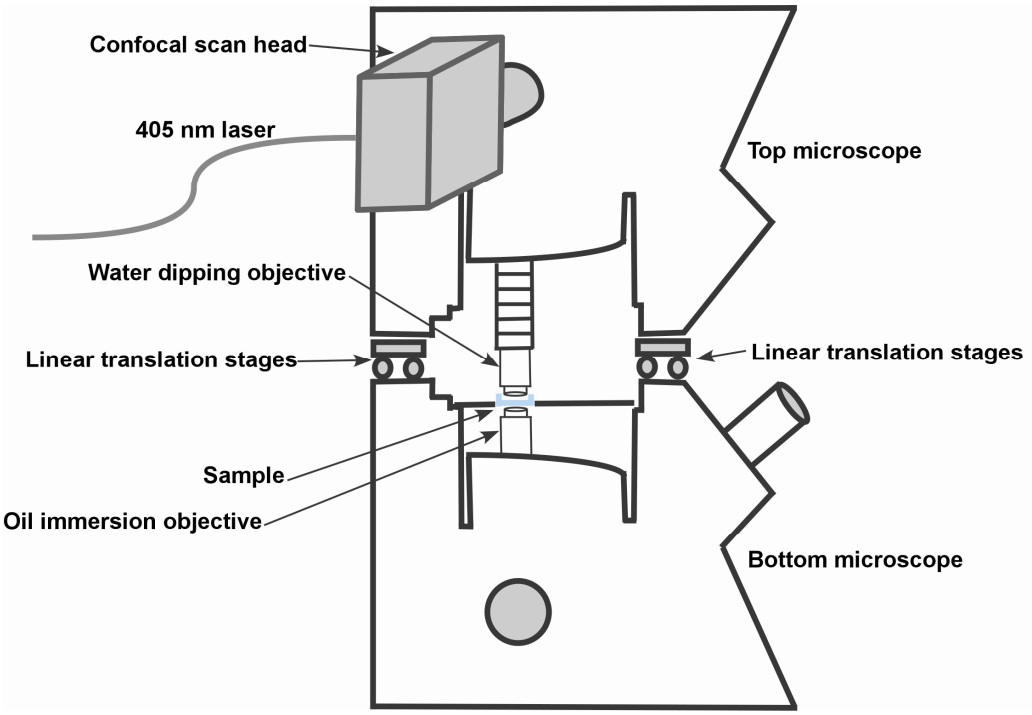

Figure 6.1

The dual microscope/dual objective configuration for localized photoactivation. One microscope body is oriented in an upside down position and mounted on the top of the other one through linear translation stages. A confocal scan head was mounted on the left sideport of the top microscope. The 405 nm laser beam was introduced to the scan head through an optical fiber. A Carl Zeiss ACHROPLAN 63x/0.95 W water-dipping objective lens was mounted on the top microscope body for localized photoactivation. The sample is excited through a Zeiss 1.45 NA 100x αPlan-Fluar oil immersion objective lens mounted in the bottom microscope. The fluorescence signal emitted from the sample is collected by the bottom objective.

Localized photoactivation-multifocal plane microscopy

Our lab has developed MUM to image multiple focal planes within cells simultaneously (Prabhat et al., 2007; Prabhat et al., 2004). The principle of MUM is shown in **Figure 6.2**. The objects in the focal plane of the objective are imaged by a camera placed at the infinity corrected detector plane of the tube lens. However, if the camera is moved toward the tube lens along the optical axis (at the translated detector plane of the tube lens), it will image another focal plane in the sample space, which is away from the standard infinity corrected focal plane of the objective. Similarly, if the camera is moved away from the tube lens along the optical axis, it will image another focal plane closer to the objective than the infinity corrected standard focal plane. Therefore, using two (or more) cameras and a dual view adaptor (s), objects in different planes of cells can be imaged simultaneously. The configuration of a LP-MUM setup that can simultaneously image two focal planes for two color channels at higher frame rates is presented in this subsection.

Four cameras were used to image two focal planes simultaneously for two color channels (green and red) in this configuration (**Figure 6.3**). Each of the cameras images one single color channel for a given focal plane by using wavelength dependent beam splitters. This design avoids the usage of a filter wheel and shutters, allowing acquisition at higher frame rates. A Zeiss 1.45 NA 100x αPlan-Fluar oil immersion objective was mounted on the bottom Zeiss Axio Observer.A1 microscope for excitation and the collection of fluorescence emission. A Sapphire 488-50 CDRH laser (Coherent, Santa Clara, CA)

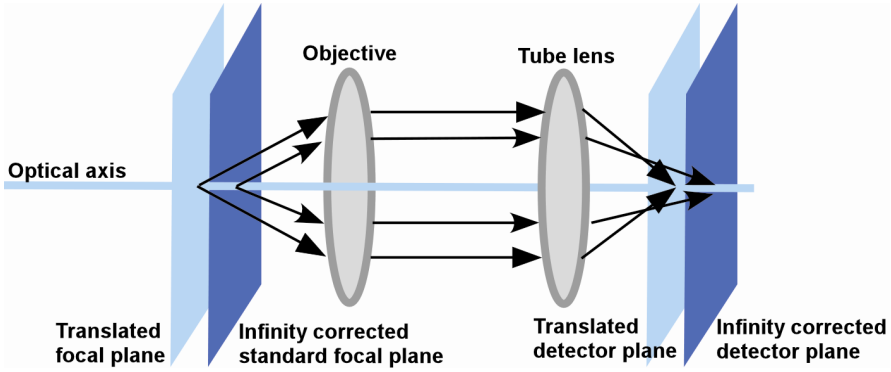

Figure 6.2

The principle of MUM. The objects in the focal plane of the objective are imaged by a camera placed at the infinity corrected detector plane of the tube lens. Another camera placed at the translated detector plane of the tube lens images objects at the translated focal plane of the objective.

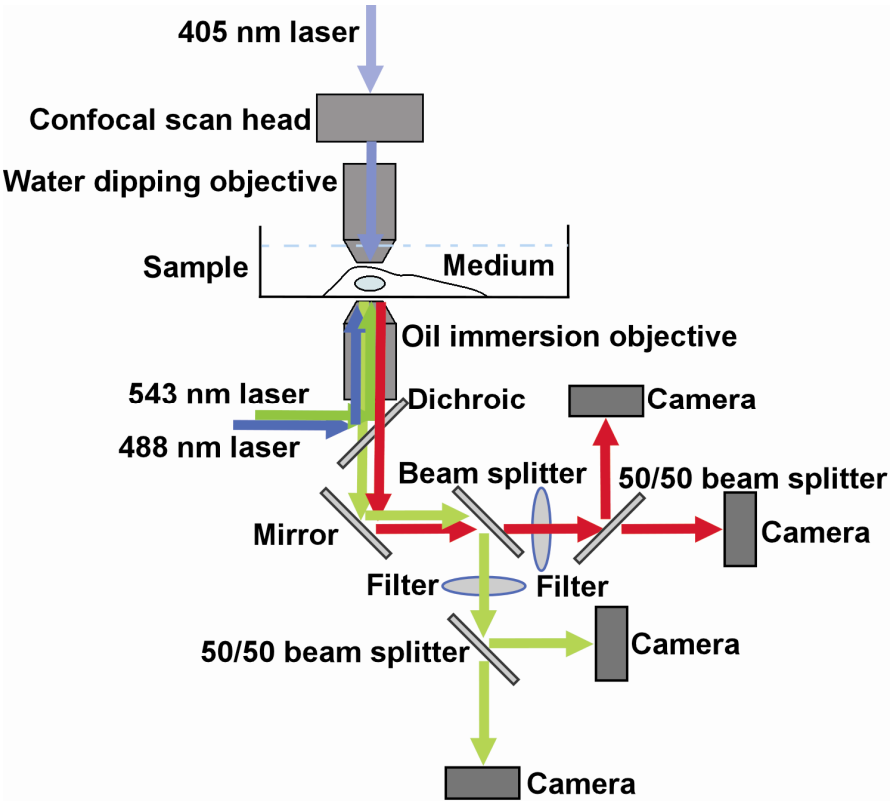

Figure 6.3

LP-MUM configuration. The LP-MUM imaging station is composed of two inverted microscope bodies. A confocal scan head and a water dipping objective were mounted on the top microscope to introduce a 405 nm photoactivation laser from the top of the sample. The sample is placed on the stage of the bottom microscope. The sample is excited and fluorescence emission is collected with an oil immersion objective mount on the bottom microscope body. Four cameras were attached to the bottom microscope through dual view adaptors.

was used for GFP/PAGFP excitation and a MGL-III-543nm-50mW laser (Opto Engine LLC, Midvale, UT) for mCherry/mRFP/Alexa 555 excitation. A 488/543/633 SPC XT dichroic from Chroma Technology was used to split the excitation and emission light. The lamp housing of the bottom microscope was removed and the excitation laser beams were introduced to the dichroic through the reflected light mount on the rear of the bottom microscope. Two Hamamatsu C-8484-05G cameras (Bridgewater, NJ) and two Andor iXon cameras (South Windsor, CT) were used for data collection. The four cameras were mounted onto three dual view adaptors attached to the left sideport of the bottom microscope. The parfocality of the four cameras and the distance between the two focal planes were calibrated as described previously (Prabhat et al., 2004). An Andor camera was placed at the standard distance (42.5 mm) from the tube lens to collect green fluorescence emission for the designed focal plane. Based on the plane calibration experiments, a Hamamatsu camera was placed at a position which is 44.5 mm from the tube lens so that it can collect red fluorescence emission from the designed focal plane. Two cameras (Hamamatsu and Andor) were placed at modified distances (34.5 mm and 36.5 mm, respectively) from the tube lenses to collect red and green fluorescence emission from a plane which is 800 nm above the designed focal plane within the cell, respectively. The fluorescence is split by a Chroma 560DCSP beamsplitter into two light paths. The mCherry/mRFP/Alexa 555 fluorescence is reflected by the beamsplitter, passes through a Chroma HQ605/75 emission filter and is projected to the two Hamamatsu cameras. The GFP/PAGFP fluorescence passes through the beamsplitter, is filtered by a Chroma HQ515/30 emission filter and guided to the two Andor cameras. Hence the EGFP/PAGFP and mCherry/mRFP/Alexa 555 images from two different focal

planes in the samples can be acquired simultaneously by four cameras. This four camera MUM setup allows us to acquire imaging data from two focal planes for two color channels (green and red) at higher frame rates, since a filter wheel and shutters are not used.

The efficiency of localized photoactivation was verified with a gel containing purified and immobilized PAGFP protein. The purified PAGFP protein was immobilized in the polymer Mowiol gel (CHAPTER 2) and locally photoactivated with the LP-MUM setup. Before imaging an experimental sample, the two objectives mounted in the top and bottom microscopes need to be aligned so that they can both focus on similar fields of view. A dense bead sample was made by plating 50 µL 0.1 µm green yellow beads (Fluoresbrite carboxylate YG microspheres 0.1 micron, Polysciences Inc, Warrington, PA) to a MatTek dish. When illuminating the bead samples with the focused 405 nm laser beam from the top, a bright spot can be seen with the bottom oil immersion objective. By adjusting the linear translation stages between the two microscope bodies, the beam of the 405 nm laser that is focused by the top water dipping objective can be placed into the field of view of the bottom oil immersion objective.

PAGFP in a volume of about 1 µm in diameter can be photoactivated (**Figure 6.4**). In the bottom panel of **Figure 6.4**, the immobilized PAGFP molecules in the gel were in the dark state initially under 488 nm excitation at 0 s. A 405 nm laser beam was switched on and focused onto a small volume in the gel for about 1-2 s. After the 405 nm laser was switched off, there is a bright spot of about 1 µm in diameter seen under excitation of the

488 nm laser in the field of view (3 s), indicating that PAGFP molecules in this volume were photoactivated. The intensity plot along a line across the brightest pixel of the spot shows that the full width at half maximum of the spot is about 1 μm. Since sorting endosomes in HMEC-1 cells are usually 1-2 μm in diameter, our setup can therefore specifically photoactivate individual sorting endosomes.

The efficiency of photoactivation was also verified with live cells. **Figure 6.5** shows that an individual endosome in a HMEC-1 cell co-transfected with mCherry-SNX4 and PAGFP-Rab11 can be photoactivated. mCherry-SNX4 were observed in ring-like sorting endosomes that are about 1-2 μm in diameter and tubulovesicular TCs in transfected cells, as shown in the right hand side of **Figure 6.5**. The PAGFP signal is originally very weak for the entire field of view. The 405 nm laser coupled to the top microscope was turned on transiently for about one second and focused onto one of the ring-like sorting endosomes by the water dipping objective. The PAGFP signal from the target sorting endosome increased significantly afterwards, as shown in the left hand side of **Figure 6.5**. Other PAGFP labeled proteins in the same cell were not photoactivated and remained undetectable.

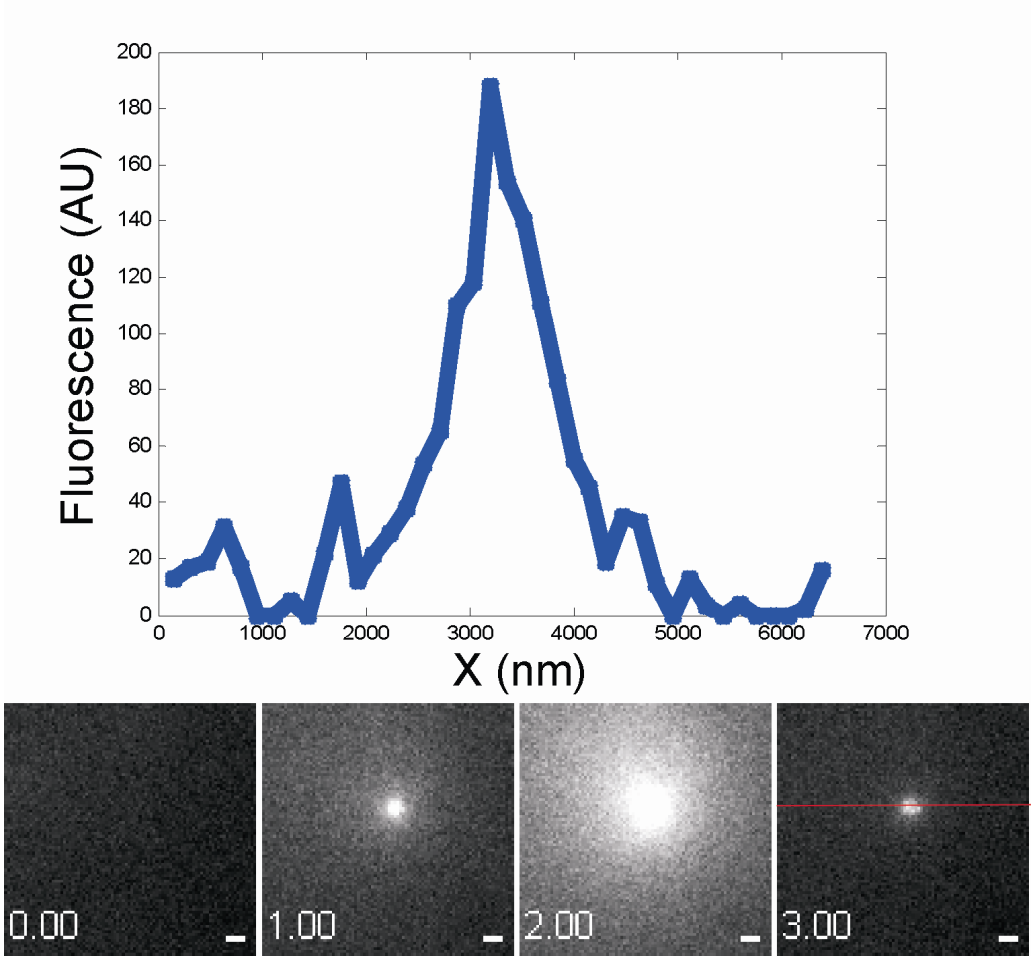

Figure 6.4

Photoactivating immobilized PAGFP molecules in a gel. Purified, recombinant PAGFP was immobilized in the polymer Mowiol gel. The immobilized PAGFP molecules in the gel were in the dark state initially under 488 nm excitation at 0 s. After illumination with a 405 nm laser beam for 1 s, PAGFP molecules in a volume about 1 µm in diameter were photoactivated. The intensity plot along the red line across the brightest pixel of the spot shows that the full width at half maximum of the spot is about 1 µm. Scale bar = 1 µm.

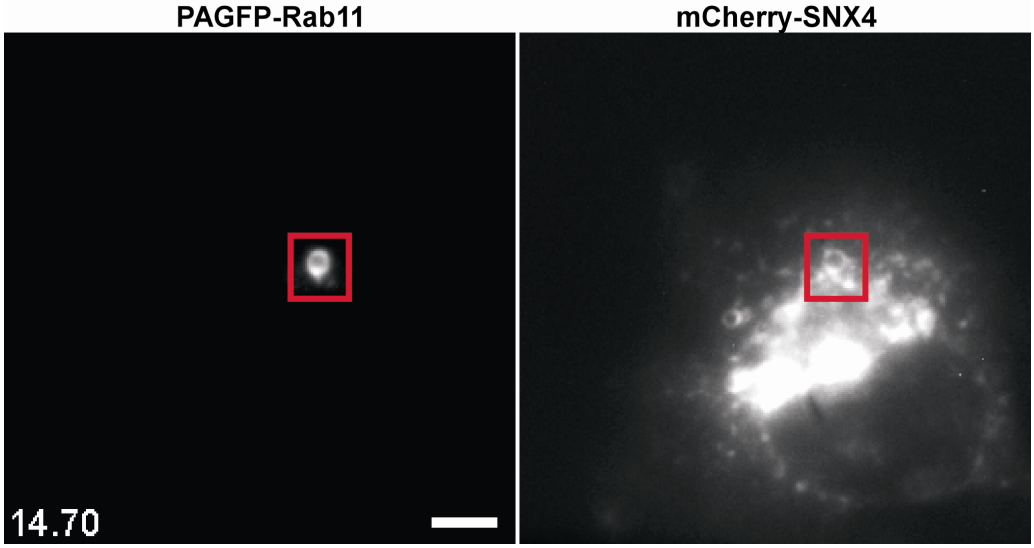

Figure 6.5

Photoactivating a single endosome. HMEC-1 cells were co-transfected with PAGFP-Rab11/mCherry-SNX4. PAGFP in an endosome highlighted by a red rectangle in the image of the mCherry-SNX4 channel (right panel) was photoactivated, as indicated by a red box in the image of the PAGFP-Rab11 channel (left panel). Scale bar = 5 μm.

Registration

The purpose of registration is to spatially align images acquired by the four different cameras. The scripts used for image registration were developed using the MATLAB (Natick, MA) technical computing language and the Image Processing Toolbox.

Bead samples were prepared by coating the glass bottoms of MatTek dishes (35-mm, glass-bottom, 10 mm microwell dishes) with 200 μL Poly-L-Lysine for 15 minutes. After 15 minutes, the Poly-L-Lysine was removed and the dishes were allowed to dry for an additional 15 minutes. Tetra-Speck Microspheres (100 nm diameter, Invitrogen) were diluted 100-fold in PBS and 200 μL diluted solution was added to the microwells of the dishes. The bead mixture was pipetted up and down several times into the microwell portions to ensure the solution was mixed well and that clumping of the beads was minimized. After 15 minutes the bead mixture was removed from the microwells 2.5 mL PBS added to the dishes. The bead samples were imaged by four cameras with exactly the same LP-MUM microscope configuration described previously on the same day as the live cell imaging experiments. The focus of the bottom-mounted oil objective was manually adjusted during acquisition to make sure that the in-focus images of the bead sample were recorded by four cameras sequentially. The images were processed by custom-written MATLAB scripts and bead objects were automatically detected with the Olivo-Marin algorithm (Olivo-Marin, 2002). The correspondence of 8-10 beads which can be identified in the fields of view of all four cameras was manually specified to obtain the registration parameters. The transformation parameters for the images from the

four cameras were determined by using the Affine transformation algorithm. The transformation parameters were first used to register the images of the bead samples for evaluation and then applied to the live cell data.

APPENDIX B MOVIE LEGENDS

Movie 3.1. Tubule-mediated transfer of FcRn from the limiting membrane of a late endosome to the intraluminal space of a lysosome. The movie corresponds to **Figure 3.6**. mRFP-FcRn is shown in red, and LAMP-1 is shown in green in the overlay data. The right column shows the single color (mRFP-FcRn) data. Arrows indicate the event of interest as described in the figure legend. Movie plays at nine times the acquisition speed. Scale bar = 1 μm.

Movie 3.2, Tubule-mediated transfer of FcRn from the limiting membrane of a late endosome to the intraluminal space of a lysosome. The movie corresponds to **Figure 3.7**. mRFP-FcRn is shown in red, and LAMP-1 is shown in green in the overlay data. The right column shows the single color (mRFP-FcRn) data. Arrows indicate the event of interest as described in the figure legend. Movie plays at six times the acquisition speed. Scale bar = 1 μm.

Movie 3.3. Tubule-mediated transfer of labeled IgG to a lysosome. The movie corresponds to **Figure 3.10**. Dextran is shown in red, FcRn-GFP is shown in green, and IgG is shown in blue in the overlay data. The right column shows the single color (IgG) data. Arrows indicate the event of interest as described in the figure legend. Movie plays at three times the acquisition speed. Scale bar = 1 μm.

Movie 3.4. IgG is transferred to a lysosome in an interaction that resembles kiss-and-linger. The movie corresponds to **Figure 3.12**. Dextran is shown in red, FcRn-GFP is shown in green, and IgG is shown in blue in the overlay data. Arrows indicate the event of interest as described in the figure legend. Movie plays at nine times the acquisition speed. Scale bar = 1 μm.

Movie 3.5. Tubule-mediated transfer of labeled IgG to a lysosome. The movie corresponds to **Figure 3.14**. Dextran is shown in red, FcRn-GFP is shown in green, and IgG is shown in blue in the overlay data. The right column shows the single color (IgG) data. Arrows indicate the event of interest as described in the figure legend. Movie plays at fifteen times the acquisition speed. Scale bar = 1 μm.

Movie 3.6. Tubule-mediated transfer of LAMP-1 from a late endosome to a lysosome. The movie corresponds to **Figure 3.17**. mRFP-FcRn is shown in red, LAMP-1 is shown in green, and IgG is shown in blue in the overlay data. Arrows indicate the event of interest as described in the figure legend. Movie plays at nine times the acquisition speed. Scale bar = 1 μm.

Movie 3.7. Tubule-mediated transfers of LAMP-1 from a lysosome to a late endosome. The movie corresponds to **Figure 3.19**. mRFP-FcRn is shown in red, LAMP-1 is shown in green, and IgG is shown in blue in the overlay data. The middle and right columns show the single color (LAMP-1 and mRFP-FcRn, respectively) data. Arrows

indicate events of interest as described in the figure legend. Movie plays at three times the acquisition speed. Scale bar = 1 μm.

Movie 3.8. Transfer of FcRn to a lysosome from a Rab5+ endosome. The movie corresponds to **Figure 3.21**. mRFP-FcRn is shown in red, Rab5 is shown in green, and dextran is shown in blue in the overlay data. The right column shows the single color (mRFP-FcRn) data. Arrows indicate the event of interest as described in the figure legend. Movie plays at nine times the acquisition speed. Scale bar = 1 μm.

Movie 3.9. Transfer of Rab7 from an endosome to a lysosome. The movie corresponds to **Figure 3.25**. mRFP-FcRn is shown in red, Rab7 is shown in green, and dextran is shown in blue in the overlay data. The single color data of mRFP-FcRn (the second column), Rab7 (the third column), and dextran (the fourth column) are also shown. Arrows indicate the event of interest as described in the figure legend. Movie plays at three times the acquisition speed. Scale bar = 1 μm.

Movie 4.1. FcRn can be seen in ring-like sorting endosomes and tubulovesicular TCs. The movie corresponds to **Figure 4.1**. Movie plays at 4 times the acquisition speed. Scale bars = 5 μm.

Movie 4.2. A FcRn+/Rab4+ looping event. The movie corresponds to **Figure 4.6**. FcRn-PAGFP and mRFP-Rab4 are shown as green and red in the overlay data, respectively. The top row shows images from the upper plane and the bottom row shows

images from the lower plane. Arrows indicate the event of interest as described in the figure legend. Movie plays at 3 times the acquisition speed. Scale bars = 1 μm.

Movie 4.3. A FcRn+/APPL1+ TC merges with a sorting endosome. The movie corresponds to **Figure 4.7**. The first and second columns show the single color data of mRFP-FcRn (red in overlay data) and GFP-APPL1 (green in overlay data), respectively. The top row shows images from the upper plane and the bottom row shows images from the lower plane. Arrows indicate the event of interest as described in the figure legend. Movie plays at 2 times the acquisition speed. Scale bars = 1 μm.

Movie 4.4. A MST-HN+/APPL1+ TC merges with a sorting endosome. The movie corresponds to **Figure 4.8**. MST-HN-A555 and GFP-APPL1 are shown as red and green in the overlay data, respectively. The top row shows images from the upper plane and the bottom row shows images from the lower plane. Arrows indicate the event of interest as described in the figure legend. Movie plays at 2 times the acquisition speed. Scale bars = 1 μm.

Movie 4.5. A SNX4+/FcRn+ TC transfers between sorting endosomes. The movie corresponds to **Figure 4.18**. The first and second columns show the single color data of GFP-SNX4 (green in overlay data) and mRFP-FcRn (red in overlay data), respectively. The top row shows images from the upper plane and the bottom row shows images from the lower plane. Arrows indicate the event of interest as described in the figure legend. Movie plays at 2 times the acquisition speed. Scale bars = 1 μm.

Movie 4.6. A SNX4+/Rab4+ TC transfers between sorting endosomes. The movie corresponds to **Figure 4.21**. The first and second columns show the single color data of mCherry-SNX4 (red in overlay data) and PAGFP-Rab4 (green in overlay data), respectively. The top row shows images from the upper plane and the bottom row shows images from the lower plane. Arrows indicate the event of interest as described in the figure legend. Movie plays at 2 times the acquisition speed. Scale bars = 1 μm.

Movie 4.7. A SNX4+/Rab4+ TC returns to a sorting endosome. The movie corresponds to **Figure 4.23**. PAGFP-Rab4 and mCherry-SNX4 are shown as green and red in the overlay data, respectively. The top row shows images from the upper plane and the bottom row shows images from the lower plane. Arrows indicate the event of interest as described in the figure legend. Movie plays at 2 times the acquisition speed. Scale bars = 1 μm.

Movie 4.8. A SNX4+/Rab11+ TC returns to a sorting endosome. The movie corresponds to **Figure 4.24**. The first and second columns show the single color data of mCherry-SNX4 (red in overlay data) and PAGFP-Rab11 (green in overlay data), respectively. Arrows indicate the event of interest as described in the figure legend. Movie plays at 5 times the acquisition speed. Scale bars = 1 μm.

Movie 4.9. A FcRn+/Rab11+ TC leaves a sorting endosome for plasma membrane. The movie corresponds to **Figure 4.25**. The first and second columns show the single color data of mRFP-FcRn (red in overlay data) and PAGFP-Rab11 (green in overlay

data), respectively. The top row shows images from the upper plane and the bottom row shows images from the lower plane. Arrows indicate the event of interest as described in the figure legend. Movie plays at 2 times the acquisition speed. Scale bars = 1 μm.

Movie 4.10. A SNX4-/Rab11+ TC leaves a sorting endosome for plasma membrane. The movie corresponds to **Figure 4.26**. The first and second columns show the single color data of mCherry-SNX4 (red in overlay data) and PAGFP-Rab11 (green in overlay data), respectively. The top row shows images from the upper plane and the bottom row shows images from the lower plane. Arrows indicate the event of interest as described in the figure legend. Movie plays at 2 times the acquisition speed. Scale bars = 1 μm.

BIBLIOGRAPHY

Abrahamson, D.R., and Rodewald, R. (1981). Evidence for the sorting of endocytic vesicle contents during the receptor-mediated transport of IgG across the newborn rat intestine. J Cell Biol *91*, 270-280.

Ahouse, J.J., Hagerman, C.L., Mittal, P., Gilbert, D.J., Copeland, N.G., Jenkins, N.A., and Simister, N.E. (1993). Mouse MHC class I-like Fc receptor encoded outside the MHC. J Immunol *151*, 6076-6088.

Antohe, F., Radulescu, L., Gafencu, A., Ghetie, V., and Simionescu, M. (2001). Expression of functionally active FcRn and the differentiated bidirectional transport of IgG in human placental endothelial cells. Human Immunol *62*, 93-105.

Berthiaume, E.P., Medina, C., and Swanson, J.A. (1995). Molecular size-fractionation during endocytosis in macrophages. J Cell Biol *129*, 989-998.

Betzig, E., Patterson, G.H., Sougrat, R., Lindwasser, O.W., Olenych, S., Bonifacino, J.S., Davidson, M.W., Lippincott-Schwartz, J., and Hess, H.F. (2006). Imaging intracellular fluorescent proteins at nanometer resolution. Science *313*, 1642-1645.

Bielli, A., Thornqvist, P.O., Hendrick, A.G., Finn, R., Fitzgerald, K., and McCaffrey, M.W. (2001). The small GTPase Rab4A interacts with the central region of cytoplasmic dynein light intermediate chain-1. Biochem Biophys Res Commun *281*, 1141-1153.

Borvak, J., Richardson, J., Medesan, C., Antohe, F., Radu, C., Simionescu, M., Ghetie, V., and Ward, E.S. (1998). Functional expression of the MHC class I-related receptor, FcRn, in endothelial cells of mice. Int Immunol *10*, 1289-1298.

Brambell, F.W. (1966). The transmission of immunity from mother to young and the catabolism of immunoglobulins. Lancet *2*, 1087-1093.

Bright, N.A., Gratian, M.J., and Luzio, J.P. (2005). Endocytic delivery to lysosomes mediated by concurrent fusion and kissing events in living cells. Curr Biol *15*, 360-365.

Bucci, C., Thomsen, P., Nicoziani, P., McCarthy, J., and van Deurs, B. (2000). Rab7: a key to lysosome biogenesis. Mol Biol Cell *11*, 467-480.

Burmeister, W.P., Gastinel, L.N., Simister, N.E., Blum, M.L., and Bjorkman, P.J. (1994). Crystal structure at 2.2 A resolution of the MHC-related neonatal Fc receptor. Nature *372*, 336-343.

Cauza, K., Hinterhuber, G., Dingelmaier-Hovorka, R., Brugger, K., Klosner, G., Horvat, R., Wolff, K., and Foedinger, D. (2005). Expression of FcRn, the MHC class I-related receptor for IgG, in human keratinocytes. J Invest Dermatol *124*, 132-139.

Christoforidis, S., McBride, H.M., Burgoyne, R.D., and Zerial, M. (1999). The Rab5 effector EEA1 is a core component of endosome docking. Nature *397*, 621-625.

Claypool, S.M., Dickinson, B.L., Yoshida, M., Lencer, W.I., and Blumberg, R.S. (2002). Functional reconstitution of human FcRn in Madin-Darby canine kidney cells requires co-expressed human beta 2-microglobulin. J Biol Chem *277*, 28038-28050.

Cullen, P.J. (2008). Endosomal sorting and signalling: an emerging role for sorting nexins. Nat Rev Mol Cell Biol *9*, 574-582.

Dall'Acqua, W.F., Woods, R.M., Ward, E.S., Palaszynski, S.R., Patel, N.K., Brewah, Y.A., Wu, H., Kiener, P.A., and Langermann, S. (2002). Increasing the affinity of a human IgG1 for the neonatal Fc receptor: biological consequences. J Immunol *169*, 5171-5180.

Daniels, G.M., and Amara, S.G. (1999). Regulated trafficking of the human dopamine transporter. Clathrin-mediated internalization and lysosomal degradation in response to phorbol esters. J Biol Chem *274*, 35794-35801.

Daro, E., van der Sluijs, P., Galli, T., and Mellman, I. (1996). Rab4 and cellubrevin define different early endosome populations on the pathway of transferrin receptor recycling. Proc Natl Acad Sci U S A *93*, 9559-9564.

de Renzis, S., Sonnichsen, B., and Zerial, M. (2002). Divalent Rab effectors regulate the sub-compartmental organization and sorting of early endosomes. Nat Cell Biol *4*, 124-133.

Delamarre, L., Pack, M., Chang, H., Mellman, I., and Trombetta, E.S. (2005). Differential lysosomal proteolysis in antigen-presenting cells determines antigen fate. Science *307*, 1630-1634.

Demarco, I.A., Periasamy, A., Booker, C.F., and Day, R.N. (2006). Monitoring dynamic protein interactions with photoquenching FRET. Nat Methods *3*, 519-524.

Deneka, M., Neeft, M., Popa, I., van Oort, M., Sprong, H., Oorschot, V., Klumperman, J., Schu, P., and van der Sluijs, P. (2003). Rabaptin-5alpha/rabaptin-4 serves as a linker between rab4 and gamma(1)-adaptin in membrane recycling from endosomes. EMBO J *22*, 2645-2657.

Dickinson, B.L., Badizadegan, K., Wu, Z., Ahouse, J.C., Zhu, X., Simister, N.E., Blumberg, R.S., and Lencer, W.I. (1999). Bidirectional FcRn-dependent IgG transport in a polarized human intestinal epithelial cell line. J Clin Invest *104*, 903-911.

Duclos, S., Corsini, R., and Desjardins, M. (2003). Remodeling of endosomes during lysosome biogenesis involves 'kiss and run' fusion events regulated by rab5. J Cell Sci *116*, 907-918.

Eggers, C.T., Schafer, J.C., Goldenring, J.R., and Taylor, S.S. (2009). D-AKAP2 interacts with Rab4 and Rab11 through its RGS domains and regulates transferrin receptor recycling. J Biol Chem *284*, 32869-32880.

Firan, M., Bawdon, R., Radu, C., Ober, R.J., Eaken, D., Antohe, F., Ghetie, V., and Ward, E.S. (2001). The MHC class I-related receptor, FcRn, plays an essential role in the maternofetal transfer of gamma-globulin in humans. Int Immunol *13*, 993-1002.

Fouraux, M.A., Deneka, M., Ivan, V., van der Heijden, A., Raymackers, J., van Suylekom, D., van Venrooij, W.J., van der Sluijs, P., and Pruijn, G.J. (2004). Rabip4' is an effector of rab5 and rab4 and regulates transport through early endosomes. Mol Biol Cell *15*, 611-624.

Gan, Z., Ram, S., Vaccaro, C., Ober, R.J., and Ward, E.S. (2009). Analyses of the recycling receptor, FcRn, in live cells reveal novel pathways for lysosomal delivery. Traffic *10*, 600-614.

Gandhi, S.P., and Stevens, C.F. (2003). Three modes of synaptic vesicular recycling revealed by single-vesicle imaging. Nature *423*, 607-613.

Ghetie, V., Hubbard, J.G., Kim, J.K., Tsen, M.F., Lee, Y., and Ward, E.S. (1996). Abnormally short serum half-lives of IgG in beta 2-microglobulin-deficient mice. Eur J Immunol *26*, 690-696.

Ghetie, V., Popov, S., Borvak, J., Radu, C., Matesoi, D., Medesan, C., Ober, R.J., and Ward, E.S. (1997). Increasing the serum persistence of an IgG fragment by random mutagenesis. Nat Biotechnol *15*, 637-640.

Ghetie, V., and Ward, E.S. (2000). Multiple roles for the major histocompatibility complex class I- related receptor FcRn. Annu Rev Immunol *18*, 739-766.

Grant, B.D., and Donaldson, J.G. (2009). Pathways and mechanisms of endocytic recycling. Nat Rev Mol Cell Biol *10*, 597-608.

Gruenberg, J. (2001). The endocytic pathway: a mosaic of domains. Nat Rev Mol Cell Biol *2*, 721-730.

Haft, C.R., de la Luz Sierra, M., Barr, V.A., Haft, D.H., and Taylor, S.I. (1998). Identification of a family of sorting nexin molecules and characterization of their association with receptors. Mole Cell Biol *18*, 7278-7287.

Hales, C.M., Vaerman, J.P., and Goldenring, J.R. (2002). Rab11 family interacting protein 2 associates with Myosin Vb and regulates plasma membrane recycling. J Biol Chem *277*, 50415-50421.

Hettema, E.H., Lewis, M.J., Black, M.W., and Pelham, H.R. (2003). Retromer and the sorting nexins Snx4/41/42 mediate distinct retrieval pathways from yeast endosomes. EMBO J *22*, 548-557.

Hoogenraad, C.C., Popa, I., Futai, K., Martinez-Sanchez, E., Wulf, P.S., van Vlijmen, T., Dortland, B.R., Oorschot, V., Govers, R., Monti, M.*, et al.* (2010). Neuron specific Rab4 effector GRASP-1 coordinates membrane specialization and maturation of recycling endosomes. PLoS Biol *8*, e1000283.

Hopkins, C.R., and Trowbridge, I.S. (1983). Internalization and processing of transferrin and the transferrin receptor in human carcinoma A431 cells. J Cell Biol *97*, 508-521.

Horgan, C.P., Hanscom, S.R., Jolly, R.S., Futter, C.E., and McCaffrey, M.W. (2010). Rab11-FIP3 links the Rab11 GTPase and cytoplasmic dynein to mediate transport to the endosomal-recycling compartment. J Cell Sci *123*, 181-191.

Husi, H., Ward, M.A., Choudhary, J.S., Blackstock, W.P., and Grant, S.G. (2000). Proteomic analysis of NMDA receptor-adhesion protein signaling complexes. Nature Neurosci *3*, 661-669.

Hutagalung, A.H., and Novick, P.J. (2011). Role of Rab GTPases in membrane traffic and cell physiology. Physiol Rev *91*, 119-149.

Imamura, T., Huang, J., Usui, I., Satoh, H., Bever, J., and Olefsky, J.M. (2003). Insulin-induced GLUT4 translocation involves protein kinase C-lambda-mediated functional coupling between Rab4 and the motor protein kinesin. Mole Cell Biol *23*, 4892-4900.

Israel, E.J., Wilsker, D.F., Hayes, K.C., Schoenfeld, D., and Simister, N.E. (1996). Increased clearance of IgG in mice that lack beta 2-microglobulin: possible protective role of FcRn. Immunology *89*, 573-578.

Jaiswal, J.K., Chakrabarti, S., Andrews, N.W., and Simon, S.M. (2004). Synaptotagmin VII restricts fusion pore expansion during lysosomal exocytosis. PLoS Biol *2*, E233.

Junghans, R.P., and Anderson, C.L. (1996). The protection receptor for IgG catabolism is the beta2-microglobulin-containing neonatal intestinal transport receptor. Proc Natl Acad Sci U S A *93*, 5512-5516.

Katayama, H., Yamamoto, A., Mizushima, N., Yoshimori, T., and Miyawaki, A. (2008). GFP-like proteins stably accumulate in lysosomes. Cell Struct Funct *33*, 1-12.

Katzmann, D.J., Babst, M., and Emr, S.D. (2001). Ubiquitin-dependent sorting into the multivesicular body pathway requires the function of a conserved endosomal protein sorting complex, ESCRT-I. Cell *106*, 145-155.

Katzmann, D.J., Odorizzi, G., and Emr, S.D. (2002). Receptor downregulation and multivesicular-body sorting. Nat Rev Mol Cell Biol *3*, 893-905.

Kim, P.K., Mullen, R.T., Schumann, U., and Lippincott-Schwartz, J. (2006). The origin and maintenance of mammalian peroxisomes involves a de novo PEX16-dependent pathway from the ER. J Cell Biol *173*, 521-532.

Krsmanovic, T., Pawelec, A., Sydor, T., and Kolling, R. (2005). Control of Ste6 recycling by ubiquitination in the early endocytic pathway in yeast. Mol Biol Cell *16*, 2809-2821.

Leprince, C., Le Scolan, E., Meunier, B., Fraisier, V., Brandon, N., De Gunzburg, J., and Camonis, J. (2003). Sorting nexin 4 and amphiphysin 2, a new partnership between endocytosis and intracellular trafficking. J Cell Sci *116*, 1937-1948.

Li, L., Omata, W., Kojima, I., and Shibata, H. (2001). Direct interaction of Rab4 with syntaxin 4. J Biol Chem *276*, 5265-5273.

Lindsay, A.J., and McCaffrey, M.W. (2004). The C2 domains of the class I Rab11 family of interacting proteins target recycling vesicles to the plasma membrane. J Cell Sci *117*, 4365-4375.

Lippincott-Schwartz, J., Altan-Bonnet, N., and Patterson, G.H. (2003). Photobleaching and photoactivation: following protein dynamics in living cells. Nat Cell Biol *Suppl*, S7-14.

Lippincott-Schwartz, J., Snapp, E., and Kenworthy, A. (2001). Studying protein dynamics in living cells. Nat Rev Mol Cell Biol *2*, 444-456.

Liu, J., Yao, F., Wu, R., Morgan, M., Thorburn, A., Finley, R.L., Jr., and Chen, Y.Q. (2002). Mediation of the DCC apoptotic signal by DIP13 alpha. J Biol Chem *277*, 26281-26285.

Luzio, J.P., Pryor, P.R., and Bright, N.A. (2007). Lysosomes: fusion and function. Nat Rev Mol Cell Biol *8*, 622-632.

Mao, X., Kikani, C.K., Riojas, R.A., Langlais, P., Wang, L., Ramos, F.J., Fang, Q., Christ-Roberts, C.Y., Hong, J.Y., Kim, R.Y.*, et al.* (2006). APPL1 binds to adiponectin receptors and mediates adiponectin signalling and function. Nat Cell Biol *8*, 516-523.

Martin, W.L., West, A.P., Jr., Gan, L., and Bjorkman, P.J. (2001). Crystal structure at 2.8 A of an FcRn/heterodimeric Fc complex: mechanism of pH-dependent binding. Mol Cell *7*, 867-877.

Maxfield, F.R., and McGraw, T.E. (2004). Endocytic recycling. Nat Rev Mol Cell Biol *5*, 121-132.

McCaffrey, M.W., Bielli, A., Cantalupo, G., Mora, S., Roberti, V., Santillo, M., Drummond, F., and Bucci, C. (2001). Rab4 affects both recycling and degradative endosomal trafficking. FEBS Lett *495*, 21-30.

McCarthy, K.M., Yoong, Y., and Simister, N.E. (2000). Bidirectional transcytosis of IgG by the rat neonatal Fc receptor expressed in a rat kidney cell line: a system to study protein transport across epithelia. J Cell Sci *113 (Pt 7)*, 1277-1285.

McNatt, M.W., McKittrick, I., West, M., and Odorizzi, G. (2007). Direct binding to Rsp5 mediates ubiquitin-independent sorting of Sna3 via the multivesicular body pathway. Mol Biol Cell *18*, 697-706.

Mellman, I., Fuchs, R., and Helenius, A. (1986). Acidification of the endocytic and exocytic pathways. Annual Rev Biochem *55*, 663-700.

Miaczynska, M., Christoforidis, S., Giner, A., Shevchenko, A., Uttenweiler-Joseph, S., Habermann, B., Wilm, M., Parton, R.G., and Zerial, M. (2004). APPL proteins link Rab5 to nuclear signal transduction via an endosomal compartment. Cell *116*, 445-456.

Miesenbock, G., De Angelis, D.A., and Rothman, J.E. (1998). Visualizing secretion and synaptic transmission with pH-sensitive green fluorescent proteins. Nature *394*, 192-195.

Mitsuuchi, Y., Johnson, S.W., Sonoda, G., Tanno, S., Golemis, E.A., and Testa, J.R. (1999). Identification of a chromosome 3p14.3-21.1 gene, APPL, encoding an adaptor molecule that interacts with the oncoprotein-serine/threonine kinase AKT2. Oncogene *18*, 4891-4898.

Nechamen, C.A., Thomas, R.M., Cohen, B.D., Acevedo, G., Poulikakos, P.I., Testa, J.R., and Dias, J.A. (2004). Human follicle-stimulating hormone (FSH) receptor interacts with the adaptor protein APPL1 in HEK 293 cells: potential involvement of the PI3K pathway in FSH signaling. Biol Reprod *71*, 629-636.

Ober, R.J., Martinez, C., Lai, X., Zhou, J., and Ward, E.S. (2004a). Exocytosis of IgG as mediated by the receptor, FcRn: an analysis at the single-molecule level. Proc Natl Acad Sci U S A *101*, 11076-11081.

Ober, R.J., Martinez, C., Vaccaro, C., Zhou, J., and Ward, E.S. (2004b). Visualizing the site and dynamics of IgG salvage by the MHC class I-related receptor, FcRn. J Immunol *172*, 2021-2029.

Olivo-Marin, J.C. (2002). Extraction of spots in biological images using multiscale products. Pattern Recog *35*, 8.

Pagano, A., Crottet, P., Prescianotto-Baschong, C., and Spiess, M. (2004). In vitro formation of recycling vesicles from endosomes requires adaptor protein-1/clathrin and is regulated by rab4 and the connector rabaptin-5. Mol Biol Cell *15*, 4990-5000.

Patel, D.A., Puig-Canto, A., Challa, D.K., Perez Montoyo, H., Ober, R.J., and Ward, E.S. (2011). Neonatal Fc receptor blockade by Fc engineering ameliorates arthritis in a murine model. J Immunol *187*, 1015-1022.

Patterson, G.H., Knobel, S.M., Sharif, W.D., Kain, S.R., and Piston, D.W. (1997). Use of the green fluorescent protein and its mutants in quantitative fluorescence microscopy. Biophys J *73*, 2782-2790.

Patterson, G.H., and Lippincott-Schwartz, J. (2002). A photoactivatable GFP for selective photolabeling of proteins and cells. Science *297*, 1873-1877.

Pfeffer, S. (2003). Membrane domains in the secretory and endocytic pathways. Cell *112*, 507-517.

Piper, R.C., and Katzmann, D.J. (2007). Biogenesis and function of multivesicular bodies. Annu Rev Cell Dev Biol *23*, 519-547.

Prabhat, P., Gan, Z., Chao, J., Ram, S., Vaccaro, C., Gibbons, S., Ober, R.J., and Ward, E.S. (2007). Elucidation of intracellular recycling pathways leading to exocytosis of the Fc receptor, FcRn, by using multifocal plane microscopy. Proc Natl Acad Sci U S A *104*, 5889-5894.

Prabhat, P., Ram, S., Ward, E.S., and Ober, R.J. (2004). Simultaneous imaging of different focal planes in fluorescence microscopy for the study of cellular dynamics in three dimensions. IEEE Trans Nanobioscience *3*, 237-242.

Presta, L.G. (2008). Molecular engineering and design of therapeutic antibodies. Cur Opin Immunol *20*, 460-470.

Progida, C., Malerod, L., Stuffers, S., Brech, A., Bucci, C., and Stenmark, H. (2007). RILP is required for the proper morphology and function of late endosomes. J Cell Sci *120*, 3729-3737.

Ram, S., Prabhat, P., Chao, J., Ward, E.S., and Ober, R.J. (2008). High accuracy 3D quantum dot tracking with multifocal plane microscopy for the study of fast intracellular dynamics in live cells. Biophys J *95*, 6025-6043.

Ram, S., Prabhat, P., Ward, E.S., and Ober, R.J. (2009). Improved single particle localization accuracy with dual objective multifocal plane microscopy. Opt Exp *17*, 6881-6898.

Reggiori, F., and Pelham, H.R. (2001). Sorting of proteins into multivesicular bodies: ubiquitin-dependent and -independent targeting. EMBO J *20*, 5176-5186.

Ren, M., Xu, G., Zeng, J., De Lemos-Chiarandini, C., Adesnik, M., and Sabatini, D.D. (1998). Hydrolysis of GTP on rab11 is required for the direct delivery of transferrin from the pericentriolar recycling compartment to the cell surface but not from sorting endosomes. Proc Natl Acad Sci U S A *95*, 6187-6192.

Rink, J., Ghigo, E., Kalaidzidis, Y., and Zerial, M. (2005). Rab conversion as a mechanism of progression from early to late endosomes. Cell *122*, 735-749.

Roopenian, D.C., and Akilesh, S. (2007). FcRn: the neonatal Fc receptor comes of age. Nature Rev Immunol *7*, 715-725.

Ryan, T.A. (2003). Kiss-and-run, fuse-pinch-and-linger, fuse-and-collapse: the life and times of a neurosecretory granule. Proc Natl Acad Sci U S A *100*, 2171-2173.

Saftig, P., and Klumperman, J. (2009). Lysosome biogenesis and lysosomal membrane proteins: trafficking meets function. Nat Rev Mol Cell Biol *10*, 623-635.

Schenck, A., Goto-Silva, L., Collinet, C., Rhinn, M., Giner, A., Habermann, B., Brand, M., and Zerial, M. (2008). The endosomal protein Appl1 mediates Akt substrate specificity and cell survival in vertebrate development. Cell *133*, 486-497.

Schonteich, E., Wilson, G.M., Burden, J., Hopkins, C.R., Anderson, K., Goldenring, J.R., and Prekeris, R. (2008). The Rip11/Rab11-FIP5 and kinesin II complex regulates endocytic protein recycling. J Cell Sci *121*, 3824-3833.

Schuster, M., Kilaru, S., Ashwin, P., Lin, C., Severs, N.J., and Steinberg, G. (2011a). Controlled and stochastic retention concentrates dynein at microtubule ends to keep endosomes on track. EMBO J *30*, 652-664.

Schuster, M., Lipowsky, R., Assmann, M.A., Lenz, P., and Steinberg, G. (2011b). Transient binding of dynein controls bidirectional long-range motility of early endosomes. Proc Natl Acad Sci U S A *108*, 3618-3623.

Sheff, D.R., Daro, E.A., Hull, M., and Mellman, I. (1999). The receptor recycling pathway contains two distinct populations of early endosomes with different sorting functions. J Cell Biol *145*, 123-139.

Shimomura, O., Johnson, F.H., and Saiga, Y. (1962). Extraction, purification and properties of aequorin, a bioluminescent protein from the luminous hydromedusan, Aequorea. J Cell Comp Physiol *59*, 223-239.

Simister, N.E., and Mostov, K.E. (1989). An Fc receptor structurally related to MHC class I antigens. Nature *337*, 184-187.

Simonsen, A., Lippe, R., Christoforidis, S., Gaullier, J.M., Brech, A., Callaghan, J., Toh, B.H., Murphy, C., Zerial, M., and Stenmark, H. (1998). EEA1 links PI(3)K function to Rab5 regulation of endosome fusion. Nature *394*, 494-498.

Skanland, S.S., Walchli, S., Brech, A., and Sandvig, K. (2009). SNX4 in complex with clathrin and dynein: implications for endosome movement. PLoS One *4*, e5935.

Skanland, S.S., Walchli, S., Utskarpen, A., Wandinger-Ness, A., and Sandvig, K. (2007). Phosphoinositide-regulated retrograde transport of ricin: crosstalk between hVps34 and sorting nexins. Traffic *8*, 297-309.

Soldati, T., Rancano, C., Geissler, H., and Pfeffer, S.R. (1995). Rab7 and Rab9 are recruited onto late endosomes by biochemically distinguishable processes. J Biol Chem *270*, 25541-25548.

Sonnichsen, B., De Renzis, S., Nielsen, E., Rietdorf, J., and Zerial, M. (2000). Distinct membrane domains on endosomes in the recycling pathway visualized by multicolor imaging of Rab4, Rab5, and Rab11. J Cell Biol *149*, 901-914.

Stenmark, H. (2009). Rab GTPases as coordinators of vesicle traffic. Nat Rev Mol Cell Biol *10*, 513-525.

Storrie, B., and Desjardins, M. (1996). The biogenesis of lysosomes: is it a kiss and run, continuous fusion and fission process? Bioessays *18*, 895-903.

Story, C.M., Mikulska, J.E., and Simister, N.E. (1994). A major histocompatibility complex class I-like Fc receptor cloned from human placenta: possible role in transfer of immunoglobulin G from mother to fetus. J Exp Med *180*, 2377-2381.

Subach, F.V., Patterson, G.H., Renz, M., Lippincott-Schwartz, J., and Verkhusha, V.V. (2010). Bright monomeric photoactivatable red fluorescent protein for two-color super-resolution sptPALM of live cells. J Am Chem Soc *132*, 6481-6491.

Traer, C.J., Rutherford, A.C., Palmer, K.J., Wassmer, T., Oakley, J., Attar, N., Carlton, J.G., Kremerskothen, J., Stephens, D.J., and Cullen, P.J. (2007). SNX4 coordinates endosomal sorting of TfnR with dynein-mediated transport into the endocytic recycling compartment. Nat Cell Biol *9*, 1370-1380.

Ullrich, O., Reinsch, S., Urbe, S., Zerial, M., and Parton, R.G. (1996). Rab11 regulates recycling through the pericentriolar recycling endosome. J Cell Biol *135*, 913-924.

Urbanowski, J.L., and Piper, R.C. (2001). Ubiquitin sorts proteins into the intralumenal degradative compartment of the late-endosome/vacuole. Traffic *2*, 622-630.

Urbanska, A., Sadowski, L., Kalaidzidis, Y., and Miaczynska, M. (2011). Biochemical Characterization of APPL Endosomes: The Role of Annexin A2 in APPL Membrane Recruitment. Traffic *12*, 1227-1241.

Vaccaro, C., Zhou, J., Ober, R.J., and Ward, E.S. (2005). Engineering the Fc region of immunoglobulin G to modulate in vivo antibody levels. Nat Biotechnol *23*, 1283-1288.

van der Sluijs, P., Hull, M., Webster, P., Male, P., Goud, B., and Mellman, I. (1992). The small GTP-binding protein rab4 controls an early sorting event on the endocytic pathway. Cell *70*, 729-740.

van Weering, J.R., Verkade, P., and Cullen, P.J. (2012). SNX-BAR-Mediated Endosome Tubulation is Co-ordinated with Endosome Maturation. Traffic *13*, 94-107.

Varsano, T., Dong, M.Q., Niesman, I., Gacula, H., Lou, X., Ma, T., Testa, J.R., Yates, J.R., 3rd, and Farquhar, M.G. (2006). GIPC is recruited by APPL to peripheral TrkA endosomes and regulates TrkA trafficking and signaling. Mol Cell Biol *26*, 8942-8952.

Wang, Y.L., and Goren, M.B. (1987). Differential and sequential delivery of fluorescent lysosomal probes into phagosomes in mouse peritoneal macrophages. J Cell Biol *104*, 1749-1754.

Wang, Z., Edwards, J.G., Riley, N., Provance, D.W., Jr., Karcher, R., Li, X.D., Davison, I.G., Ikebe, M., Mercer, J.A., Kauer, J.A.*, et al.* (2008). Myosin Vb mobilizes recycling endosomes and AMPA receptors for postsynaptic plasticity. Cell *135*, 535-548.

Ward, E.S. (1992). Secretion of T cell receptor fragments from recombinant Escherichia coli cells. J Mol Biol *224*, 885-890.

Ward, E.S., Gussow, D., Griffiths, A.D., Jones, P.T., and Winter, G. (1989). Binding activities of a repertoire of single immunoglobulin variable domains secreted from Escherichia coli. Nature *341*, 544-546.

Ward, E.S., Martinez, C., Vaccaro, C., Zhou, J., Tang, Q., and Ober, R.J. (2005). From sorting endosomes to exocytosis: association of Rab4 and Rab11 GTPases with the Fc receptor, FcRn, during recycling. Mol Biol Cell *16*, 2028-2038.

Ward, E.S., and Ober, R.J. (2009). Chapter 4: Multitasking by exploitation of intracellular transport functions the many faces of FcRn. Adv Immunol *103*, 77-115.

White, I.J., Bailey, L.M., Aghakhani, M.R., Moss, S.E., and Futter, C.E. (2006). EGF stimulates annexin 1-dependent inward vesiculation in a multivesicular endosome subpopulation. EMBO J *25*, 1-12.

Wiedenmann, J., Ivanchenko, S., Oswald, F., Schmitt, F., Rocker, C., Salih, A., Spindler, K.D., and Nienhaus, G.U. (2004). EosFP, a fluorescent marker protein with UV-inducible green-to-red fluorescence conversion. Proc Natl Acad Sci U S A *101*, 15905-15910.

Worby, C.A., and Dixon, J.E. (2002). Sorting out the cellular functions of sorting nexins. Nat Rev Mol Cell Biol *3*, 919-931.

Yao, X., Zhang, J., Zhou, H., Wang, E., and Xiang, X. (2012). In vivo roles of the basic domain of dynactin p150 in microtubule plus-end tracking and dynein function. Traffic *13*, 375-387.

Yoshida, M., Claypool, S.M., Wagner, J.S., Mizoguchi, E., Mizoguchi, A., Roopenian, D.C., Lencer, W.I., and Blumberg, R.S. (2004). Human neonatal Fc receptor mediates transport of IgG into luminal secretions for delivery of antigens to mucosal dendritic cells. Immunity *20*, 769-783.

Yoshida, M., Kobayashi, K., Kuo, T.T., Bry, L., Glickman, J.N., Claypool, S.M., Kaser, A., Nagaishi, T., Higgins, D.E., Mizoguchi, E.*, et al.* (2006). Neonatal Fc receptor for IgG regulates mucosal immune responses to luminal bacteria. J Clin Invest *116*, 2142-2151.

Yudowski, G.A., Puthenveedu, M.A., Henry, A.G., and von Zastrow, M. (2009). Cargo-mediated regulation of a rapid Rab4-dependent recycling pathway. Mol Biol Cell *20*, 2774-2784.

Zerial, M., and McBride, H. (2001). Rab proteins as membrane organizers. Nat Rev Mol Cell Biol *2*, 107-117.

Zhang, J., Campbell, R.E., Ting, A.Y., and Tsien, R.Y. (2002). Creating new fluorescent probes for cell biology. Nat Rev Mol Cell Biol *3*, 906-918.

Zhou, J., Mateos, F., Ober, R.J., and Ward, E.S. (2005). Conferring the binding properties of the mouse MHC class I-related receptor, FcRn, onto the human ortholog by sequential rounds of site-directed mutagenesis. J Mol Biol *345*, 1071-1081.

Zhu, X., Meng, G., Dickinson, B.L., Li, X., Mizoguchi, E., Miao, L., Wang, Y., Robert, C., Wu, B., Smith, P.D., *et al.* (2001). MHC class I-related neonatal Fc receptor for IgG is functionally expressed in monocytes, intestinal macrophages, and dendritic cells. J Immunol *166*, 3266-3276.

Zoncu, R., Perera, R.M., Balkin, D.M., Pirruccello, M., Toomre, D., and De Camilli, P. (2009). A phosphoinositide switch controls the maturation and signaling properties of APPL endosomes. Cell *136*, 1110-1121.